Université de Toulouse

THÈSE

En vue de l'obtention du

DOCTORAT DE L'UNIVERSITÉ DE TOULOUSE

Délivré par l'Université Toulouse III – Paul Sabatier

Discipline ou spécialité: Physique

Présentée et soutenue par:

Stefano DI SABATINO

Le 5 novembre 2015

Titre:

Reduced Density-Matrix Functional Theory: Correlation and Spectroscopy

---

Jury:

Dr.	Arjan BERGER	Examinateur
Prof. Dr.	Silke BIERMANN	Rapporteur
Prof. Dr.	Eberhard K. U. GROSS	Rapporteur
Prof. Dr.	Christoph MEIER	Examinateur
Dr.	Pina ROMANIELLO	Directeur de thèse
Dr.	Francesco SOTTILE	Examinateur

Ecole doctorale: Sciences de la matière
Unité de recherche: Laboratoire de Physique Théorique, IRSAMC
Directeur de thèse: Pina ROMANIELLO

Reduced Density-Matrix Functional Theory: Correlation and Spectroscopy

Stefano Di Sabatino

Alla mia famiglia

Contents

Conclusions and outlooks 107

Chapter 1

Introduction

In quantum mechanics a many-particle system is completely characterized by the wavefunction $\Psi(\mathbf{x}_1, \mathbf{x}_2, ..., \mathbf{x}_N; t)$, which is solution of the time-dependent Schrödinger equation

$$\mathrm{i}\frac{\partial}{\partial t}\Psi(\mathbf{x}_1, \mathbf{x}_2, ..., \mathbf{x}_N; t) = \hat{H}(t)\Psi(\mathbf{x}_1, \mathbf{x}_2, ..., \mathbf{x}_N; t),$$

where the Hamiltonian $\hat{H}(t)$ consists of a kinetic energy operator, a (time-dependent) potential operator and a two-particle operator. Here the coordinates $\mathbf{x}_i$ comprise the space-coordinate $\mathbf{r}_i$ and the spin-coordinate s_i. The many-body wavefunction depends on three spatial variables for each of the N electrons; the problem hence becomes quickly hard to solve, if not intractable, with increasing system size. However, in general, we are not interested in the complete wavefunction but rather in the expectation value of some physical observables. The wavefunction, thus, contains a large amount of information, most of which is washed out when calculating the observables of interest.

In condensed-matter physics, important formalisms for predicting and interpreting material properties, such as Density Functional Theory (DFT), Many-Body Perturbation Theory (MBPT) and Dynamical Mean Field Theory (DMFT), avoid the use of the wavefunction and use simpler quantities, such as the electron density or the one-body Green's function (1-GF). The price to pay for such a simplified framework is that one has to introduce effective potentials in which the complexity of the original problem is hidden. These potentials comprise the many-body effects of the system and, in general, need to be approximated. Moreover, there is also the issue of the observables, whose expression in terms of the fundamental variable of the problem is not always known. Of course the more information is contained in the basic variable the easier it is to deal with these two aspects.

Let us consider DFT [54, 58], for example. In this framework one replaces the interacting system with a fictitious system of non-interacting particles, the Kohn-Sham (KS) system, in which, under the influence of an effective potential (the Kohn-Sham potential), the electron density of the interacting system is reproduced. One then only has to solve a set of single-particle equations. These equations have to be solved self-consistently since the KS potential is a functional of the density. However, the KS

potential is in general unknown and finding approximations is a difficult task because the KS system does not have a clear physical meaning. Moreover only a few observables are known as functionals of the density. This is the case for the ground-state total energy or the fundamental gap, but in some other cases one relies on approximations. For example, the KS eigenvalues are in general different from the quasiparticle energies of the interacting system; nevertheless, empirical evidence shows that in many circumstances the single-particle KS spectrum is in good agreement with experimental direct and inverse photo-emission spectra. However, for strongly correlated systems, the results of the DFT approach are in disagreement with experiment. Let us consider the example of NiO as a prototypical strongly correlated material. This material is an antiferromagnetic insulator below the Néel temperature and it remains an insulator in the paramagnetic phase. The photoemission spectrum is very similar for the paramagnetic and the antiferromagnetic phases, with a band gap of about 4.3 eV [96, 107]. This clearly indicates that the magnetic order is not the leading mechanism responsible for the gap. The occurrence of the gap is the result of the strong Coulomb repulsion between electrons in the narrow partially-filled d states [86, 120]. The physics underlying the origin of the gap can be understood using the example of the Hubbard dimer at half filling in the atomic limit. In the symmetric dimer (singlet ground state) electrons localize on either site with equal probability (unless a small perturbation is present). Therefore the exact spectral function, which is related to the photoemission spectrum, shows two peaks: a removal peak at zero and an addition peak at U (the on-site Coulomb interaction), for both spin-up and spin-down channels. In this case it is important that an additional electron knows whether it meets a spin-up or a spin-down electron on a given site. In other words, it is a problem of correlation between two spins. DFT, within the standard local density approximation (LDA) [87], predicts NiO to be an insulator if spin polarization is taken into account [106], although the band gap is severely underestimated, but it predicts a metal in absence of magnetic ordering [72].

Another popular approach is Many-Body Perturbation Theory (MBPT) based on Green's functions. At the equilibrium, the one-body Greens function (1-GF) yields the ground-state expectation values of one-body operators, and the total energy. Moreover, it gives access to photoemission spectra through the imaginary part of the 1-GF (i.e., the spectral function). The 1-GF, therefore, contains more information than the simple electron density. MBPT is computationally more demanding than DFT, however it has the advantage that approximations with a clearer physical meaning can be more easily designed than in the context of density functionals. Within the so called GW approximation [50] to electron correlation, MBPT has become the method of choice for the calculations of quasiparticle band structures [6, 7, 79, 113, 114, 117] and direct and inverse photo-emission spectra [17, 30, 37, 67, 84] of many materials improving substantially over the results provided by static mean-field electronic structure methods. However GW suffers from some fundamental shortcomings for example, self-screening [80, 95], lack of full self-consistency (in extended systems) [15, 102, 112],

lack of size-consistency [25] and, in particular, it does not describe strong correlation (without imposing a magnetic ordering) [95]. For example paramagnetic NiO is described as a metal also by GW. This is because GW, besides exchange, gives a classical description of the system and of its response to an additional electron or hole [95].

A different approach based on GFs which can treat the missing physics is Dynamical Mean Field Theory (DMFT). This theory is based on mapping the complicated problem of a lattice model (the Hubbard model) onto a problem of a single site embedded in an effective medium which is determined self-consistently [39]. When applied to real materials an effective Hamiltonian for strongly localized electrons in d or f states is used, that is determined by the s and p electrons of the system. Much effort is devoted towards an *ab initio* calculation of the effective interaction between d or f electrons [12]. Since DMFT treats local correlations explicitly it is a powerful tool for the study of strongly correlated systems. Within this framework NiO is correctly described [59, 60].

In between the density and the 1-GF there is another quantity of interest, the one-body reduced density matrix (1-RDM), which is the basic variable of Reduced Density-Matrix Functional Theory (RDMFT). Within RDMFT, the ground-state properties of a physical system are functionals of the ground-state 1-RDM [44, 69], thanks to the one-to-one mapping between the (non-degenerate) ground-state wavefunction of the system and the corresponding 1-RDM [44]. In particular the ground-state total energy is a functional of the 1-RDM and energy minimization under the constraint that the 1-RDM is N-representable determines the exact 1-RDM. This procedure is, in general, computationally less expensive than calculating the 1-GF. The main advantage of RDMFT over DFT is that the kinetic energy functional is known exactly as a functional of the 1-RDM, only the exchange-correlation energy has to be approximated. Once the 1-RDM of the system is determined by means of a variational principle, all the observables of the system can be calculated, provided that their expression as functional of the 1-RDM is known. This is not the case for the photoemission spectra. Recently, an approximate procedure to calculate quasiparticle energies and photoemission spectra within RDMFT has been proposed [99], which is inspired by Koopmans' theorem. When applied to a series of transition-metal oxides, the method seems to capture the essential physics of strong electron correlations. These are, however, only empirical evidences, and an in-depth analysis is missing. It is therefore important to study these aspects in a systematic way in order to advance our understanding of an approach which is used all over physics and chemistry.

In this thesis we focus on the description of spectroscopy, in particular photoemission, and strong correlation within RDMFT.

Photoemission spectroscopy

Experimentally, direct and inverse photoemission spectroscopies (PES/IPES) give direct insights in the electronic structure of the materials. Figure 1.1 shows a schematic

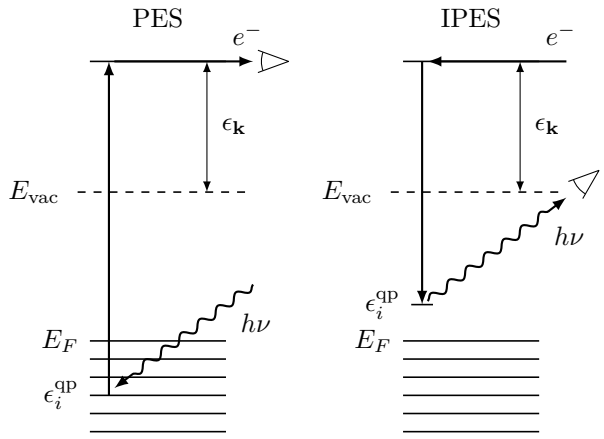

Figure 1.1: Schematic representation of direct photoemission (PES) and inverse photoemission (IPES) spectroscopies.

representation of PES and IPES experiments. In PES the sample is exposed to a beam of monochromatic radiation inducing photoelectric ionization [27, 53]. Photoelectrons are emitted with kinetic energy $\epsilon_{\mathbf{k}}$, given by

$$\epsilon_{\mathbf{k}} = h\nu + \epsilon_i^{\text{qp}}, \tag{1.1}$$

where $h\nu$ is the energy of the impinging photon and ϵ_i^{qp} is the quasi-particle energy of the level i, calculated with respect to the vacuum level, that the electron was occupying before being extracted from the sample. In inverse photoemission experiments the sample is exposed to a beam of electrons, the impinging electrons can lose their energy and be captured by the system *via* the emission of photons, whose energy is given by Eq. (1.1).

In a photoemission experiment the electrons extracted from the system are measured by a detector. The photocurrent, $J_{\mathbf{k}}(\omega)$, is the probability per unit time of emitting an electron with momentum $\hbar\mathbf{k}$ when the sample is irradiated with a photon of angular frequency ω. According to Fermi's golden rule the photocurrent is given by

$$J_{\mathbf{k}}(\omega) = \sum_l \left| \langle N-1, l; \mathbf{k}| \, \hat{\Delta} \, |N\rangle \right|^2 \delta(\epsilon_{\mathbf{k}} - \epsilon_l - \omega),$$

where $\hat{\Delta}$ is the dipole transition operator. The perturbation induces a transition from the initial state $|N\rangle$ with N electrons in the ground state to the final state $|N-1, l; \mathbf{k}\rangle$ in which the sample with $N-1$ electrons is in the excited state l and the photoelectron has momentum $\hbar\mathbf{k}$. The energy conservation requires that

$$\epsilon_{\mathbf{k}} = h\nu + E(N) - E_l(N-1),$$

therefore, knowing the frequency of the photon and measuring the kinetic energy of the photoelectron, one can determine the binding energy $\epsilon_l = E(N) - E_l(N-1)$. If we consider the photoelectron state completely decoupled from the sample, according to the sudden approximation, we can write $|N-1, l; \mathbf{k}\rangle = \hat{c}_{\mathbf{k}}^\dagger \, |N-1, l\rangle$, where $\hat{c}_{\mathbf{k}}^\dagger$ is the creation operator. Expanding the dipole transition operator in a complete set of

single-particle wavefunctions we have $\hat{\Delta} = \sum_{ij} \Delta_{ij} \hat{c}_i^\dagger \hat{c}_j$, which can be used to evaluate

$$\begin{aligned}\langle N-1, l; \mathbf{k}| \hat{\Delta} |N\rangle &= \langle N-1, l| \hat{c}_\mathbf{k} \sum_{ij} \Delta_{ij} \hat{c}_i^\dagger \hat{c}_j |N\rangle \\ &= \sum_j \Delta_{\mathbf{k}j} \langle N-1, l| \hat{c}_j |N\rangle ,\end{aligned}$$

where we used the fact that $\hat{c}_\mathbf{k} \hat{c}_i^\dagger \hat{c}_j = \delta_{\mathbf{k}i} \hat{c}_j + \hat{c}_i^\dagger \hat{c}_j \hat{c}_\mathbf{k}$, obtained using the anticommutation relation of $\hat{c}_\mathbf{k}$ and $c_i^\dagger$, and we assumed that the ground state has no component in the state $|\mathbf{k}\rangle$, *i.e.*, $\hat{c}_\mathbf{k} |N\rangle = 0$, as this state is a very high energy state. Let us introduce the matrix elements

$$A_{ij}(\omega) = \sum_l \langle N| \hat{c}_i^\dagger |N-1, l\rangle \langle N-1, l| \hat{c}_j |N\rangle \delta(\omega - \epsilon_l);$$

the photocurrent $J_\mathbf{k}(\omega)$ can thus be rewritten as

$$J_\mathbf{k}(\omega) = \sum_{ij} \Delta_{\mathbf{k}i} A_{ij}(\epsilon_\mathbf{k} - \omega) \Delta_{j\mathbf{k}}.$$

If we assume that the matrix elements of the dipole transition operator $\hat{\Delta}$ are constant and that the diagonal elements of A are the most relevant, we obtained

$$J_\mathbf{k}(\omega) = |\Delta|^2 \sum_i A_{ii}(\epsilon_\mathbf{k} - \omega). \tag{1.2}$$

The photocurrent is thus given by the product of the trace of A and Δ. In Chap. 3 we will see that $A_{ij}(\omega)$ are the matrix elements of the spectral function, and can be directly obtained from the imaginary part of the 1-GF.

Strong correlation and Hubbard model

NiO was taken by Mott as a paradigmatic material for Mott-Hubbard insulators, which can be described in terms of the Hubbard model [55]. According to this model, a solid is described as a regular lattice with one orbital per site and takes into account both the itinerant and the localized nature of electrons. The Hamiltonian of the Hubbard model, in second quantization, reads as

$$\hat{H} = -t \sum_{\langle i,j \rangle} \sum_\sigma \hat{c}_{i\sigma}^\dagger \hat{c}_{j\sigma} + \frac{U}{2} \sum_i \sum_{\sigma,\sigma'} \hat{c}_{i\sigma}^\dagger \hat{c}_{i\sigma'}^\dagger \hat{c}_{i\sigma'} \hat{c}_{i\sigma} + \epsilon_0 \sum_i \sum_\sigma \hat{c}_{i\sigma}^\dagger \hat{c}_{i\sigma} + \hat{V}_0.$$

Here $c_{i\sigma}^\dagger$ and $c_{i\sigma}$ are the creation and annihilation operators for an electron at site i with spin σ, U is the on-site (spin-independent) interaction, $-t$ is the hopping kinetic energy and ϵ_0 is the orbital energy. The summation $\sum_{\langle i,j \rangle}$ is restricted to the nearest-neighbor sites. The Hamiltonian further contains a potential V_0 that can be chosen to fix the zero-energy scale. The physics of the Hubbard model arises from

the competition between the hopping term, which prefers to delocalize electrons, and the on-site interaction, which favors localization. The ratio U/t is a measure for the relative contribution of both terms and is the intrinsic, dimensionless coupling constant of the Hubbard model. Depending on this ratio the system can be a metal or an insulator. When the hopping term dominates ($t \gg U$) the interaction can be neglected and the energy levels then form a band; the system is metallic, except when the band is completely filled. In the opposite case ($U \gg t$) electrons are distributed in such a way to minimize doubly occupancies, thus electrons distribute as uniformly as possible. If we deal with an half-filled system, at each site there is exactly one electron and hopping is suppressed. Thus, in this limiting case the half-filled system is an insulator. Between these two limiting cases there exists a critical value of U at which a metal-insulator transition (Mott transition) takes place [77].

This model can be solved exactly for small clusters [24], for the infinite one dimensional chain [66] and for infinite dimensions [38]. We will resort to this model throughout the thesis to illustrate the underlying physics of various approximations to electron correlation and to observables. We will also use it for benchmarking.

Outline of the thesis

In this thesis we study how spectroscopy and electron correlation are described in Reduced Density-Matrix Functional Theory. To do this we will exploit the link between reduced density matrices and Green's functions. The thesis is organized as follows. The first two chapters are devoted to the presentation of the theoretical background. In chapter 2 we introduce the basic concepts of Reduced Density-Matrix Functional Theory (RDMFT). We discuss the Hohenberg-Kohn theorem, for local and non-local external potentials, which states that there exists a one-to-one mapping between the (non-degenerate) ground-state wavefunction of the system and the corresponding 1-RDM. As a consequence of this theorem all the ground-state properties of a physical system are functionals of the ground-state 1-RDM. We discuss the variational principle which allows one to determine the 1-RDM. In practice, however, approximations to the exchange-correlation energy are needed. Finally some of these approximations are discussed.

In chapter 3 we introduce the basic concepts of Many-Body Perturbation Theory, whose basic variables are the Green's functions. In particular we focus on the one-body Green's function and its link to observables, such as the density, the 1-RDM, and the photoelectron spectrum. We discuss the Dyson equation to determine the one-body Green's function in terms of an effective potential, the so-called self-energy, which contains the many-body effects of the system. Various approximations to the self-energy are discussed, namely GW, Hartree-Fock, second Born and T matrix.

In chapter 4 we explore the performance of approximations to electron correlation in RDMFT and of approximations to the observables calculated within this theory using

the Hubbard model. This allows us to analyze the underlying physics and to elucidate the origin of the observed trends. In particular we explore how degeneracies and spin-symmetry breaking are treated in RDMFT and we show how the spectroscopic properties change with different spin structures.

In chapter 5 we derive a method for the calculation of photoemission spectra in terms of reduced density matrices. We start from the spectral representation of the 1-GF, whose imaginary part is related to photoemission spectra, and we introduce an effective energy that accounts for all poles of the 1-GF. We test simple approximations to this effective energy both on model system and the realistic case of bulk NiO.

Chapter 6 is more explorative and deals with time-dependent phenomena within RDMFT. The time evolution of the 1-RDM is related to the 2-RDM. The difficult task is to find approximations to the 2-RDM. We explore new approximation by exploiting the link between reduced density matrices and GFs. These approximations, however, depend on GFs and, moreover they can break down at strong correlation. We therefore derive an adiabatic approximation from the exact ground-state 2-RDM of the two-level Anderson model, which is suitable to study strong correlation. We illustrate the performance on the simple two-level Anderson model.

Chapter 2

Reduced Density-Matrix Functional Theory

In this chapter we introduce the basic concepts of Reduced Density-Matrix Functional Theory (RDMFT). We discuss the Hohenberg-Kohn theorem for local and non-local external potentials, which states that there exists a one-to-one mapping between the (non-degenerate) ground-state wavefunction of the system and the corresponding one-body reduced density matrix (1-RDM). As a consequence of this theorem all the ground-state properties of a physical system are functionals of the ground-state 1-RDM. We discuss the variational principle which allows us to determine the 1-RDM. In practice, however, approximations to the exchange-correlation energy are needed. We will discuss some of them at the end of this chapter.

2.1 Preliminaries

Let us consider a stationary system of N interacting electrons. The quantum mechanical behavior is completely described by the Schrödinger equation

$$\hat{H}\,|\Psi\rangle = E\,|\Psi\rangle\,. \tag{2.1}$$

where $|\Psi\rangle$ is an eigenstate and E the corresponding eigenenergy of the N-particle system. Here $\hat{H}$ is the Hamiltonian operator of the system and is given by

$$\hat{H} = \hat{T} + \hat{V} + \hat{W}, \tag{2.2}$$

where $\hat{T}$, $\hat{V}$ and $\hat{W}$ are the operators corresponding to the kinetic energy, the external potential and the two-particle interaction, respectively. In second quantization they

are explicitly given by

$$\hat{T} = \int d\mathbf{x}\hat{\psi}^\dagger(\mathbf{x}) \left(-\frac{\nabla^2_{\mathbf{r}}}{2}\right) \hat{\psi}(\mathbf{x}),$$
$$\hat{V} = \int d\mathbf{x}d\mathbf{x}'\hat{\psi}^\dagger(\mathbf{x}')v_{\text{ext}}(\mathbf{x},\mathbf{x}')\hat{\psi}(\mathbf{x}),$$
$$\hat{W} = \frac{1}{2}\int d\mathbf{x}'d\mathbf{x}'\hat{\psi}^\dagger(\mathbf{x})\hat{\psi}^\dagger(\mathbf{x}')v_c(\mathbf{r},\mathbf{r}')\hat{\psi}(\mathbf{x}')\hat{\psi}(\mathbf{x}),$$

where $\mathbf{x}$ is a combined space-spin coordinate $\mathbf{x} \equiv (\mathbf{r}, s)$ and $\int d\mathbf{x} = \sum_s \int d\mathbf{r}$. $\hat{\psi}(\mathbf{x})$ and $\hat{\psi}^\dagger(\mathbf{x})$ are the field operators in the Schrödinger picture and we assumed that particles interact via the Coulomb potential $v_c(\mathbf{r},\mathbf{r}') = 1/|\mathbf{r}-\mathbf{r}'|$. We note that atomic units are used throughout this work. Here we consider a non-local external potential $v_{\text{ext}}(\mathbf{x},\mathbf{x}')$ as it will be useful for the following discussion. Non-local potentials are encountered if one wants to deal, for example, with spin-dependent potentials, magnetic fields or if one wants to study valence electrons using a pseudopotential to treat nuclei and core electrons.

The density matrix $\Gamma^{(N)}$ for a pure state of N electrons is defined, in second quantization, as

$$\Gamma^{(N)}(\mathbf{x}_1,...,\mathbf{x}_N;\mathbf{x}'_1,...,\mathbf{x}'_N) \equiv \langle\Psi|\,\hat{\psi}^\dagger(\mathbf{x}'_N)...\hat{\psi}^\dagger(\mathbf{x}'_1)\hat{\psi}(\mathbf{x}_1)...\hat{\psi}(\mathbf{x}_N)\,|\Psi\rangle\,.$$

This is equivalent to

$$\Gamma^{(N)}(\mathbf{x}_1,...,\mathbf{x}_N;\mathbf{x}'_1,...,\mathbf{x}'_N) \equiv N!\,\Psi^*(\mathbf{x}'_1,...,\mathbf{x}'_N)\Psi(\mathbf{x}_1,...,\mathbf{x}_N),$$

where $\Psi(\mathbf{x}_1,...,\mathbf{x}_N) = \langle\mathbf{x}_1,...,\mathbf{x}_N|\Psi\rangle$ is the wavefunction corresponding to $|\Psi\rangle$. The n-body reduced density matrix (n-RDM) is defined as

$$\begin{aligned}\Gamma^{(n)}(\mathbf{x}_1,...,\mathbf{x}_n;\mathbf{x}'_1,...,\mathbf{x}'_n) \equiv\ & \langle\Psi|\,\hat{\psi}^\dagger(\mathbf{x}'_n)...\hat{\psi}^\dagger(\mathbf{x}'_1)\hat{\psi}(\mathbf{x}_1)...\hat{\psi}(\mathbf{x}_n)\,|\Psi\rangle \\ =\ & \frac{N!}{(N-n)!}\int d\mathbf{x}_{n+1}...d\mathbf{x}_N\Psi^*(\mathbf{x}'_1,...,\mathbf{x}'_n,\mathbf{x}_{n+1},...,\mathbf{x}_N) \\ & \times\Psi(\mathbf{x}_1,...,\mathbf{x}_N). \end{aligned} \tag{2.3}$$

In particular for the two-body reduced density matrix (2-RDM) and the one-body reduced density matrix (1-RDM) $\gamma \equiv \Gamma^{(1)}$, definition (2.3) reduces respectively to

$$\begin{aligned}\Gamma^{(2)}(\mathbf{x}_1,\mathbf{x}_2;\mathbf{x}'_1,\mathbf{x}'_2) \equiv\ & \langle\Psi|\,\hat{\psi}^\dagger(\mathbf{x}'_2)\hat{\psi}^\dagger(\mathbf{x}'_1)\hat{\psi}(\mathbf{x}_1)\hat{\psi}(\mathbf{x}_2)\,|\Psi\rangle \\ =\ & N(N-1)\int d\mathbf{x}_3...d\mathbf{x}_N\Psi^*(\mathbf{x}'_1,\mathbf{x}'_2,\mathbf{x}_3,...,\mathbf{x}_N)\Psi(\mathbf{x}_1,...,\mathbf{x}_N), \end{aligned} \tag{2.4}$$

and

$$\begin{aligned}\gamma(\mathbf{x},\mathbf{x}') \equiv\ & \langle\Psi|\,\hat{\psi}^\dagger(\mathbf{x}')\hat{\psi}(\mathbf{x})\,|\Psi\rangle \\ =\ & N\int d\mathbf{x}_2...d\mathbf{x}_N\Psi^*(\mathbf{x}',\mathbf{x}_2,...,\mathbf{x}_N)\Psi(\mathbf{x},\mathbf{x}_2,...,\mathbf{x}_N). \end{aligned} \tag{2.5}$$

According to these definitions the 1-RDM normalizes to the total number of electrons

$$\mathrm{Tr}\,\gamma(\mathbf{x},\mathbf{x}') \equiv \int d\mathbf{x}\gamma(\mathbf{x},\mathbf{x}) = N.$$

From the definition (2.3) one can see that the n-body and the $(n-1)$-body reduced density matrices are related *via*

$$\Gamma^{(n-1)}(\mathbf{x}_1,...,\mathbf{x}_{n-1};\mathbf{x}'_1,...,\mathbf{x}'_{n-1}) = \frac{1}{N-n+1} \times \int d\mathbf{x}_n \Gamma^{(n)}(\mathbf{x}_1,...,\mathbf{x}_{n-1},\mathbf{x}_n;\mathbf{x}'_1,...,\mathbf{x}'_{n-1},\mathbf{x}_n).$$

In particular for $n = 2$

$$\gamma(\mathbf{x},\mathbf{x}') = \frac{1}{N-1}\int d\mathbf{x}_2 \Gamma^{(2)}(\mathbf{x},\mathbf{x}_2;\mathbf{x}',\mathbf{x}_2). \tag{2.6}$$

It is also worth noting that

$$\rho(\mathbf{x}) = \gamma(\mathbf{x},\mathbf{x}) = N\int d\mathbf{x}_2...d\mathbf{x}_N \Psi^*(\mathbf{x},\mathbf{x}_2,...,\mathbf{x}_N)\Psi(\mathbf{x},\mathbf{x}_2,...,\mathbf{x}_N), \tag{2.7}$$

i.e., the diagonal of the 1-RDM gives the electron density ρ.

We can now express the total energy of the system, $E = \langle\Psi|\,\hat{H}\,|\Psi\rangle$, in terms of reduced density matrices. It reads as

$$E = \int d\mathbf{x} \lim_{\mathbf{x}'\to\mathbf{x}} \left(-\frac{\nabla^2_{\mathbf{r}}}{2}\right)\gamma(\mathbf{x},\mathbf{x}') + \int d\mathbf{x}d\mathbf{x}' v_{\mathrm{ext}}(\mathbf{x},\mathbf{x}')\gamma(\mathbf{x},\mathbf{x}') + \frac{1}{2}\int d\mathbf{x}d\mathbf{x}' v_c(\mathbf{r},\mathbf{r}')\Gamma^{(2)}(\mathbf{x},\mathbf{x}';\mathbf{x},\mathbf{x}'), \tag{2.8}$$

where we used Eqs (2.4) and (2.5). This means that the total energy of the system is completely determined by the 1-RDM and the diagonal of the 2-RDM.

Using Eq. (2.6) the total energy can be rewritten as a functional of the 2-RDM alone. One might think to minimize this functional with respect to the 2-RDM to obtain the ground-state total energy. However there is a major obstacle in following this direction. The trial 2-RDMs must correspond to some antisymmetric wavefunction, *i.e.*, they must be N-representables. The set of necessary and sufficient conditions for the 2-RDM to be N-representable is not known. Recently a set of necessary conditions has been derived which is however not sufficient [73, 74]. Varying the 2-RDM without imposing sufficient constraints can lead to a lower energy than the ground-state energy.

The set of necessary and sufficient conditions for the 1-RDM to be N-representable is, instead, known and it turns out to be extremely simple as it will be discussed in the next section. One can, thus, use the 1-RDM as fundamental variable and express the total energy (2.8) and the ground-state expectation value of any operator as a functional of the 1-RDM. This is justified by a theorem, similar to the Hohenberg-Kohn theorem [54] of Density Functional Theory (DFT), which guarantees a one-to-one mapping between the 1-RDM γ and the ground-state wavefunction Ψ_0.

2.2 Hohenberg-Kohn theorems

Before proving the map $\gamma \leftrightarrow \Psi_0$ in the general case of a nonlocal external potential $v_{\text{ext}}(\mathbf{r}, \mathbf{r}')$, it is instructive to review the case of a local external potential $v_{\text{ext}}(\mathbf{r}, \mathbf{r}') = v_{\text{ext}}(\mathbf{r})\delta(\mathbf{r} - \mathbf{r}')$.

2.2.1 Local potentials

In the case of external local potentials the first Hohenberg-Kohn theorem states that there exists a one-to-one mapping $\rho \leftrightarrow v_{\text{ext}}$ (in case of a non-degenerate ground state). The proof is as follows. First we notice that the map $v_{\text{ext}} \to \rho$ is provided by the time-independent Schrödinger equation (2.1) and Eq. (2.7). The external potential, indeed, determines the ground state Ψ_0, from which ρ is calculated through Eq. (2.7).

The inverse map $\rho \to v_{\text{ext}}$ can be proven by *reductio ad absurdum*. First we show that two potentials v_{ext} and v'_{ext} differing by more than a constant, will not lead to the same wavefunction ($\Psi_0 \to v_{\text{ext}}$). Let us assume that both potentials give the same ground state Ψ_0. The Schrödinger equations are

$$\hat{H}\Psi_0 = E_0\Psi_0, \tag{2.9}$$

$$\hat{H}'\Psi_0 = E'_0\Psi_0, \tag{2.10}$$

where $\hat{H}$ and $\hat{H}'$ contain the potentials v_{ext} and v'_{ext}, respectively. Subtracting Eq. (2.10) from Eq. (2.9) we get

$$(\hat{H} - \hat{H}')\Psi_0 = (E_0 - E'_0)\Psi_0,$$

from which it follows that

$$(\hat{V} - \hat{V}')\Psi_0 = (E_0 - E'_0)\Psi_0. \tag{2.11}$$

Since $\hat{V}$ and $\hat{V}'$ are multiplicative operators (because we look at local potentials), we see from Eq. (2.11) that if in some region $v_{\text{ext}} \neq v'_{\text{ext}} + \text{const.}$ then Ψ_0 must vanish in that region for the above equation to hold. The wavefunction Ψ_0 cannot vanish on a set with nonzero measure [65], so we can divide by Ψ_0 arriving at the contradiction $\hat{V} - \hat{V}' = \text{const}$. Therefore, local potentials that give the same ground-state wavefunction cannot differ by more than a constant.

We now need to prove the map $\rho \to \Psi_0$. Let v_{ext} and v'_{ext} be two potentials that differ by more than a constant. Since the corresponding wavefunctions Ψ and Ψ' are different by the previous theorem, we have

$$\begin{aligned} E &= \langle\Psi_0|\,\hat{H}\,|\Psi_0\rangle < \langle\Psi'_0|\,\hat{H}\,|\Psi'_0\rangle \\ &= \langle\Psi'_0|\,\hat{H}'\,|\Psi'_0\rangle + \int d\mathbf{r}[v_{\text{ext}}(\mathbf{r}) - v'_{\text{ext}}(\mathbf{r})]\rho'(\mathbf{r}) \\ &= E' + \int d\mathbf{r}[v_{\text{ext}}(\mathbf{r}) - v'_{\text{ext}}(\mathbf{r})]\rho'(\mathbf{r}). \end{aligned}$$

Interchanging the roles of v_{ext} and v'_{ext}, we have

$$E' < E + \int d\mathbf{r}[v'_{\text{ext}}(\mathbf{r}) - v_{\text{ext}}(\mathbf{r})]\rho(\mathbf{r}).$$

Adding the two inequalities we obtain

$$\int d\mathbf{r}[v'_{\text{ext}}(\mathbf{r}) - v_{\text{ext}}(\mathbf{r})][\rho'(\mathbf{r}) - \rho(\mathbf{r})] < 0.$$

If the two ground-state densities were the same, we would have the contradiction $0 < 0$; therefore different ground states must have different ground-state densities. This defines the map $\rho\ (\to \Psi_0) \to v_{\text{ext}}$, and thus the one-to-one map $\rho \leftrightarrow v_{\text{ext}}$ is constructed.

This theorem has an important consequence: the ground-state wavefunction can be written as a functional of the density, $\Psi_0[\rho]$. As a consequence, the ground-state expectation values of any operator $\hat{O}$ is also a functional of the density

$$O[\rho] \equiv \langle \Psi_0[\rho] | \hat{O} | \Psi_0[\rho] \rangle .$$

In particular, the total energy functional can be written as

$$\begin{aligned} E[\rho] &= \langle \Psi_0[\rho] | \hat{T} + \hat{V} + \hat{W} | \Psi_0[\rho] \rangle \\ &= \langle \Psi_0[\rho] | \hat{T} + \hat{W} | \Psi_0[\rho] \rangle + \int d\mathbf{r}\rho(\mathbf{r}) v_{\text{ext}}(\mathbf{r}) \\ &= F[\rho] + \int d\mathbf{r}\rho(\mathbf{r}) v_{\text{ext}}(\mathbf{r}), \end{aligned}$$

where $F[\rho]$ is defined independently of the external potential and, thus, it is a universal functional of the density.

Let ρ_0 be the ground-state density corresponding to the potential v_{ext}, then thanks to the variational principle we have for an arbitrary ρ

$$\begin{aligned} E[\rho] &= \langle \Psi_0[\rho] | \hat{T} + \hat{V}_0 + \hat{W} | \Psi_0[\rho] \rangle \\ &\geq \langle \Psi_0[\rho_0] | \hat{T} + \hat{V}_0 + \hat{W} | \Psi_0[\rho_0] \rangle = E[\rho_0]. \end{aligned}$$

This proves the second Hohenberg-Kohn theorem, which states that the exact density minimizes the ground-state energy functional:

$$E_0 = \inf_{\rho} \left\{ \langle \Psi_0[\rho] | \hat{T} + \hat{W} | \Psi_0[\rho] \rangle + \int d\mathbf{r}\rho(\mathbf{r}) v_{\text{ext}}(\mathbf{r}) \right\},$$

where the infimum should be restricted to all pure-state v-representable densities ρ. A density is said to be pure-state v-representable if it is the density associated with the antisymmetric ground-state wavefunction of a Hamiltonian with some external potential $v_{\text{ext}}(\mathbf{r})$. The conditions for a density to be v-representable are unknown.

However DFT can be formulated in a way that only requires the density to be N-representable (see, *e.g.*, Ref. [85]). A density is N-representable if it can be obtained through Eq. (2.7) from some antisymmetric wavefunction. The conditions for a density ρ to be N-representable are [44]

$$\rho(\mathbf{r}) \geq 0, \qquad \int d\mathbf{r}\rho(\mathbf{r}) = N, \qquad \text{and} \qquad \int d\mathbf{r}|\nabla\rho(\mathbf{r})^{1/2}|^2 < \infty.$$

2.2.2 Non-local potentials

Gilbert [44] provided a generalization of the Hohenberg-Kohn theorem to the case of nonlocal potentials. The first difficulty one encounters is that it is not possible to show the existence of a one-to-one mapping between the external potential and the ground-state wavefunction. This is a consequence of the fact that the potential is not a multiplicative operator [44]. However one can show that the map between Ψ_0 and γ is one-to-one, which is sufficient to justify a Reduced Density-Matrix Functional Theory. The proof follows the same line of argument as for the case of local potentials. First, Ψ_0 determines γ through the definition of the latter (see Eq. (2.5)). This is the $\Psi_0 \to \gamma$ map. The inverse map $\gamma \to \Psi_0$ is demonstrated by *reductio ad absurdum*.

Let v_{ext} and v'_{ext} be two potentials that generate two distinct ground-states Ψ_0 and Ψ'_0, respectively. By the variational principle we have

$$\begin{aligned} E &= \langle\Psi_0|\,\hat{H}\,|\Psi_0\rangle < \langle\Psi'_0|\,\hat{H}\,|\Psi'_0\rangle \\ &= \langle\Psi'_0|\,\hat{H}'\,|\Psi'_0\rangle + \int d\mathbf{x}d\mathbf{x}'[v_{\text{ext}}(\mathbf{x},\mathbf{x}') - v'_{\text{ext}}(\mathbf{x},\mathbf{x}')]\gamma'(\mathbf{x},\mathbf{x}') \\ &= E' + \int d\mathbf{x}d\mathbf{x}'[v_{\text{ext}}(\mathbf{x},\mathbf{x}') - v'_{\text{ext}}(\mathbf{x},\mathbf{x}')]\gamma'(\mathbf{x},\mathbf{x}'). \end{aligned}$$

Interchanging the roles of v_{ext} and v'_{ext}, we have

$$E' < E + \int d\mathbf{x}d\mathbf{x}'[v'_{\text{ext}}(\mathbf{x},\mathbf{x}') - v_{\text{ext}}(\mathbf{x},\mathbf{x}')]\gamma(\mathbf{x},\mathbf{x}').$$

Adding the two inequalities we obtain

$$\int d\mathbf{x}d\mathbf{x}'[v'_{\text{ext}}(\mathbf{x},\mathbf{x}') - v_{\text{ext}}(\mathbf{x},\mathbf{x}')][\gamma'(\mathbf{x},\mathbf{x}') - \gamma(\mathbf{x},\mathbf{x}')] < 0.$$

If the two ground-state 1-RDMs were the same, we would have the contradiction $0 < 0$. Therefore different ground states must have different 1-RDMs. This concludes the proof that the relation between the ground-state wavefunction and the ground-state 1-RDM is one-to-one ($\Psi_0 \leftrightarrow \gamma$).

This theorem implies that the ground-state wavefunction can be expressed as a functional of the 1-RDM, $\Psi_0[\gamma]$. Therefore the expectation values of any ground-state operator can be written as a functional of the 1-RDM

$$O[\gamma] \equiv \langle\Psi_0[\gamma]|\,\hat{O}\,|\Psi_0[\gamma]\rangle\,.$$

In particular the total energy functional is given by

$$\begin{aligned} E[\gamma] &= \langle \Psi_0[\gamma] | \, \hat{T} + \hat{V} + \hat{W} \, | \Psi_0[\gamma] \rangle \\ &= \int d\mathbf{x} d\mathbf{x}' h(\mathbf{x}, \mathbf{x}') \gamma(\mathbf{x}, \mathbf{x}') + \langle \Psi_0[\gamma] | \, \hat{W} \, | \Psi_0[\gamma] \rangle \, , \end{aligned} \tag{2.12}$$

where

$$h(\mathbf{x}, \mathbf{x}') = \delta(\mathbf{x} - \mathbf{x}') \left(-\frac{\nabla^2_{\mathbf{r}}}{2} \right) + v_{\text{ext}}(\mathbf{x}, \mathbf{x}')$$

is the one-body part of the Hamiltonian. Here it is evident the advantage of using the 1-RDM instead of the density ρ as a basic variable: the kinetic energy term is a well-known functional of the 1-RDM. This is not the case in DFT.

Let us now suppose that γ is the ground-state 1-RDM corresponding to the external potential v_{ext} and γ' the ground-state 1-RDM corresponding to a different v'_{ext}. Using the variational principle, we have

$$\begin{aligned} E[\gamma'] &= \int d\mathbf{x} d\mathbf{x}' h(\mathbf{x}, \mathbf{x}') \gamma'(\mathbf{x}, \mathbf{x}') + \langle \Psi_0[\gamma'] | \, \hat{W} \, | \Psi_0[\gamma'] \rangle \\ &= \langle \Psi_0[\gamma'] | \, \hat{T} + \hat{V} + \hat{W} \, | \Psi_0[\gamma'] \rangle \\ &\geq \langle \Psi_0[\gamma] | \, \hat{T} + \hat{V} + \hat{W} \, | \Psi_0[\gamma] \rangle = E[\gamma]. \end{aligned}$$

The exact 1-RDM, thus, minimizes the total energy functional. The ground state energy can be found as

$$E_0 = \inf_{\gamma} \left\{ \langle \Psi_0[\gamma] | \, \hat{W} \, | \Psi_0[\gamma] \rangle + \int d\mathbf{x} d\mathbf{x}' h(\mathbf{x}, \mathbf{x}') \gamma(\mathbf{x}, \mathbf{x}') \right\}. \tag{2.13}$$

Note that the energy functional (2.12) is defined only for pure state v-representable 1-RDM, thus the infimum should be restricted to this class of 1-RDMs. However the conditions for a 1-RDM to be v-representable are unknown.

The problem is solved by minimizing the functional (2.13) over a larger set of 1-RDM, *i.e.*, the ensemble N-representable 1-RDMs. By definition, a 1-RDM γ is said to be ensemble N-representable if a set of pure states $|\Psi_i\rangle$ and weights w_i, with $\sum_i w_i = 1$, exists such that

$$\gamma(\mathbf{x}, \mathbf{x}') = \sum_i w_i \, \langle \Psi_i | \, \hat{\psi}^\dagger(\mathbf{x}') \hat{\psi}(\mathbf{x}) \, | \Psi_i \rangle \, .$$

The states $|\Psi_i\rangle$ form a mixed state characterized by the density matrix operator $\hat{\Gamma}^{(N)} = \sum_i w_i \, |\Psi_i\rangle \, \langle \Psi_i|$ with $\gamma(\mathbf{x}, \mathbf{x}') = \text{Tr} \, [\hat{\Gamma}^{(N)} \hat{\psi}^\dagger(\mathbf{x}') \hat{\psi}(\mathbf{x})]$.

For ensemble N-representable 1-RDM the functional $W[\gamma]$ can be defined as

$$W[\gamma] \equiv \inf_{\hat{\Gamma}^{(N)} \to \gamma} \text{Tr} \, [\hat{\Gamma}^{(N)} \hat{W}], \tag{2.14}$$

where now the infimum goes over all the ensemble density matrices which yield the given 1-RDM γ. If the ground-state is non-degenerate, the minimum of (2.14) corresponds to a pure state. In case the ground-state is degenerate, the minimization will give a linear combination of the 1-RDMs with the lowest energy [44].

The advantage of this extension is that the necessary and sufficient ensemble N-representability conditions for the 1-RDM are known and they turn out to be particularly simple [21, 69]: given the spectral representation of γ in terms of its eigenvalues n_i (occupation numbers) and eigenfunction ϕ_i (natural spin orbitals, or for simplicity natural orbitals)

$$\gamma(\mathbf{x}, \mathbf{x}') = \sum_i n_i \phi_i(\mathbf{x}) \phi_i^*(\mathbf{x}'),$$

the 1-RDM is ensemble N-representable if

$$0 \leq n_i \leq 1 \tag{2.15}$$

and

$$\sum_i n_i = N. \tag{2.16}$$

Condition (2.15) is related to the fact that an orbital cannot be occupied by more than one electron, according to Pauli principle. While condition (2.16) simply reflects the fact that the total number of electrons is equal to N.

2.3 Energy as functional of the 1-RDM

As discussed in the previous section, the total energy can be expressed as a functional of the 1-RDM

$$E[\gamma] = E_{\text{kin}}[\gamma] + E_{\text{ext}}[\gamma] + E_{\text{int}}[\gamma],$$

where E_{kin}, E_{ext} and E_{int} are respectively the kinetic, external and interaction energies. The kinetic and external energies have a simple functional dependence in terms of the 1-RDM. The main advantage of RDMFT over DFT is that the kinetic energy is known exactly as a functional of γ

$$E_{\text{kin}}[\gamma] = \int d\mathbf{x} \lim_{\mathbf{x}' \to \mathbf{x}} \left(-\frac{\nabla_{\mathbf{r}}^2}{2} \right) \gamma(\mathbf{x}, \mathbf{x}').$$

The energy due to the external potential can also be expressed in a simple way in terms of the 1-RDM

$$E_{\text{ext}}[\gamma] = \int d\mathbf{x} d\mathbf{x}' v_{\text{ext}}(\mathbf{x}, \mathbf{x}') \gamma(\mathbf{x}, \mathbf{x}').$$

Only the interaction part cannot be easily expressed in term of the 1-RDM. We can rewrite the interaction energy as a sum of the following contributions

$$E_{\text{int}}[\gamma] = E_H[\gamma] + E_x[\gamma] + E_c[\gamma].$$

The first term is the Hartree energy and reads as

$$E_H[\gamma] = \frac{1}{2}\int d\mathbf{x}d\mathbf{x}' v_c(\mathbf{r},\mathbf{r}')\gamma(\mathbf{x},\mathbf{x})\gamma(\mathbf{x}',\mathbf{x}'). \tag{2.17}$$

It is referred usually as the classical part of the interaction, in fact it can be regarded as the potential energy associated to a charge distribution $\rho(\mathbf{x}) = \gamma(\mathbf{x},\mathbf{x})$. The exchange energy also can be expressed easily in terms of the 1-RDM and reads as

$$E_x[\gamma] = -\frac{1}{2}\int d\mathbf{x}d\mathbf{x}' v_c(\mathbf{r},\mathbf{r}')\gamma(\mathbf{x},\mathbf{x}')\gamma(\mathbf{x}',\mathbf{x}). \tag{2.18}$$

Only the remaining correlation energy $E_c[\gamma]$ needs to be approximated.

Most of the approximate functionals proposed in literature are implicit functionals of the 1-RDM; they are explicit functional of the occupation numbers n_i and natural orbitals ϕ_i, $E[\{n_i\},\{\phi_i\}]$. Some of the approximations proposed in literature will be presented in Sec. 2.6.

2.4 Energy minimization

The total energy functional $E[\{n_i\},\{\phi_i\}]$ has to be minimized under the constraints that the 1-RDM is ensemble N-representable ($0 \leq n_i \leq 1$, $\sum_i n_i = N$) and under the orthonormality requirement for the natural orbitals,

$$\langle\phi_i|\phi_j\rangle = \int d\mathbf{x}\phi_i^*(\mathbf{x})\phi_j(\mathbf{x}) = \delta_{ij}.$$

Bounds on the occupation numbers can be enforced, for example, setting $n_i = \cos^2\theta_i$ and varying θ_i without constraints. The other two conditions can be taken into account easily using the method of Lagrange multipliers. We can define the auxiliary functional

$$\Omega[\{\theta_i\},\{\phi_i\}] = E[\{n_i(\theta_i)\},\{\phi_i\}] - \mu\left(\sum_j \cos^2\theta_j - N\right) - \sum_{jk}\lambda_{jk}\left(\langle\phi_j|\phi_k\rangle - \delta_{jk}\right). \tag{2.19}$$

The functional (2.19) has to be stationary with respect to variations in $\{\theta_i\}$, $\{\phi_i(\mathbf{x})\}$, and $\{\phi_i^*(\mathbf{x})\}$

$$\begin{aligned}\delta\Omega = &\sum_i \sin(2\theta_i)\left[\mu - \frac{\partial E}{\partial n_i}\right]\delta\theta_i \\ &+ \sum_i \int d\mathbf{x}\left[\frac{\delta E}{\delta\phi_i(\mathbf{x})} - \sum_k \lambda_{ki}\phi_k^*(\mathbf{x})\right]\delta\phi_i(\mathbf{x}) \\ &+ \sum_i \int d\mathbf{x}\delta\phi_i^*(\mathbf{x})\left[\frac{\delta E}{\delta\phi_i^*(\mathbf{x})} - \sum_k \lambda_{ik}\phi_k(\mathbf{x})\right] = 0.\end{aligned} \tag{2.20}$$

The stationarity with respect to θ_i brings to the relation

$$\sin(2\theta_i)\left[\mu - \frac{\partial E}{\partial n_i}\right] = 0, \tag{2.21}$$

where the partial derivative $\partial E/\partial n_i$ is taken holding the natural orbitals fixed. There are two possible solutions to Eq. (2.21). The first is

$$\sin(2\theta_i) = 0,$$

which is satisfied by $\theta_i = 0$ or $\theta_i = \pi/2$, which correspond to $n_i = 0$ or $n_i = 1$, respectively. The states corresponding to occupation numbers either 0 or 1 are usually referred as "pinned" states [52]. If an occupation number is equal to one it means that the corresponding natural orbital is present in all the determinants with non-zero coefficient in the full CI expansion. This situation is rather exceptional for the exact wavefunction of a system of interacting particles. However most of the approximate 1-RDM functional known produce occupation numbers equal to one for most of the core states.

The second solution is

$$\frac{\partial E}{\partial n_i} = h_{ii} + \frac{\partial E_{\text{int}}}{\partial n_i} = \mu, \tag{2.22}$$

where $h_{ii} = \int d\mathbf{x} d\mathbf{x}' \phi_i^*(\mathbf{x}) h(\mathbf{x}, \mathbf{x}') \phi_i(\mathbf{x}')$. Equation (2.22) is satisfied only by partially occupied orbitals.

For a fixed set of occupation numbers $\{n_i\}$, the equations resulting from the variation with respect to the natural orbitals $\{\phi_i\}$ and their complex conjugates $\{\phi_i^*\}$ are respectively

$$\frac{\delta E}{\delta \phi_i(\mathbf{x})} = n_i \int d\mathbf{x}' \phi_i^*(\mathbf{x}') h(\mathbf{x}', \mathbf{x}) + \frac{\delta E_{\text{int}}}{\delta \phi_i(\mathbf{x})} = \sum_k \lambda_{ki} \phi_k^*(\mathbf{x}) \tag{2.23}$$

and

$$\frac{\delta E}{\delta \phi_i^*(\mathbf{x})} = n_i \int d\mathbf{x}' h(\mathbf{x}, \mathbf{x}') \phi_i(\mathbf{x}') + \frac{\delta E_{\text{int}}}{\delta \phi_i^*(\mathbf{x})} = \sum_k \lambda_{ik} \phi_k(\mathbf{x}). \tag{2.24}$$

In principle one has to solve the system of equations consisting of Eqs (2.22), (2.23), and (2.24) combined with the additional constraints for the Lagrange multipliers. This system of equations is nonlinear, so it is a formidable task to solve it in a direct way. In practice the minimum of the functional (2.20) can be found using a conjugate gradient scheme where the gradient is evaluated using (2.22), (2.23), and (2.24) at each iteration. But in this case particular attention should be paid to the fact that this scheme does not guarantee that the global minimum is reached.

Piris and Ugalde proposed an alternative method for the optimization with respect to the natural orbitals [89]. The optimal natural orbitals are obtained through an iterative diagonalization of an Hermitian matrix derived from the Lagrange multipliers λ_{ij} of Eqs (2.23) and (2.24).

2.5 Spin treatment

In the previous section we considered a combined space-spin variable $\mathbf{x} \equiv (\mathbf{r}, s)$. The natural spin orbitals can be written explicitly as two component spinors

$$\phi_i(\mathbf{x}) = a_{i\uparrow}\varphi_{i\uparrow}(\mathbf{r})\chi_\uparrow + a_{i\downarrow}\varphi_{i\downarrow}(\mathbf{r})\chi_\downarrow$$

where $\chi_\uparrow = \binom{1}{0}$ and $\chi_\downarrow = \binom{0}{1}$, and $|a_{j\uparrow}|^2 + |a_{j\downarrow}|^2 = 1$ to guarantee the normalization. The 1-RDM assumes the form of a 2×2 matrix

$$\gamma(\mathbf{x}, \mathbf{x}') = \begin{pmatrix} \gamma_{\uparrow\uparrow}(\mathbf{r}, \mathbf{r}') & \gamma_{\uparrow\downarrow}(\mathbf{r}, \mathbf{r}') \\ \gamma_{\downarrow\uparrow}(\mathbf{r}, \mathbf{r}') & \gamma_{\downarrow\downarrow}(\mathbf{r}, \mathbf{r}') \end{pmatrix}$$

and the spectral representation is given by

$$\gamma_{\sigma\sigma'}(\mathbf{r}, \mathbf{r}') = \sum_i n_i a^*_{i\sigma'} a_{i\sigma} \varphi^*_{i\sigma'}(\mathbf{r}')\varphi_{i\sigma}(\mathbf{r}).$$

However in many physical circumstances the treatment can be significantly simplified. If the Hamiltonian does not mix the two spin channels, as would be the case for the spin-orbit coupling or inhomogeneous external magnetic fields, and we do not have to deal with spontaneous symmetry breaking, the two spin channels decouple. In the case of homogeneous magnetic fields we can work with spin-dependent occupation numbers and natural orbitals, *i.e.*, we have two sets of occupation numbers and natural orbitals, one for each spin channel. As an intermediate approximate step we could consider spin-dependent occupation numbers but spin independent natural orbitals, this if often referred to as restricted open-shell treatment. For closed-shell systems both spin channels are completely equivalent so a restricted spin treatment is possible, in which both occupation numbers and natural orbitals are independent of the spin of the electron.

2.6 Approximations for $E_{\mathbf{xc}}[\gamma]$

As discussed in the previous sections the functional dependence of the Hartree and the exchange energies is known exactly in terms of the 1-RDM (see Eqs (2.17) and (2.18)). In terms of occupation numbers and natural orbitals the Hartree-Fock energy reads as

$$\begin{aligned} E_{\mathrm{HF}}[\{n_i\}, \{\phi_i\}] = \frac{1}{2}\sum_{jk} n_j n_k \int d\mathbf{x} d\mathbf{x}' \phi^*_j(\mathbf{x})\phi^*_k(\mathbf{x}')v_c(\mathbf{r}, \mathbf{r}')\phi_j(\mathbf{x})\phi_k(\mathbf{x}') \\ - \frac{1}{2}\sum_{jk} n_j n_k \int d\mathbf{x} d\mathbf{x}' \phi^*_j(\mathbf{x})\phi^*_k(\mathbf{x}')v_c(\mathbf{r}, \mathbf{r}')\phi_k(\mathbf{x})\phi_j(\mathbf{x}'). \end{aligned}$$

The correlation energy functional $E_c[\gamma]$, instead, is not known and thus needs to be approximated. It is important to note that, although the exact E_c is not known,

some exact constraints that it should satisfy are known [19]. This knowledge can be used to construct physically meaningful approximations. Most of the approximations combine exchange and correlation parts in simple expressions of the form

$$E_{\rm xc}[\{n_i\},\{\phi_i\}] = -\frac{1}{2}\sum_{jk} f(n_j,n_k)\int d\mathbf{x}d\mathbf{x}'\phi_j^*(\mathbf{x})\phi_k^*(\mathbf{x}')v_c(\mathbf{r},\mathbf{r}')\phi_k(\mathbf{x})\phi_j(\mathbf{x}'), \quad (2.25)$$

i.e., they have the form of the exchange energy modified by the function $f(n_j,n_k)$. This kind of functionals are usually referred to as of J-K type, as they only involve direct Coulomb (J) and exchange (K) integrals over the natural orbitals. In the following we discuss in more detail the J-K type functionals which will be used in the next chapters of the thesis.

2.6.1 Müller functional

Many of the approximations proposed in literature can be traced back to the work of Müller [78]. He proposed the following factorization for the 2-RDM

$$\begin{aligned}\Gamma^{(2)}(\mathbf{x}_1,\mathbf{x}_2;\mathbf{x}_1',\mathbf{x}_2') = \gamma(\mathbf{x}_1,\mathbf{x}_1')\gamma(\mathbf{x}_2,\mathbf{x}_2') \\ - \sum_{ij} n_i^{\frac{1}{2}+p} n_j^{\frac{1}{2}-p}\phi_i(\mathbf{x}_1)\phi_i^*(\mathbf{x}_2')\phi_j(\mathbf{x}_2)\phi_j^*(\mathbf{x}_1'),\end{aligned} \quad (2.26)$$

with $-1/2 \leq p \leq 1/2$. As shown by Müller, with the form (2.26), the probability of finding an electron at $\mathbf{r}$ when a second one is at $\mathbf{r}'$ becomes negative in the neighborhood of $\mathbf{r}'$. This unphysical negative probability is minimal for $p = 0$. In this case, the Müller approximation reduces to

$$\Gamma^{(2)}(\mathbf{x}_1,\mathbf{x}_2;\mathbf{x}_1',\mathbf{x}_2') = \gamma(\mathbf{x}_1,\mathbf{x}_1')\gamma(\mathbf{x}_2,\mathbf{x}_2') - \gamma^{\frac{1}{2}}(\mathbf{x}_2,\mathbf{x}_1')\gamma^{\frac{1}{2}}(\mathbf{x}_1,\mathbf{x}_2'),$$

where $\gamma^{1/2}$ can be defined using the spectral representation of the 1-RDM

$$\gamma^{\frac{1}{2}}(\mathbf{x}_1,\mathbf{x}_2) = \sum_i n_i^{\frac{1}{2}}\phi_i(\mathbf{x}_1)\phi_i^*(\mathbf{x}_2).$$

This factorization for the 2-RDM results in an exchange-correlation energy of the form (2.25) with

$$f^{\rm Müller}(n_j,n_k) = \sqrt{n_j n_k}. \quad (2.27)$$

Interestingly Buijse and Baerends arrived at the same functional following a different approach [14]. The Müller functional severely overestimates the correlation energy of all the systems it has been applied to [18, 23, 62]. It provides a lower bound to the total energy as was shown by Frank *et al.* [33].

2.6.2 Goedecker-Umrigar functional

The Müller functional only partially cancels the interaction of the electron with itself in the Hartree energy, due to the square root and the fractional nature of occupation numbers. Goedecker and Umrigar [45] proposed a correction to the Müller functional by explicitly removing all terms with $j = k$, resulting in the formula

$$f^{\mathrm{GU}}(n_j, n_k) = \sqrt{n_j n_k} - \delta_{jk}(n_j - n_j^2).$$

This functional is orbital self-interaction free, *i.e.*, the interaction of an orbital with itself is excluded. However due to the fractional nature of occupation numbers a particular electron can be distributed over several orbitals, thus it is not possible to completely exclude self interaction. However in many practical cases occupation numbers are often close to either zero or one, and, therefore, the orbital self interaction is close to the total self interaction.

For atoms and molecules at equilibrium geometry the GU functional gives much better correlation energies than the Müller functional. But it fails to reproduce the correct dissociation limit of small molecules [103]. When applied to the homogeneous electron gas (HEG), the GU functional, as the Müller functional, leads to rather inaccurate correlation energies [62]; moreover they fail to reproduce the fundamental gap for band as well as Mott insulators [98].

2.6.3 Corrected Hartree-Fock functional

Csányi and Arias [23] derived a functional starting from a tensor product expansion of the 2-RDM. They called their approximation Corrected Hartree-Fock (CHF). It reads as

$$f^{\mathrm{CHF}}(n_j, n_k) = n_j n_k + \sqrt{n_j(1 - n_j)}\sqrt{n_k(1 - n_k)}.$$

When applied to the HEG [23], the CHF functional coincides with the Müller functional in the low density limit. When density increases, however, the CHF severely overestimates correlation and the solution tends quickly to the HF solution. The same is also observed for other systems. For example, for H_2 at equilibrium CHF gives the HF solution [20].

2.6.4 Power functional

Recently Sharma *et al.* [98] proposed a generalization of the Müller functional (2.27) which reads as

$$f^{\mathrm{Power}}(n_j, n_k) = n_j^{\alpha} n_k^{\alpha},$$

with $1/2 \leq \alpha \leq 1$. This simple form interpolates between the uncorrelated HF limit ($\alpha = 1$) and the overcorrelated Müller ($\alpha = 1/2$), thus α can be considered as a mixing parameter. This functional has been tested both on finite and extended

systems [62, 63, 98, 99]. This functional was shown to perform very well in predicting ground-state properties and photoemission spectra for solids. In particular band gaps for semiconductors and insulators, including transition metal oxides, are in good agreement with experiments [98, 99]. A few optimal values of α have been proposed in literature: $\alpha = 0.525$ for stretched H_2, $\alpha = 0.578$ for molecules at equilibrium, $\alpha = 0.55$ for the HEG, $0.65 \leq \alpha \leq 0.7$ for solids [63, 98]. The optimal value for α thus depends on the kind of system considered.

Chapter 3

Many-Body Perturbation Theory

In this chapter we introduce the basic concepts of Many-Body Perturbation Theory based on Green's functions [1, 32, 46, 51]. In particular we focus on the one-body Green's function and its link to observables, such as the electron density, the one-body reduced density matrix, and the photoelectron spectrum. We discuss the Dyson equation to determine the one-body Green's function in terms of an effective potential, the so-called self-energy, which contains the many-body effects of the system. Various approximations to the self-energy are reported, namely GW, Hartree-Fock, second Born and T matrix.

3.1 Green's functions

At zero temperature the time-ordered equilibrium n-body Green's function (n-GF) is defined as

$$G^{(n)}(1,2,...,n;1',2',...,n') \equiv (-\mathrm{i})^n \frac{\langle\Psi_0|\, T[\hat{\psi}_H(1)...\hat{\psi}_H(n)\hat{\psi}_H^\dagger(n')...\hat{\psi}_H^\dagger(1')]\,|\Psi_0\rangle}{\langle\Psi_0|\Psi_0\rangle}, \quad (3.1)$$

where $1,2,...,n$ stand for combined space-spin-time coordinates, *i.e.*, $1 \equiv (\mathbf{r}_1, s_1, t_1)$, etc.; $|\Psi_0\rangle$ is the ground state of the system in the Heisenberg picture, $\hat{\psi}_H$ and $\hat{\psi}_H^\dagger$ are the field operators in the Heisenberg picture

$$\hat{\psi}_H(1) = e^{\mathrm{i}\hat{H}t_1}\hat{\psi}(\mathbf{x}_1)e^{-\mathrm{i}\hat{H}t_1}, \quad (3.2)$$

where $\hat{\psi}(\mathbf{x}_1)$ is the field operator in the Schrödinger picture. T is the Wick time ordering operator, which, when applied to a product of operators, arranges them in a chronological order of their time arguments with a multiplicative factor ± 1 depending on whether the chronological order is an even or odd permutation of the original order. In the following, to simplify the notation, we will assume that $|\Psi_0\rangle$ is normalized, *i.e.*, $\langle\Psi_0|\Psi_0\rangle = 1$.

The one-body Green's function (1-GF), according to Eq. (3.1), is defined as

$$G(1,1') = -\mathrm{i}\,\langle\Psi_0|\, T[\hat{\psi}_H(1)\hat{\psi}_H^\dagger(1')]\,|\Psi_0\rangle\,. \quad (3.3)$$

The time-ordered product can be written explicitly as

$$T[\hat{\psi}_H(1)\hat{\psi}_H^\dagger(1')] = \begin{cases} \hat{\psi}_H(1)\hat{\psi}_H^\dagger(1') & \text{for } t_1 > t_{1'} \\ -\hat{\psi}_H^\dagger(1')\hat{\psi}_H(1) & \text{for } t_{1'} > t_1, \end{cases}$$

from which

$$\begin{aligned} G(1,1') = &- \mathrm{i}\theta(t_1 - t_{1'}) \langle\Psi_0| \hat{\psi}_H(1)\hat{\psi}_H^\dagger(1') |\Psi_0\rangle \\ &+ \mathrm{i}\theta(t_{1'} - t_1) \langle\Psi_0| \hat{\psi}_H^\dagger(1')\hat{\psi}_H(1) |\Psi_0\rangle , \end{aligned} \tag{3.4}$$

where $\theta(t)$ is the Heaviside step function. Equation (3.4) suggests a simple interpretation of the 1-GF: it expresses the probability amplitude for an electron (hole) which at time t_1' (t_1) is added to the N-electron system (in its ground-state) at position $\mathbf{r}_1'$ ($\mathbf{r}_1$) with spin s_1' (s_1) to be found at position $\mathbf{r}_1$ ($\mathbf{r}_1'$) with spin s_1 (s_1') at time $t_1 > t_1'$ ($t_1' > t_1$).

Even if the 1-GF does not contain all the information of the ground-state wavefunction, we can still obtain from it all the observable properties of greatest interest, namely the ground-state expectation value of any one-particle operator, the ground-state total energy, and the one-particle excitation spectrum of the system. Let us discuss these properties in more detail.

Given a one-particle operator $\hat{O}$ in second quantization form

$$\hat{O} = \int d\mathbf{x}\hat{\psi}^\dagger(\mathbf{x})o(\mathbf{x})\hat{\psi}(\mathbf{x}),$$

where $o(\mathbf{x}_1)$ is the single particle operator in first quantization form,[1] the ground-state expectation value can be evaluated as

$$\begin{aligned} \langle\Psi_0| \hat{O} |\Psi_0\rangle &= \int d\mathbf{x} o(\mathbf{x}) \langle\Psi_0| \hat{\psi}^\dagger(\mathbf{x})\hat{\psi}(\mathbf{x}) |\Psi_0\rangle \\ &= \lim_{\mathbf{x}'\to\mathbf{x}} \int d\mathbf{x} o(\mathbf{x}) \langle\Psi_0| \hat{\psi}^\dagger(\mathbf{x}')\hat{\psi}(\mathbf{x}) |\Psi_0\rangle \\ &= -\mathrm{i} \lim_{\mathbf{x}'\to\mathbf{x}} \lim_{t'\to t^+} \int d\mathbf{x} o(\mathbf{x}) G(\mathbf{x}t;\mathbf{x}'t'), \end{aligned}$$

where t^+ stands for $t+\delta$, with δ an infinitesimal positive real number. Note that in the last step we used the definitions (3.2) and (3.4). Thus the 1-GF allows us to calculate the ground-state expectation value of any one-particle operator. For example, the electron density of the system is the diagonal in space, spin and time of the 1-GF, $n(\mathbf{x}) = -\mathrm{i}G(\mathbf{x}t;\mathbf{x}t^+)$, whereas the one-body reduced density matrix (1-RDM) is the diagonal in time of the 1-GF $\gamma(\mathbf{x},\mathbf{x}') = -\mathrm{i}G(\mathbf{x}t,\mathbf{x}'t^+)$.

The 1-GF can also be used to calculate the total energy, which in principle contains a two-body operator. The Galitskii-Migdal formula [36] gives the total ground-state

[1] For simplicity we consider here a local operator.

energy in terms of the 1-GF, and it reads as

$$E_0 = -\frac{\mathrm{i}}{2}\int d\mathbf{x}\lim_{t'\to t^+}\lim_{\mathbf{x}'\to\mathbf{x}}\left[\mathrm{i}\frac{\partial}{\partial t}+h(\mathbf{r})\right]G(\mathbf{x}t,\mathbf{x}'t'), \tag{3.5}$$

where $h(\mathbf{r}) = -\nabla^2_{\mathbf{r}}/2+v_{\mathrm{ext}}(\mathbf{r})$ is the one-particle Hamiltonian, with v_{ext} a local external potential.

The relation of the 1-GF with the one-particle excitation spectrum will be discussed in the next subsection, where the Lehmann representation of the 1-GF will be introduced.

3.1.1 Lehmann representation

In the following we will write the 1-GF in such a way to make clear its connection with the excitation energies of the system.

In absence of a time-dependent external potential, due to the homogeneity of time, the 1-GF depends only on the time difference $\tau = t_1 - t_1'$. Introducing, in Eq. (3.4), the resolution of the identity $\sum_k\sum_M \left|\Psi_k^M\right\rangle\left\langle\Psi_k^M\right| = \hat{1}$ in the Fock space, where $\left|\Psi_k^M\right\rangle$ indicates the k-th eigenstate of the M-electron system, we obtain

$$\begin{aligned}G(\mathbf{x},\mathbf{x}';\tau) = &-\mathrm{i}\theta(\tau)\sum_m \left\langle\Psi_0\right|\hat{\psi}_H(\mathbf{x}t)\left|\Psi_m^{N+1}\right\rangle\left\langle\Psi_m^{N+1}\right|\hat{\psi}_H^\dagger(\mathbf{x}'t')\left|\Psi_0\right\rangle\\ &+\mathrm{i}\theta(-\tau)\sum_n \left\langle\Psi_0\right|\hat{\psi}_H^\dagger(\mathbf{x}'t')\left|\Psi_n^{N-1}\right\rangle\left\langle\Psi_n^{N-1}\right|\hat{\psi}_H(\mathbf{x}t)\left|\Psi_0\right\rangle,\end{aligned} \tag{3.6}$$

where we have used the fact that field operators select only states with $N+1$ particles if $\tau > 0$ or with $N-1$ particles if $\tau < 0$. We can explicitly indicate the time dependence of the field operators in Eq. (3.6) using Eq. (3.2) and obtain the following expression for the 1-GF

$$\begin{aligned}G(\mathbf{x},\mathbf{x}';\tau) = &-\mathrm{i}\theta(\tau)\sum_m \left\langle\Psi_0\right|\hat{\psi}(\mathbf{x})\left|\Psi_m^{N+1}\right\rangle\left\langle\Psi_m^{N+1}\right|\hat{\psi}^\dagger(\mathbf{x}')\left|\Psi_0\right\rangle e^{\mathrm{i}(E_0^N-E_m^{N+1})\tau}\\ &+\mathrm{i}\theta(-\tau)\sum_n \left\langle\Psi_0\right|\hat{\psi}^\dagger(\mathbf{x}')\left|\Psi_n^{N-1}\right\rangle\left\langle\Psi_n^{N-1}\right|\hat{\psi}(\mathbf{x})\left|\Psi_0\right\rangle e^{-\mathrm{i}(E_0^N-E_n^{N-1})\tau}.\end{aligned} \tag{3.7}$$

The terms

$$f_m(\mathbf{x}) = \left\langle\Psi_0\right|\hat{\psi}(\mathbf{x})\left|\Psi_m^{N+1}\right\rangle,$$

and

$$g_n(\mathbf{x}) = \left\langle\Psi_n^{N-1}\right|\hat{\psi}(\mathbf{x})\left|\Psi_0\right\rangle$$

are generally referred to as the Feynman-Dyson amplitudes. Thus Eq. (3.7) assumes the more compact form

$$\begin{aligned}G(\mathbf{x},\mathbf{x}';\tau) = &-\mathrm{i}\theta(\tau)\sum_m f_m(\mathbf{x})f_m^*(\mathbf{x}')e^{\mathrm{i}(E_0^N-E_m^{N+1})\tau}\\ &+\mathrm{i}\theta(-\tau)\sum_n g_n(\mathbf{x})g_n^*(\mathbf{x}')e^{-\mathrm{i}(E_0^N-E_n^{N-1})\tau}.\end{aligned} \tag{3.8}$$

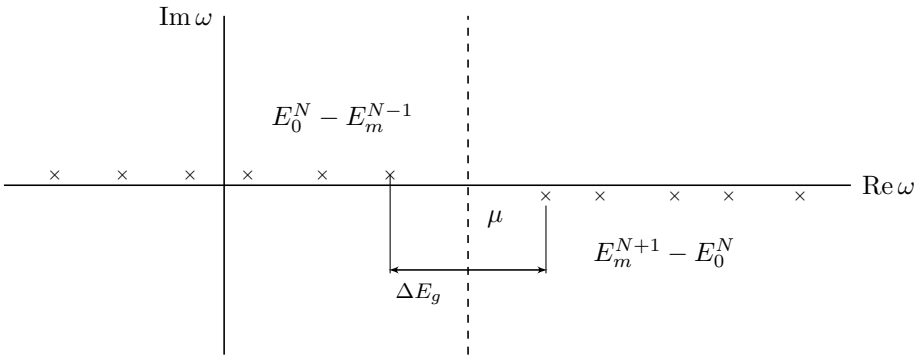

Figure 3.1: Singularities of $G(\mathbf{x}, \mathbf{x}'; \omega)$ in the complex plane. The removal energies $E_0^N - E_m^{N-1}$ are located above the real axis, whereas the addition energies $E_m^{N+1} - E_0^N$ are located below. The chemical potential μ lies inside the band gap ΔE_g.

Note that the amplitudes f_m as well as g_n are, in general, not orthogonal nor linearly independent. One can only prove that the total set is complete:

$$\sum_m f_m(\mathbf{x}) f_m^*(\mathbf{x}') + \sum_n g_n(\mathbf{x}) g_n^*(\mathbf{x}') = \delta(\mathbf{x} - \mathbf{x}'). \tag{3.9}$$

Using the following relation

$$\int_{-\infty}^{\infty} dt \left[\theta(\pm t) e^{-\mathrm{i}\alpha t}\right] e^{\mathrm{i}\omega t} = \lim_{\eta \to 0^+} \frac{\pm \mathrm{i}}{\omega - \alpha \pm \mathrm{i}\eta},$$

we can obtain the Fourier transform of Eq. (3.8). We arrive at the Lehmann representation in frequency space for the 1-GF

$$G(\mathbf{x}, \mathbf{x}'; \omega) = \lim_{\eta \to 0^+} \left[\sum_m \frac{f_m(\mathbf{x}) f_m^*(\mathbf{x}')}{\omega - (E_m^{N+1} - E_0^N) + \mathrm{i}\eta} + \sum_n \frac{g_n(\mathbf{x}) g_n^*(\mathbf{x}')}{\omega - (E_0^N - E_n^{N-1}) - \mathrm{i}\eta} \right]. \tag{3.10}$$

From Eq. (3.10) it becomes clear that the 1-GF has poles at the electron addition $(E_m^{N+1} - E_0^N)$ and removal $(E_0^N - E_n^{N-1})$ energies of the system.

In Fig. 3.1 it is depicted the polar structure of the 1-GF. The smallest electron removal energy gives the ionization potential IP $= -(E_0^N - E_0^{N-1})$, while the electron affinity is defined as EA $= E_0^N - E_0^{N+1}$. If the system under study is a metal, then IP=EA is the chemical potential μ. If, instead, the system is insulating, then one can define the band gap ΔE_g as

$$\Delta E_g = \mathrm{IP} - \mathrm{EA} = E_0^{N+1} + E_0^{N-1} - 2E_0^N.$$

In this case, the chemical potential μ lies somewhere inside the band gap.

3.1.2 1-GF in a basis set

Let $\{\phi_i(\mathbf{x})\}$ be a complete set of orthonormal orbitals in the one-particle Hilbert space, then we can express the field operators in this basis as

$$\hat{\psi}(\mathbf{x}) = \sum_i \phi_i(\mathbf{x})\hat{c}_i,$$

$$\hat{\psi}^\dagger(\mathbf{x}) = \sum_i \phi_i^*(\mathbf{x})\hat{c}_i^\dagger.$$

The operators $\hat{c}_i$ and $\hat{c}^\dagger$ are known as the creation and annihilation operators respectively.

We can then write the 1-GF as

$$G(\mathbf{x},\mathbf{x}';\omega) = \sum_{ij} G_{ij}(\omega)\phi_i(\mathbf{x})\phi_j^*(\mathbf{x}'),$$

with

$$\begin{aligned} G_{ij}(\omega) &= \int d\mathbf{x}d\mathbf{x}'\phi_i^*(\mathbf{x})G(\mathbf{x},\mathbf{x}';\omega)\phi_j(\mathbf{x}') \\ &= \sum_m \frac{\langle\Psi_0|\,\hat{c}_i\,|\Psi_m^{N+1}\rangle\langle\Psi_m^{N+1}|\,\hat{c}_j^\dagger\,|\Psi_0\rangle}{\omega-(E_m^{N+1}-E_0^N)+\mathrm{i}\eta} + \sum_n \frac{\langle\Psi_0|\,\hat{c}_j^\dagger\,|\Psi_n^{N-1}\rangle\langle\Psi_n^{N-1}|\,\hat{c}_i\,|\Psi_0\rangle}{\omega-(E_0^N-E_n^{N-1})-\mathrm{i}\eta}. \end{aligned}$$

In this way the space-spin variables are discretized. Note that if we deal with a non-interacting system, for which the Hamiltonian reads as $\hat{H} = \sum_i[-\nabla_{\mathbf{r}_i}^2/2 + v_{\mathrm{ext}}(\mathbf{r}_i)]$ then the 1-GF can be written as

$$G(\mathbf{x},\mathbf{x}';\omega) = \sum_i \frac{\phi_i(\mathbf{x})\phi_i^*(\mathbf{x}')}{\omega-\epsilon_i^0+\mathrm{sign}(\epsilon_i^0-\mu)\mathrm{i}\eta} \tag{3.11}$$

where ϕ_i and ϵ_i^0 are the independent-particle wavefunctions and the corresponding energies, respectively.

3.1.3 Spectral function and connection with experiments

It is convenient to define the spectral function in terms of the imaginary part of the 1-GF according to

$$A(\mathbf{x},\mathbf{x}';\omega) = \frac{1}{\pi}\mathrm{sign}(\mu-\omega)\,\mathrm{Im}\,G(\mathbf{x},\mathbf{x}';\omega). \tag{3.12}$$

Using the Lehmann representation for the 1-GF (Eq. (3.10)), the spectral function reads as

$$A(\mathbf{x},\mathbf{x}';\omega) = \sum_m f_m(\mathbf{x})f_m^*(\mathbf{x}')\delta(\omega-(E_m^{N+1}-E_0^N)) + \sum_n g_n(\mathbf{x})g_n^*(\mathbf{x}')\delta(\omega-(E_0^N-E_n^{N-1})). \tag{3.13}$$

The full 1-GF can be obtained back from the spectral function using the relation

$$G(\mathbf{x},\mathbf{x}';\omega) = \int_{-\infty}^{\mu} d\omega' \frac{A(\mathbf{x},\mathbf{x}';\omega')}{\omega - \omega' - \mathrm{i}\eta} + \int_{\mu}^{\infty} d\omega' \frac{A(\mathbf{x},\mathbf{x}';\omega')}{\omega - \omega' + \mathrm{i}\eta}.$$

This means that the spectral function contains the same information as the 1-GF, but it has the main advantage of being a positive real-valued function, while the 1-GF is in general a complex function.

The spectral function satisfies the following normalization condition

$$\int_{-\infty}^{\infty} d\omega A(\mathbf{x},\mathbf{x}';\omega) = \delta(\mathbf{x}-\mathbf{x}'), \tag{3.14}$$

which can be obtained by integrating Eq. (3.13) with respect to ω and using the completeness relation (3.9). Several observables have a simple link to the spectral function. For example the ground state electron density $\rho(\mathbf{r})$ can be calculated as

$$\rho(\mathbf{r}) = \int_{-\infty}^{\mu} d\omega A(\mathbf{r},\mathbf{r};\omega),$$

while an expression for the ground-state energy in terms of the spectral function can be derived from the Galitskii-Migdal formula (3.5) and reads as

$$E_0 = \frac{1}{2}\sum_{ij}\int_{-\infty}^{\mu} d\omega \left[\omega\delta_{ij} + h_{ij}\right] A_{ji}(\omega), \tag{3.15}$$

where we introduced a complete set of orthonormal one-electron wavefunctions $\{\phi_i\}$, and defined the matrix elements of the spectral function and the one-particle Hamiltonian as

$$A_{ij}(\omega) = \int d\mathbf{x}d\mathbf{x}'\phi_i^*(\mathbf{x})A(\mathbf{x},\mathbf{x}';\omega)\phi_j(\mathbf{x}'), \tag{3.16}$$

and

$$h_{ij} = \int d\mathbf{x}\phi_i^*(\mathbf{x})h(\mathbf{x})\phi_j(\mathbf{x}),$$

respectively. Using Eq. (3.16) together with (3.14) we obtain the sum rule

$$\int_{-\infty}^{\infty} A_{ij}(\omega) = 1.$$

Moreover, one can obtain from the spectral function the distribution of one-electron states as

$$n_i = \langle\Psi_0|\, c_i^\dagger c_i \,|\Psi_0\rangle = \int_{-\infty}^{\mu} d\omega A_{ii}(\omega).$$

If for example we choose the states i to be the momentum eigenstates, we obtain the momentum distribution, a key quantity in, *e.g.*, Compton scattering [56, 81].

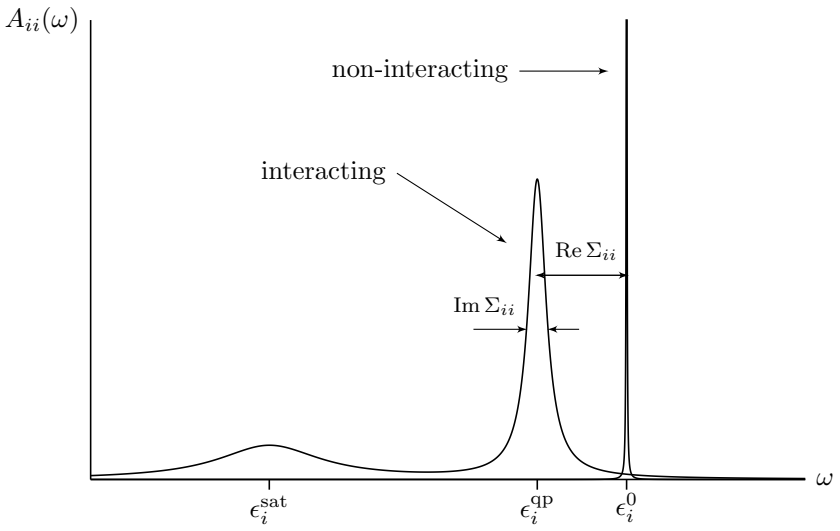

Figure 3.2: Example of spectral function. In a non-interacting system, excitations are a series of delta peaks (ϵ_i^0). When interactions among electrons are taken into account, each peak is shifted, and, since the lifetime of the excitation is finite, it is broadened. This is the quasiparticle peak (ϵ_i^{qp}). In addition to the main quasiparticle peak, new features, called satellites ($\epsilon_i^{\mathrm{sat}}$), can appear.

Finally the spectral function gives information about the photoelectron spectrum of a system, as one can see comparing Eq. (3.13) with Eq. (1.2). Using Eq. (3.11), the spectral function for a non-interacting system takes the simple form

$$A(\mathbf{x}, \mathbf{x}'; \omega) = \sum_i \phi_i(\mathbf{x})\phi_i^*(\mathbf{x})\delta(\omega - \epsilon_i^0).$$

Thus for a non-interacting system the matrix elements $A_{ij}(\omega)$ defined in (3.16) have a simple δ-peak located at the non-interacting energy ϵ_i^0.

In case of an interacting system the single-particle energies ϵ_i^0 are corrected by an effective complex-valued non-local and frequency-dependent potential Σ (see next section) which takes into account the many body effects of the system. If for simplicity we neglect the non-diagonal part of G and Σ, we have

$$G_{ii}(\omega) = \frac{1}{\omega - \epsilon_i^0 - \Sigma_{ii}(\omega)}.$$

The spectral function then takes the following form

$$A_{ii}(\omega) = \frac{1}{\pi} \frac{|\,\mathrm{Im}\,\Sigma_{ii}(\omega)|}{[\omega - \epsilon_i^0 - \mathrm{Re}\,\Sigma_{ii}(\omega)]^2 + [\mathrm{Im}\,\Sigma_{ii}(\omega)]^2}.$$

As shown in Fig. 3.2, $A_{ii}(\omega)$ has a main peak, called the quasiparticle (qp) peak, at $\epsilon_i^{\mathrm{qp}} = \epsilon_i^0 + \mathrm{Re}\,\Sigma_{ii}(\epsilon_i^{\mathrm{qp}})$. The width of this peak is $\mathrm{Im}\,\Sigma_{ii}(\epsilon_i^{\mathrm{qp}})$ and is related to the inverse

lifetime of the excitation i. As a consequence of the frequency dependence of the self-energy, an interacting system may have extra peaks that are not directly related to one-particle excitations, *i.e.*, they are not quasiparticles. These extra features of the spectral function are called satellites.

3.2 How to determine G?

The definition (3.3) is not very useful for determining the 1-GF, since it assumes that the ground-state $|\Psi_0\rangle$ is known, which, in general is not the case. A practical route to get the 1-GF is by its propagation in time.

3.2.1 Equations of motion

The equation of motion for the 1-GF can be obtained by differentiating the definition (3.4) with respect to t_1 (for more details on the derivation, see, e.g., Refs [22, 57, 104]). One can use the equation of motion of the field operators in the Heisenberg picture

$$\mathrm{i}\frac{\partial\hat{\psi}_H(1)}{\partial t_1} = [\hat{\psi}_H(1), \hat{H}],$$

and similarly for $\hat{\psi}^\dagger_H$. Using the Hamiltonian operator $\hat{H}$ given in Eq. (2.2) we can evaluate the commutator. This yields the following expression

$$\begin{aligned}\mathrm{i}\frac{\partial G(1,1')}{\partial t_1} &= \delta(1-1') + h(1)G(1,1') \\ &\quad - \mathrm{i}\int d2v_c(1^+,2)\,\langle\Psi_0|\,T[\hat{\psi}^\dagger_H(2)\hat{\psi}_H(2)\hat{\psi}_H(1)\hat{\psi}^\dagger_H(1')]\,|\Psi_0\rangle\,, \qquad (3.17)\end{aligned}$$

where $v_c(1,2) = v_c(\mathbf{x}_1,\mathbf{x}_2)\delta(t_1-t_2)$ is the Coulomb potential. The expectation value of the time-ordered product in the last term on the right-hand side can be related to the 2-GF, if a positive infinitesimal time δ is added to t_2 in $\psi^\dagger_H(2)$ and the limit $\delta\to 0$ is inserted in the integral sign. Now that there are two different indices 2 and 2^+, the time ordering operator is defined unambiguously and we can permute the field operators in order to obtain the 2-GF,

$$\begin{aligned}\langle\Psi_0|\,T[\hat{\psi}^\dagger_H(2^+)\hat{\psi}_H(2)\hat{\psi}_H(1)\hat{\psi}^\dagger_H(1')]\,|\Psi_0\rangle &= -\,\langle\Psi_0|\,T[\hat{\psi}_H(1)\hat{\psi}_H(2)\hat{\psi}^\dagger_H(2^+)\hat{\psi}^\dagger_H(1')]\,|\Psi_0\rangle \\ &= G^{(2)}(1,2;1',2^+).\end{aligned}$$

Equation (3.17) then becomes

$$\left[\mathrm{i}\frac{\partial}{\partial t_1} - h(1)\right]G(1,1') + \mathrm{i}\int d2v_c(1^+,2)G^{(2)}(1,2;1',2^+) = \delta(1-1'). \qquad (3.18)$$

In a similar manner we can obtain the equation of motion for the n-GF, in terms of the $(n+1)$-GF and the $(n-1)$-GF [22, 57]. So we have an infinite set of coupled equations which is completely equivalent to the Schrödinger equation.

In practice one should truncate this hierarchy to close the system of equations at a given order n. It is therefore necessary to express the $(n+1)$-GF in terms of lower-order GFs. This can be very involved and, moreover, it is not obvious how to cut the hierarchy. This can be avoided by introducing an effective potential which has folded in it this hierarchy.

3.2.2 Dyson equation and self-energy

As a preliminary step, in order to rewrite Eq. (3.18) in a more convenient form for the following discussion, it is useful to define the non interacting 1-GF, $G_0(1,1')$, as the solution of

$$\left[\mathrm{i}\frac{\partial}{\partial t_1} - h(1)\right] G_0(1,1') = \delta(1-1'). \tag{3.19}$$

Using Eq. (3.19), the equation of motion of the 1-GF can be recast in the following integral form

$$G(1,1') = G_0(1,1') - \mathrm{i}\int d2d2' G_0(1,2') v_c(2'^+,2) G^{(2)}(2',2;1',2^+), \tag{3.20}$$

where G_0 determines the appropriate initial condition in time.[2] An equivalent form can be obtained multiplying both sides of Eq. (3.20) by $G^{-1}(1',2)G_0^{-1}(3,1)$,[3] integrating with respect to 1 and $1'$ and changing the name of the variables, it reads as

$$G_0^{-1}(1,1') + \mathrm{i}\int d2d2' v_c(1^+,2) G^{(2)}(1,2;2',2^+) G^{-1}(2',1') = G^{-1}(1,1').$$

This last equation suggests the introduction of the self-energy Σ defined as

$$\Sigma(1,1') = -\mathrm{i}\int d2d2' v_c(1^+,2) G^{(2)}(1,2;2',2^+) G^{-1}(2',1'), \tag{3.21}$$

so that Eq. (3.20) can be rewritten as

$$G(1,1') = G_0(1,1') + \int d2d2' G_0(1,2)\Sigma(2,2')G(2',1'). \tag{3.22}$$

This is the well-known Dyson equation for the 1-GF; it is a closed equation if Σ is known. The self-energy plays the role of an effective potential in which the effects of the rest of the system are folded. That is why it is a complicated object: it is in

[2] The non-interacting 1-GF must satisfy the Kubo-Martin-Schwinger conditions, which means that there is only one solution G_0 to the equation $\int d2 G_0^{-1}(1,2)G_0(2,1') = \delta(1-1')$. For an extensive discussion see Ref. [57].

[3] The inverse of the 1-GF, G^{-1} is defined according to

$$\int d2 G(1,2)G^{-1}(2,1') = \int d2 G^{-1}(1,2)G(2,1') = \delta(1-1').$$

general a non-local frequency-dependent complex-valued function. The self-energy is not known in general and approximations are needed. The advantage of the Dyson equation is that, if one approximates Σ, even at low order in the interaction, solving the Dyson equation for the 1-GF produces contributions to all orders, as one can see by iterating Eq (3.22)

$$G(1,1') = G_0(1,1') + \int d2d2' G_0(1,2)\Sigma(2,2')G_0(2',1') + \int d2d2'd3d3' G_0(1,2)\Sigma(2,2')G_0(2',3)\Sigma(3,3')G(3',1') + ...$$

To make more explicit the physical content of Σ we can use the Schwinger relation[4] (see Refs [71, 97])

$$\frac{\delta G(1,1';[\varphi])}{\delta\varphi(2)} = -G^{(2)}(1,2;1',2^+;[\varphi]) + G(1,1';[\varphi])G(2,2^+;[\varphi]), \tag{3.24}$$

which relates the 2-GF to the 1-GF and its variation with respect to a fictitious external potential φ. Thus, we can express the self-energy given by Eq. (3.21) in terms of the

[4]A fictitious time-dependent external potential φ has to be introduced in order to evaluate the variational derivative of the quantities of interest with respect to this potential. At the end of the derivation this potential is made to vanish. In presence of an external potential, the Hamiltonian reads as $\hat{H} = \hat{H}_0 + \hat{H}'$, where $\hat{H}_0$ is the unperturbed Hamiltonian and $\hat{H}'$ contains the external potential. The generalization of definition (3.3) reads as

$$G(1,1';[\varphi]) = -\mathrm{i}\frac{\langle\Psi_0|\, T[\hat{S}(\infty,-\infty;[\varphi])\hat{\psi}_I(1)\hat{\psi}_I^\dagger(1')]\,|\Psi_0\rangle}{\langle\Psi_0|\,\hat{S}(\infty,-\infty;[\varphi])\,|\Psi_0\rangle}, \tag{3.23}$$

where we made explicit the functional dependence on the external potential φ. Here $\hat{\psi}_I$ and $\hat{\psi}_I^\dagger$ are the field operators in the interaction picture, and $\hat{S}(t,t_0)$ is the time evolution operator defined as

$$\hat{S}(t,t_0;[\varphi]) = T\left[\exp\left(-\mathrm{i}\int_{t_0}^{t} d\tau \hat{H}'_I(\tau;[\varphi])\right)\right],$$

with

$$\hat{H}'_I(\tau;[\varphi]) = \int d\mathbf{x}\varphi(\mathbf{x},\tau)\hat{\psi}_I^\dagger(\mathbf{x},\tau)\hat{\psi}_I(\mathbf{x},\tau).$$

By taking the functional derivative of (3.23) with respect to the external potential we can obtain the Schwinger relation (3.24). For the details of the derivation, see Ref. [22].

Note that the state vectors and operators in the interaction and Schrödinger pictures are respectively related by

$$|\Psi(t)\rangle_I = e^{\mathrm{i}\hat{H}_0 t}\,|\Psi(t)\rangle_S\,,$$

and

$$\hat{O}_I(t) = e^{\mathrm{i}\hat{H}_0 t}\hat{O}_S e^{-\mathrm{i}\hat{H}_0 t}.$$

In the interaction picture the operators satisfy the following equation of motion

$$\mathrm{i}\frac{d}{dt}\hat{O}_I(t) = \left[\hat{O}_I(t),\hat{H}_0\right] + \mathrm{i}\left[\frac{\partial\hat{O}(t)}{\partial t}\right]_I.$$

1-GF alone using relation (3.24). We arrive at

$$\Sigma(1,1') = v_H(1)\delta(1-1') + \mathrm{i}\int d2d2' v_c(1,2)\left.\frac{\delta G(1,2';[\varphi])}{\delta\varphi(2)}\right|_{\varphi=0} G^{-1}(2',1'), \tag{3.25}$$

where $v_H(1) = -\mathrm{i}\int d2 v_c(1,2)G(2,2^+)$ is the Hartree potential. The following relation[5]

$$\frac{\delta G(1,2';[\varphi])}{\delta\varphi(2)} = -\int d3d4 G(1,3;[\varphi])\,\frac{\delta G^{-1}(3,4;[\varphi])}{\delta\varphi(2)} G(4,2';[\varphi]) \tag{3.26}$$

can be used to rewrite the self-energy (3.25) in an alternative way which reads as

$$\Sigma(1,1') = v_H(1)\delta(1-1') - \mathrm{i}\int d2d3 v_c(1^+,2)G(1,3)\left.\frac{\delta G^{-1}(3,1';[\varphi])}{\delta\varphi(2)}\right|_{\varphi=0}. \tag{3.27}$$

The functional derivative $\delta G^{-1}/\delta\varphi$ in the last term on the right-hand side of Eq. (3.27) can be performed using G^{-1} obtained from the Dyson equation, which in presence of an external potential, reads as

$$G^{-1}(1,1';[\varphi]) = G_0^{-1}(1,1') - \varphi(1)\delta(1-1') - \Sigma(1,1';[\varphi]). \tag{3.28}$$

Using Eq. (3.28) we can rewrite Eq. (3.27) as

$$\begin{aligned}\Sigma(1,1') = {} & v_H(1)\delta(1-1') + \mathrm{i}v_c(1^+,1')G(1,1') \\ & + \mathrm{i}\int d2d3\; v_c(1^+,2)G(1,3)\left.\frac{\delta\Sigma(3,1';[\varphi])}{\delta\varphi(2)}\right|_{\varphi=0},\end{aligned}$$

and applying the chain rule $\delta\Sigma/\delta\varphi = (\delta\Sigma/\delta G)(\delta G/\delta\varphi)$ we finally arrive at

$$\begin{aligned}\Sigma(1,1') = {} & v_H(1)\delta(1-1') + \mathrm{i}v_c(1^+,1')G(1,1') \\ & + \mathrm{i}\int d2d3d4d5\, v_c(1^+,2)G(1,3)\Xi(3,5;1',4)L(4,2;5,2^+)\end{aligned} \tag{3.29}$$

where the effective interaction $\Xi(3,5;1',4) = \delta\Sigma(3,1')/\delta G(4,5)$ and the generalized response function $L(4,2;5,2') = \delta G(4,5)/\delta\varphi(2',2)$ have been introduced. This way of writing the self-energy immediately shows the physics behind it: the particle can scatter against the density of the system (Hartree term), it can exchange with another particle of the system (exchange term), and it can perturb the system, *i.e.*, it can have an effective interaction with the system (Ξ), the system responds (L), and the particle feels this response through the Coulomb interaction.

Approximations to Ξ and L give various approximations to Σ, as we will show in Sec. 3.2.4. Before discussing the approximations, we take a more conventional route to tackle the problem of finding a suitable approximation to Σ: the Hedin equations.

[5]This relation can be obtained considering the identity $\int d2 G(1,2;[\varphi])G^{-1}(2,1';[\varphi]) = \delta(1-1')$ and taking the functional derivative with respect to φ.

3.2.3 Hedin's equations and GW approximation

Hedin derived a set of coupled equations that in principle yields the exact self-energy [50]. The basic quantities entering these equations are the interacting 1-GF and the dynamically screened Coulomb interaction W. In a many-electron system, W is much weaker than the bare Coulomb interaction v_c, therefore its use in a perturbative development is well motivated. In the following we will omit the functional dependence on the fictitious external potential φ to simplify the notation. It is also assumed that at equilibrium all functional derivatives involving φ are evaluated at $\varphi = 0$.

First, we can introduce the local classical potential $V = v_H + \varphi$. We can regard Σ as a functional of V instead of φ, and making use of the chain rule we can rewrite Eq. (3.27) as

$$\Sigma(1,1') = v_H(1)\delta(1-1') - \mathrm{i}\int d2d3d4 v_c(1^+,2)G(1,3)\frac{\delta G^{-1}(3,1')}{\delta V(4)}\frac{\delta V(4)}{\delta\varphi(2)}.$$

We can introduce the time-ordered inverse dielectric matrix

$$\varepsilon^{-1}(1,2) = \frac{\delta V(1)}{\delta\varphi(2)},$$

from which we can define the dynamically-screened Coulomb potential

$$W(1,2) = \int d3\varepsilon^{-1}(1,3)v_c(3,2). \tag{3.30}$$

W is the potential at point 1 due to the presence of a test charge at point 2, including the effect of the polarization of the system. It represents the effective interaction between two electrons and it is much weaker than the bare Coulomb potential v_c if the polarization is large. We further introduce the scalar irreducible vertex function

$$\tilde{\Gamma}(1,1';2) = -\frac{\delta G^{-1}(1,1')}{\delta V(2)}. \tag{3.31}$$

Here the term irreducible refers to the fact that the derivative in Eq. (3.31) is performed with respect to the total potential V. The self-energy Σ can then be rewritten as

$$\begin{aligned}\Sigma(1,1') &= v_H(1)\delta(1-1') + \Sigma_{\mathrm{xc}}(1,1') \\ &= v_H(1)\delta(1-1') + \mathrm{i}\int d3d4 G(1,3)W(4,1^+)\tilde{\Gamma}(3,1';4),\end{aligned}$$

where we introduced the exchange-correlation part of the self-energy $\Sigma_{\mathrm{xc}} = \Sigma - v_H$.

To evaluate the irreducible vertex function $\tilde{\Gamma}$, we can start from the definition

(3.31) and using the Dyson equation $G^{-1} = G_0^{-1} - V - \Sigma_{\rm xc}$ we obtain

$$\begin{aligned}\tilde{\Gamma}(1,2;3) &= \delta(1-2)\delta(2-3) + \frac{\delta\Sigma_{\rm xc}(1,2)}{\delta V(3)} \\ &= \delta(1-2)\delta(2-3) + \int d4d5 \frac{\delta\Sigma_{\rm xc}(1,2)}{\delta G(4,5)} \frac{\delta G(4,5)}{\delta V(3)} \\ &= \delta(1-2)\delta(2-3) + \int d4d5d6d7 \frac{\delta\Sigma_{\rm xc}(1,2)}{\delta G(4,5)} G(4,6)G(7,5)\tilde{\Gamma}(6,7;3).\end{aligned} \tag{3.32}$$

The second line is obtained making use of the chain rule $\delta\Sigma_{\rm xc}/\delta V = (\delta\Sigma_{\rm xc}/\delta G)(\delta G/\delta V)$, whereas in the third line we used Eq. (3.26) with φ replaced by V. Equation (3.32) is a closed integral equation for the 3-point vertex function in terms of a 4-point kernel $\delta\Sigma_{\rm xc}/\delta G$.

We now need an equation for the inverse dielectric matrix $\varepsilon^{-1} = \delta V/\delta\varphi$ which enters in the definition of W. It can be worked out as follows

$$\begin{aligned}\varepsilon^{-1}(1,2) &= \delta(1-2) - \mathrm{i}\int d3 v_c(1,3)\frac{\delta G(3,3^+)}{\delta\varphi(2)} \\ &= \delta(1-2) + \int d3 v_c(1,3)\chi(3,2),\end{aligned} \tag{3.33}$$

where the reducible polarizability χ is defined as

$$\chi(1,2) = -\mathrm{i}\frac{\delta G(1,1^+)}{\delta\varphi(2)} = \frac{\delta\rho(1)}{\delta\varphi(2)},$$

and it gives the change in the electron density upon a change in the external field. Here the term reducible refers to the fact that the derivative is performed with respect to the external potential φ. In a similar way one can define an irreducible polarizability

$$\tilde{\chi}(1,2) = -\mathrm{i}\frac{\delta G(1,1^+)}{\delta V(2)} = \frac{\delta\rho(1)}{\delta V(2)}.$$

The relation which links the two polarizabilities can be obtained by using the chain rule

$$\begin{aligned}\chi(1,2) &= -\,\mathrm{i}\int d3 \frac{\delta G(1,1^+)}{\delta V(3)}\frac{\delta V(3)}{\delta\varphi(2)} \\ &= \tilde{\chi}(1,2) + \int d3d4 \tilde{\chi}(1,3)v_c(3,4)\chi(4,2).\end{aligned} \tag{3.34}$$

The irreducible polarizability can now be expressed in terms of the 1-GF and $\tilde{\Gamma}$ again using relation (3.26)

$$\begin{aligned}\tilde{\chi}(1,2) &= \mathrm{i}\int d3d4 G(1,3)\frac{\delta G^{-1}(3,4)}{\delta V(2)}G(4,1) \\ &= -\,\mathrm{i}\int d3d4 G(1,3)G(4,1)\tilde{\Gamma}(3,4;2).\end{aligned}$$

Σ_{GW} =

Figure 3.3: Feynman diagram representation of the GW self-energy. The bold straight line represents the interacting 1-GF, and the wiggly line the screened Coulomb potential W.

Summarizing the results obtained above, we have Hedin's set of coupled integral equations [50, 51]:

$$G(1,1') = G_0(1,1') + \int d2d2' G_0(1,2)\Sigma(2,2')G(2',1'), \tag{3.35}$$

$$\Sigma(1,2) = v_H(1)\delta(1-2) + \mathrm{i}\int d3d4 G(1,4)W(3,1^+)\tilde{\Gamma}(4,2;3), \tag{3.36}$$

$$\tilde{\Gamma}(1,2;3) = \delta(1-2)\delta(2-3) + \int d4d5d6d7 \frac{\delta\Sigma_{\mathrm{xc}}(1,2)}{\delta G(4,5)} G(4,6)G(7,5)\tilde{\Gamma}(6,7;3),$$

$$\tilde{\chi}(1,2) = -\mathrm{i}\int d3d4 G(1,3)G(4,1)\tilde{\Gamma}(3,4;2), \tag{3.37}$$

$$W(1,2) = v_c(1,2) + \int d3d4 v_c(1,3)\tilde{\chi}(3,4)W(4,2). \tag{3.38}$$

Equation (3.38) has been obtained working out the definition (3.30) together with Eqs (3.33) and (3.34). The irreducible vertex function $\tilde{\Gamma}$ and the dynamically-screened potential W satisfy Dyson-like equations, like the 1-GF. This set of equations should in principle be solved iteratively: starting with some hypothesis on Σ and G, one can evaluate $\tilde{\Gamma}$, then $\tilde{\chi}$, W and Σ. Now one can calculate a new G and start again the same procedure. In principle, repeating an infinite number of times this iteration, it gives us the exact solution.

In practice, however, one uses approximations. For example by setting $\tilde{\Gamma}(1,2;3) = \delta(1-2)\delta(2-3)$ one gets the so-called GW approximation, $\Sigma = v_H + \mathrm{i}GW$. One has then to solve self consistently only the set of Eqs (3.35)–(3.38). However also this can be quite involved, especially in solids. A commonly used approach is one-shot GW, in which one stops at the first iteration. The GW self-energy is depicted in Fig. 3.3 using Feynman diagrams.

3.2.4 T matrix, second Born and Hartree-Fock

The GW approximation can also be derived from Eq. (3.29). In situations where the screening is important we can use a good approximation to L and for Ξ the rough approximation $\Xi \approx \delta v_H/\delta G$. This leads to GW. Other approximations to Ξ and L yield other approximations to Σ [94]. In the following we briefly discuss the approximations which, besides GW, will be used in this thesis, namely, T matrix, second Born, and Hartree-Fock.

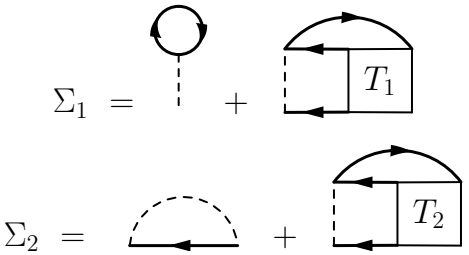

Figure 3.4: Feynman diagram representation of the particle-particle T-matrix self-energy. The bold straight line represent the interacting 1-GF, the dashed line the Coulomb potential v_c.

3.2.5 T-matrix approximation

In situation where the screening is not important, but it is rather the quantum nature of the electron to emerge, we can use the rough approximation $L \approx GG$, and concentrate on a clever approximation for Ξ. Using for the self-energy the ansatz

$$\Sigma(1,1') = \int d2d4G(4,2)T(1,2;1',4),$$

one can do the approximation

$$\frac{\delta\Sigma(3,1')}{\delta G(4,5)} \approx T(3,5;1',4)$$

in Eq. (3.29). In this way one can find the following Dyson equations for $T = T_1 + T_2$

$$\begin{aligned} T_1(1,2;1',4) = & -\mathrm{i}v_c(1,2)\delta(1-1')\delta(4-2) \\ & +\mathrm{i}\int d3d5v_c(1,2)G(1,3)G(2,5)T_1(3,5;1',4), \end{aligned}$$

$$\begin{aligned} T_2(1,2;1',4) = & \mathrm{i}v_c(1,2)\delta(2-1')\delta(4-1) \\ & +\mathrm{i}\int d3d5v_c(1,2)G(1,3)G(2,5)T_2(3,5;1',4). \end{aligned}$$

The four-point interaction $T = T_1 + T_2$ can now be identified with the particle-particle T matrix [36, 57]. In a similar way one can derive the electron-hole T matrix [94]. The Feynman diagram representation of the particle-particle T matrix is reported in Fig. 3.4.

Hartree-Fock approximation

The expansion to first order in the Coulomb potential of the T-matrix self-energy, gives the Hartree-Fock self-energy

$$\begin{aligned} \Sigma_{\mathrm{HF}}(1,1') &= -\mathrm{i}\delta(1-1')\int d2v_c(1,2)G(2,2^+) + \mathrm{i}v_c(1,1')G(1,1'^+) \\ &= v_H(1)\delta(1-1') + \mathrm{i}v_c(1,1')G(1,1'^+). \end{aligned} \tag{3.39}$$

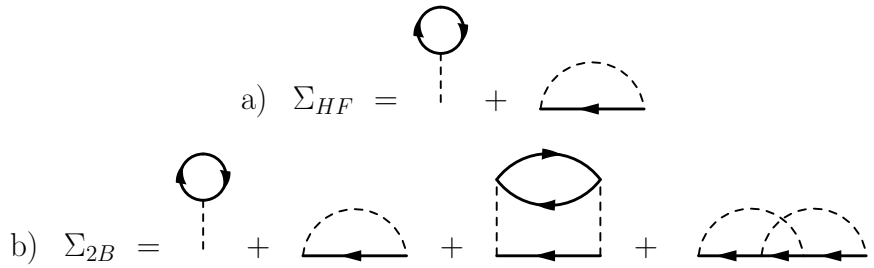

Figure 3.5: Feynman diagram representation of the a) Hartree-Fock and b) second Born self-energies. The bold straight lines represent the interacting 1-GF, the dashed lines the Coulomb potential v_c.

The first term is the Hartree potential, while the second is the Fock exchange self-energy

$$\Sigma_x(1,1') = \mathrm{i}v_c(1^+,1')G(1,1'),$$

where the sign "+" for times has been moved in a consistent way, since the Coulomb interaction is instantaneous. The δ function in time contained in v_c selects only contributions of the 1-GF from negative times, *i.e.*, from removal energies. Moreover the fact that v_c is instantaneous yields a self-energy which is static in frequency space. The Hartree-Fock self-energy is depicted in Fig. 3.5(a).

Second Born approximation

An expansion to second-order in v_c of the T matrix gives the second Born approximation

$$\Sigma_{2B}(1,1') = \Sigma_{\mathrm{HF}}(1,1') + \Sigma^{(2)}(1,1'),$$

where Σ_{HF} is the Hartree-Fock self-energy given by Eq. (3.39) and

$$\Sigma^{(2)}(1,1') = \Sigma^{(2a)}(1,1') + \Sigma^{(2b)}(1,1'),$$

is the sum of the two terms

$$\Sigma^{(2a)}(1,1') = -\mathrm{i}^2 G(1,1') \int d2d3 v_c(1,2)G(2,3)G(3,2)v_c(3,1'),$$

and

$$\Sigma^{(2b)}(1,1') = \mathrm{i}^2 \int d2d3 G(1,2)v_c(1,3)G(2,3)G(3,1')v_c(2,1').$$

These terms are usually referred to as the second-order direct and exchange terms. They are depicted in Fig. 3.5(b).

Chapter 4

Correlation and spectroscopy in Reduced Density-Matrix Functional Theory

In this chapter we explore the performance of approximations to electron correlation in Reduced Density-Matrix Functional Theory (RDMFT) and of approximations to the observables calculated within this theory. Our analysis focuses on the calculation of total energies, occupation numbers, removal/addition energies, and spectral functions. We use the exactly solvable Hubbard dimer at 1/4 and 1/2 fillings as test systems. This allows us to analyze the underlying physics and to elucidate the origin of the observed trends. For comparison, we also report the results of the GW approximation, where the self-energy functional is approximated, but no further hypothesis are made concerning the approximations of the observables. In particular, we focus on the atomic limit, where the two sites of the dimer are pulled apart and electrons localize on either site with equal probability, unless a small perturbation is present: this is the regime of strong electron correlation. In this limit, using the Hubbard dimer at 1/2 filling with or without a spin-symmetry-broken ground-state, allows us to explore how degeneracies and spin-symmetry breaking are treated in RDMFT. We find that, within the used approximations, neither in RDMFT nor in GW the signature of strong correlation is present, when looking at the removal/addition energies and spectral function from the spin-singlet ground-state, whereas both give the exact result for the spin-symmetry broken case. Moreover, we show how the spectroscopic properties change from one spin structure to the other.

4.1 Introduction

Within Reduced Density-Matrix Functional Theory (RDMFT), as we discussed in Chap. 2, the ground-state properties of a physical system are functionals of the ground-state one-body reduced density matrix (1-RDM) ; thanks to the one-to-one mapping

between the (non-degenerate) ground-state wavefunction of the system and the corresponding 1-RDM . In particular the ground-state total energy is a functional of the 1-RDM (γ) and energy minimization under the constraint that γ is ensemble N-representable determines the exact γ. In practice, however, approximations to the exchange-correlation energy $E_{\rm xc}[\gamma]$ are needed. Several approximations have been proposed and most of them are implicit functionals of the 1-RDM; they are explicit functionals of the natural orbitals ϕ_i and occupation numbers n_i. The total energy is then a functional of ϕ_i and n_i. Once the 1-RDM of the system is known, all the observables of the system can be calculated, provided that their expression as functional of the 1-RDM is known.

Such a functional has not been found yet for the spectral function, which determines, for example, photoemission spectra. Various ways to calculate removal/addition energies have been proposed [88, 99]. For example, removal energies can be calculated by using the method proposed by Pernal and Cioslowski [88], which is based on the extended Koopmans theorem (EKT) [26, 75]. So far, the method has been used only for finite systems. Numerical evidence suggests that EKT is at least exact for the lowest ionization potential [42, 43, 76, 105]. In Ref. [99] an approximate procedure to calculate quasiparticle energies and photoemission spectra within RDMFT has been proposed, which is also inspired by Koopmans theorem. When applied to a series of transition-metal oxides, the method seems to capture the essential physics of strong electron correlations. These are, however, only empirical evidences, and an in-depth analysis is missing. This is not simple because several approximations are involved: (i) an approximate exchange-correlation energy functional, (ii) an approximate expression for the removal and addition energies, and (iii) an approximate expression for the spectral function. It is therefore important to study these aspects in a systematic way in order to advance our understanding of an approach which is used all over physics and chemistry.

To do this, we need a simple system, preferably with a known exact solution for benchmarking, with a direct link between the molecular orbitals and natural orbitals and with the possibility to study quasi-degeneracies and (spin and charge) symmetry breaking. An ideal candidate is the Hubbard dimer: it is exactly solvable, the natural orbitals correspond to the bonding/antibonding orbitals, and the atomic limit $t \to 0$ offers a playground to explore degeneracies and symmetry breaking. In the atomic limit, when the two sites are pulled apart, electrons localize on either site with equal probability, unless a small perturbation is present. In this limit, explicit correlation between particles is crucial: this is the regime of strong electron correlation. In this limit, all the eigenstates of the system at 1/4 filling acquire equal energy and they become degenerate with the charge-symmetry broken states; at 1/2 filling the spin-singlet ground-state becomes degenerate with the spin-triplet state as well as with the spin-symmetry-broken states (see Tables I and II in Ref. [95]). This scenario is general and common also to other molecules, such as, *e.g.*, H_2 at dissociation, which is a paradigmatic example in quantum chemistry (see, *e.g.*, Refs.

[8, 16, 25, 34, 41, 82, 93, 101, 102, 119]). Analogies can be found also in infinite systems, as, for example, in the homogeneous electron gas (HEG). In the HEG the analogous of the bonding/antibonding orbitals are the eigenstates of the perfectly translationally invariant system, which are also the natural orbitals. At low densities, electrons localize to minimize the electron-electron interaction and the translational symmetry is spontaneously broken.

In the following, therefore, we will use the Hubbard dimer at 1/4 and 1/2 filling as a test case, and we will suggest extrapolation to real systems when appropriate.

The chapter is organized as follows. In Sec. 4.2 is shown how the occupation numbers are related to the multi-determinant nature of the wavefunction. In Sec. 4.3 the methods currently used to compute the spectral function within RDMFT are reviewed and analyzed. In Sec. 4.4 MBPT and RDMFT results for occupation numbers, total energy, removal/addition energies, and spectral function are compared to exact results and analyzed. In Sec. 4.6 we discuss how correlation is related to the measurements a physical system is subjected to. Finally we extrapolate these considerations to real systems. Conclusions are given in Sec. 4.7

4.2 Occupation numbers, 1-RDM and ground-state wave function

Natural occupation numbers are strictly related to the multideterminant nature of the wavefunction of a physical system. To illustrate this, let us expand the many-body wavefunction in terms of Slater determinants constructed from the eigenfunctions of the 1-RDM $\{\phi_i\}$, $\Psi_0(\mathbf{x}_1, ..., \mathbf{x}_N) = \sum_i C_i \Phi_i(\mathbf{x}_1, ..., \mathbf{x}_N)$. The 1-RDM then reads as [40]

$$\begin{aligned}\gamma(\mathbf{x}, \mathbf{x}') &= N \int d\mathbf{x}_2 ... d\mathbf{x}_N \sum_{ij} C_i^* C_j \Phi_i^*(\mathbf{x}', \mathbf{x}_2, ..., \mathbf{x}_N) \Phi_j(\mathbf{x}, \mathbf{x}_2, ..., \mathbf{x}_N) \\ &= \sum_i |C_i|^2 \gamma_i(\mathbf{x}, \mathbf{x}'),\end{aligned}$$

where $\gamma_i(\mathbf{x}, \mathbf{x}') = \sum_k \phi_k^i(\mathbf{x}) \phi_k^{i*}(\mathbf{x}')$ is the 1-RDM associated to the i-th Slater determinant. If the wavefunction of the system is described by a single Slater determinant, as in the case of a single (spin-polarized) electron (see the Hubbard dimer at 1/4 filling in Sec. 4.4.1), then the natural occupation numbers are either 1 or 0. If instead more determinants are involved, the natural occupation numbers, in general, take fractional values between 0 and 1. This can be nicely illustrated by considering a two-electron system with a singlet wavefunction $\Psi_0(\mathbf{x}_1, \mathbf{x}_2) = \sum_{i=1,2} C_i \Phi_i(\mathbf{x}_1, \mathbf{x}_2)$, where $\Phi_1 = |b\uparrow, b\downarrow\rangle$ and $\Phi_2 = |a\uparrow, a\downarrow\rangle$ are Slater determinants constructed from bonding and antibonding orbitals $\{\phi_i\}$, respectively (see the Hubbard dimer at 1/2 filling in Sec. 4.4.1). Note that the bonding/antibonding orbitals in the Hubbard dimer

correspond to the natural orbitals. The 1-RDM reads as

$$\begin{aligned}\gamma(\mathbf{x},\mathbf{x}') &= |C_1|^2 \sum_{i=b\uparrow,b\downarrow} \phi_i(\mathbf{x})\phi_i^*(\mathbf{x}') + |C_2|^2 \sum_{i=a\uparrow,a\downarrow} \phi_i(\mathbf{x})\phi_i^*(\mathbf{x}') \\ &= \sum_{i=b\uparrow,b\downarrow,a\uparrow,a\downarrow} n_i\phi_i(\mathbf{x})\phi_i^*(\mathbf{x}'),\end{aligned}$$

with $n_{b\uparrow} = n_{b\downarrow} = |C_1|^2$ and $n_{a\uparrow} = n_{a\downarrow} = |C_2|^2$, and $|C_1|^2 + |C_2|^2 = 1$ since the wavefunction Ψ_0 is normalized. In general, the relation between C_i and natural occupation numbers is more complicated than in this example, but the fact that fractional occupation numbers reflect the multideterminant nature of the wavefunction and hence the degree of correlation in a system remains still valid.

4.3 Spectral function in RDMFT

Recently, Sharma *et al.* [99] proposed the following approximate expression for the spectral function within RDMFT:

$$A(\omega) \approx \sum_i \left[n_i \delta(\omega - \epsilon_i^-) + (1 - n_i)\delta(\omega + \epsilon_i^+) \right], \tag{4.1}$$

where $\epsilon_i^\pm = E_0^N - E_i^{N\pm1}$, with E_0^N the ground-state energy of the N-electron system and $E_i^{N\pm1}$ the i-th state energy of the $(N \pm 1)$-electron system. To arrive at Eq. (4.1), one starts from the exact expression $A(\omega) = \mathrm{sign}(\mu - \omega)\,\mathrm{Im}\,G(\omega)/\pi$ (see Sec. 3.1.3) and approximates the ground and excited states of the $(N+1)$- and $(N-1)$-electron systems by adding an electron, $|\Psi_i^{N+1}\rangle = \frac{1}{\sqrt{1-n_i}} c_i^\dagger |\Psi_0^N\rangle$, or a hole, $|\Psi_i^{N-1}\rangle = \frac{1}{\sqrt{n_i}} c_i |\Psi_0^N\rangle$, to the ground-state of the N-electron system. This is in the spirit of Koopmans theorem and it is an approximation, because, in general, the set of states obtained in this way are not eigenstates of the $(N+1)$- and $(N-1)$-electron system, respectively, and do not form a complete set. Along the same line, the energies ϵ_i^- and ϵ_i^+ in Eq. (4.1) are calculated in an approximate way as

$$\epsilon_k^- = -\epsilon_k^+ = \epsilon_k = E[\{n_i\},\{\phi_i\}]|_{n_k=1} - E[\{n_i\},\{\phi_i\}]|_{n_k=0}\,, \tag{4.2}$$

where $E[\{n_i\},\{\phi_i\}]|_{n_k=1}$ ($E[\{n_i\},\{\phi_i\}]|_{n_k=0}$) is the total energy for the N-particle system with all the occupation numbers fixed at their optimal value (*i.e.*, the value that minimizes the energy functional) except for the occupation number n_k which is fixed to 1 (0). We will refer to this method as DIF, to keep contact with other works on the subject [123]. Using (4.2) for the calculation of removal and addition energies, the expression of the spectral function in (4.1) simplifies to $A(\omega) = \sum_i \delta(\omega - \epsilon_i)$.

We note that the energies calculated using Eq. (4.2) have both removal and addition characters, because, in general, the state k is partially filled. Equation (4.2) can,

indeed, be rewritten as the sum of two contributions

$$\begin{aligned}\epsilon_k = &\Big(E[\{n_i\},\{\phi_i\}]|_{n_k=1} - E[\{n_i\},\{\phi_i\}]|_{n_k=n_k^{\mathrm{opt}}} \Big) \\ &+ \Big(E[\{n_i\},\{\phi_i\}]|_{n_k=n_k^{\mathrm{opt}}} - E[\{n_i\},\{\phi_i\}]|_{n_k=0} \Big),\end{aligned} \tag{4.3}$$

where n_k^{opt} are the occupation numbers which minimize the total energy. The first term on the right-hand side of Eq. (4.3) corresponds to the addition of a fraction of electron equal to $1 - n_k^{\mathrm{opt}}$ while the second to the removal of a fraction of electron equal to n_k^{opt}.

Moreover, the number of energies calculated using (4.2) equals the number of occupation numbers (*i.e.*, the dimension of the natural orbital basis set), which is in general smaller than the exact number of removal and addition energies; it equals, indeed, the number of noninteracting states and hence the number of quasiparticles. Note that quasiparticle peaks in the spectral function can be directly linked to peaks in the non-interacting spectral function, whereas satellites are additional structures which are generated by the frequency-dependence of the self-energy and, therefore, have zero spectral weight for vanishing interaction. The spectral weight of a quasiparticle peak, instead, remains constant or might decrease by increasing the interaction, the weight being transferred to the satellites. This can be illustrated using the Hubbard dimer. As shown in Sec. 6.3 for this model system the basis of natural orbitals $\{\phi_i\}$ diagonalizes also the 1-GF for any frequency; therefore, one can write

$$G(\mathbf{x}_1,\mathbf{x}_2;\omega) = \sum_i G_i(\omega)\phi_i(\mathbf{x}_1)\phi_i^*(\mathbf{x}_2),$$

and for the occupation numbers, one gets

$$n_i = -\mathrm{i}\int \frac{d\omega}{2\pi} G_i(\omega) e^{\mathrm{i}\omega 0^+}. \tag{4.4}$$

If G_i has more than one pole, then the total number of removal/addition energies that one should find is larger than the number of occupation numbers. Therefore, equation (4.2), in general, describes a mixture of quasiparticle and satellite energies, as will be illustrated in Sec. 6.3.

The total energy difference, Eq. (4.2), can be further approximated as

$$E[\{n_i\},\{\phi_i\}]|_{n_k=1} - E[\{n_i\},\{\phi_i\}]|_{n_k=0} \approx \left.\frac{\partial E}{\partial n_k}\right|_{n_k=1/2}, \tag{4.5}$$

which is justified if the total energy is nearly linear in the occupation number n_k [64]. This method will be referred to as DER. Using Eqs. (4.1) and (4.5), the spectral function of several transition metal oxides has been calculated, showing that some experimental features are captured [99].

As an alternative to Eq. (4.2) (or (4.5)), removal energies can be calculated by using the EKT as proposed by Pernal and Cioslowski [88]. The method is based on the diagonalization of the Lagrangian matrix,

$$\Lambda_{ij} = \frac{1}{\sqrt{n_i n_j}} \left[n_i h_{ji} + \sum_{klm} \Gamma^{(2)}_{iklm} V_{jkml} \right],$$

with $h_{ji} = \int d\mathbf{x}\, \phi_j^*(\mathbf{x}) h(\mathbf{x}) \phi_i(\mathbf{x})$,

$$\Gamma^{(2)}_{iklm} = \int d\mathbf{x}'_1 d\mathbf{x}'_2 d\mathbf{x}_1 d\mathbf{x}_2\, \Gamma^{(2)}(\mathbf{x}'_1, \mathbf{x}'_2; \mathbf{x}_1, \mathbf{x}_2) \phi_m^*(\mathbf{x}_2) \phi_l^*(\mathbf{x}_1) \phi_k(\mathbf{x}'_2) \phi_i(\mathbf{x}'_1),$$

and

$$V_{jkml} = \int d\mathbf{x}_1 d\mathbf{x}_2 \phi_j^*(\mathbf{x}_1) \phi_k^*(\mathbf{x}_2) v_c(\mathbf{r}_1, \mathbf{r}_2) \phi_m(\mathbf{x}_1) \phi_l(\mathbf{x}_2).$$

The eigenvalues of Λ are the removal energies. The underlying physics of this method is similar to that of the approximations used to derive Eq. (4.1), although more advanced: in the EKT, the $(N-1)$-electron states are obtained as a linear combination of states obtained by removing an electron from the ground-state of the N-electron system, $|\Psi^{N-1}\rangle = \sum_i B_i c_i |\Psi_0^N\rangle$; the energy of the so obtained $(N-1)$-electron states is minimized with respect to the coefficients B_i, unlike in the DIF/DER method. In practice, the EKT has only been applied to finite systems. For the Hubbard dimer at 1/4 and 1/2 fillings, it delivers the exact removal energies when combined with the exact exchange-correlation energy functional. Therefore, in this work, we will use it to test approximations to the xc energy functional. Note that the lowest addition energy can be obtained from the highest removal energy of the $(N+1)$-system (if the latter is stable).

4.4 Correlation in the Hubbard dimer

In this section, we will illustrate the physics behind different approximations to correlation as well as to observables in RDMFT and show how it compares with the standard G_0W_0 method used in MBPT. To this purpose we use the Hubbard dimer, a simple prototype of a strongly correlated system that can be solved exactly [55]. The Hamiltonian of the Hubbard dimer reads as

$$H = -t \sum_{\substack{i,j=1,2 \\ i \neq j}} \sum_{\sigma} c^\dagger_{i\sigma} c_{j\sigma} + \frac{U}{2} \sum_{i=1,2} \sum_{\sigma,\sigma'} c^\dagger_{i\sigma} c^\dagger_{i\sigma'} c_{i\sigma'} c_{i\sigma} + \epsilon_0 \sum_{i=1,2} \sum_{\sigma} c^\dagger_{i\sigma} c_{i\sigma} + V_0.$$

Here, $c^\dagger_{i\sigma}$ and $c_{i\sigma}$ are the creation and annihilation operators for an electron at site i with spin σ, U is the on-site (spin-independent) interaction, $-t$ is the hopping kinetic energy, and ϵ_0 is the orbital energy. The Hamiltonian further contains a potential V_0

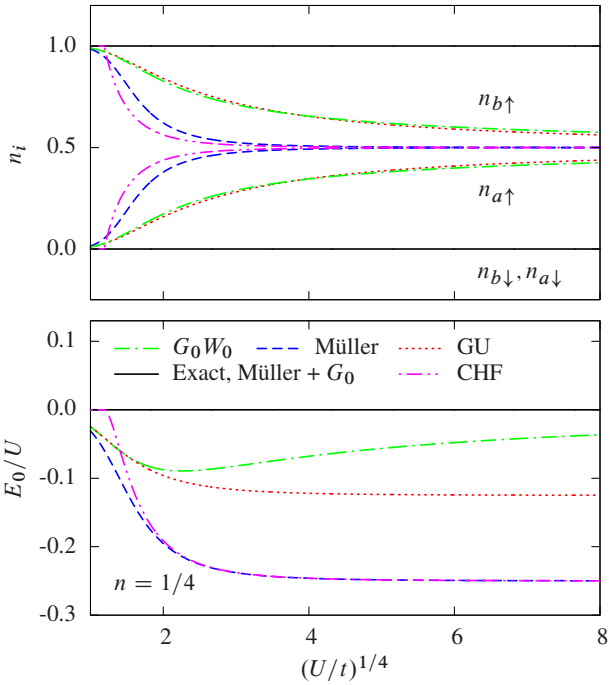

Figure 4.1: Occupation numbers (upper panel) and total energy (lower panel) as function of U/t at 1/4 filling: exact vs Müller functional, GU functional, CHF functional, and G_0W_0. Total energies obtained using G_0 occupation numbers in the Müller functional, and using the G_0W_0 Green's function in the Galitskii-Migdal formula (labeled Müller+G_0 and G_0W_0, respectively), are also reported.

that can be chosen to fix the zero-energy scale. The physics of the Hubbard model [55] arises from the competition between the hopping term, which prefers to delocalize electrons, and the on-site interaction, which favors localization. The ratio U/t is a measure for the relative contribution of both terms and is the intrinsic, dimensionless coupling constant of the Hubbard model, which will be used in the following.

We refer to App. B for the exact results of the model at 1/4 and 1/2 filling, respectively. Here, we will use both the bonding/antibonding basis set, which is conceptually similar to a molecular-like basis set, and the site basis, which can be considered as an atomic-like basis set (see App. A). The bonding/antibonding basis diagonalizes the 1-RDM of the fully symmetric dimer, *i.e.*, this basis set is the basis of natural orbitals. The site basis, instead, is the basis of natural orbitals for the symmetry-broken dimer. The site basis offers a clearer picture of electron addition and removal for the Hubbard model, where the electron-electron interaction is on site. The eigenstates of the Hubbard Hamiltonian are given as linear combinations of Slater determinants built from the bonding/antibonding or the site basis functions. In the following, the notation $|A\sigma, B\sigma', ...\rangle$ indicates a Slater determinant with on its diagonal an electron in the orbital A with spin σ, an electron in the orbital B with spin σ', and so on. In the case of one electron, the Slater determinant $|A\sigma\rangle$ is a one-electron function.

4.4.1 Total energy and occupation numbers

1/4 filling

In the case of the Hubbard dimer at 1/4 filling, the ground-state wavefunction reads

$|\Psi_0\rangle = |b\uparrow\rangle$ in the bonding/antibonding basis, *i.e.*, one single Slater determinant with one spin-up electron in the bonding orbital (equivalently, the spin-down situation could be chosen). The exact 1-RDM is idempotent for any U/t value at zero temperature, with the occupation number of the bonding (antibonding) orbital $n_{b\uparrow} = 1$ and $n_{b\downarrow} = 0$ ($n_{a\uparrow} = n_{a\downarrow} = 0$) (see Fig. 4.1, upper panel[1]). When projected on the site basis, one gets $|\Psi_0\rangle = (|1\uparrow\rangle + |2\uparrow\rangle)/\sqrt{2}$. This means that the electron has equal probability 1/2 of being on site 1 or site 2. Often, the electronic structure is probed by electron addition or removal, like in inverse or direct photoemission experiments. In the atomic limit (small hopping $t \to 0$, for which $U/t \to \infty$ for U fixed), one can imagine that the electron spends a long time on one site; there are therefore two possible addition energies: one at ϵ_0 when the addition electron goes to the unoccupied site and one at $\epsilon_0 + U$ when it goes to the occupied one. In this case, there is no correlation in the ground-state, since the occupation numbers are zero or one, but electron addition leads to two strongly correlated electrons: the added electron has to see the electron in the system. When we use the Müller functional, the optimal occupation numbers $n_{b\uparrow}$ and $n_{a\uparrow}$ tend to 0.5 with increasing U/t (see Fig. 4.1, upper panel). By increasing α up to 1 (Hartree-Fock) one approaches the exact situation; this is because exchange and Hartree energies completely cancel each other in the case of one electron. For comparison, we report also the results obtained using the functional proposed by Goedecker and Umrigar (GU) [45] and the so-called corrected Hartree-Fock (CHF) functional proposed by Csányi and Arias [23], which are variants of the original Müller functional. The GU functional slows down the eventual merging of bonding and antibonding occupation numbers at 1/2, whereas the CHF is on top of the HF results for small interaction and tends towards the Müller results when increasing the interaction. Interestingly the occupation numbers calculated from the G_0W_0 1-GF are almost on top of the GU functional results. To obtain G_0W_0 occupation numbers, we use Eq. (4.4), with the G_0W_0 1-GF on the right-hand side.

Total energy results are reported in the lower panel of Fig. 4.1. All the approximations used underestimate the total energy, the exception being the Müller functional when fed with exact occupation numbers (obtained from G_0 at 1/4 filling[2]), which is on top of the exact result ("Müller+G_0" in Fig. 4.1). This finding is also observed at 1/2 filling. However, at one fourth filling, the exact occupation numbers being 1 or 0, any $0 \leq \alpha \leq 1$ would give the exact total energy. For comparison, we also reported the total energy obtained using the Galitskii-Migdal equation (3.5) with the G_0W_0 Green's function, which is similar to the results obtained using the GU functional below $(U/t)^{1/4} \simeq 2$. In the atomic limit, however, the G_0W_0 total energy tends to the exact one as was already noticed in Ref. [95], whereas the GU functional gives a lower

[1]Note that here and in Fig. 4.2 we use $(U/t)^{1/4}$ on the horizontal axis to facilitate the comparison with Ref. [82] at 1/2 filling.

[2]For one electron, the hole part of the non-interacting Green's function, *i.e.*, the part related to removal energies, is exact, because the removed electron does not interact with other electrons in the system; the exact occupation numbers can hence be calculated from G_0 according to Eq. (4.4).

energy. For the CHF functional, we observe the same trend as for the occupation numbers.

In conclusion, at one fourth filling, we find that the Hartree-Fock approximation gives the exact occupation numbers, whereas the Müller functional gives results which quickly depart from the exact ones. Using the GU functional gives results in between these two extremes for any U/t; G_0W_0 occupation numbers are almost on top of the GU functional results. Finally, the CHF results are on top of the HF results at weak interaction, whereas they tend to the Müller results for strong interaction. Concerning the total energy, all Müller-like functionals fed with exact occupation numbers give the exact results. All the other approximations tend to underestimate the total energy.

1/2 filling

The wavefunction at 1/2 filling reads as $|\Psi_0\rangle = \sqrt{n_b}\,|b\uparrow, b\downarrow\rangle - \sqrt{n_a}\,|a\uparrow, a\downarrow\rangle$ (with $n_b = n_{b\uparrow} = n_{b\downarrow}$ and $n_a = n_{a\uparrow} = n_{a\downarrow}$) in the bonding/antibonding basis. Note that $|\Psi_0\rangle$ depends on the square root of the occupation numbers; the success of the Müller functional with $\alpha = 0.5$ at 1/2 filling is linked to this. This functional is indeed closely related to the exact reduced density-matrix functional for two-electron systems, which is the Löwdin-Shull functional [70]. The exact 2-RDM for such systems has an expansion in coefficients which are the square roots of the natural occupation numbers up to a sign [111]. A proper selection of the signs (which, in general, is unknown) gives the exact result for two-electron systems, which, for the Hubbard dimer, reads as $\Gamma^{(2)} = U/2 - U\sqrt{n_b n_a}$. At $U/t = 0$, the wavefunction is the single Slater determinant $|\Psi_0\rangle = |b\uparrow, b\downarrow\rangle$; increasing U/t, also the antibonding orbital becomes important, and eventually the full wavefunction becomes a linear combination of the Slater determinants $|b\uparrow, b\downarrow\rangle$ and $|a\uparrow, a\downarrow\rangle$ with equal weight (see Fig. 4.2, upper panel). When projected on the site basis, the ground-state wavefunction reads $|\Psi_0\rangle = A\,(|1\uparrow, 2\downarrow\rangle - |1\downarrow, 2\uparrow\rangle) + B\,(|1\uparrow, 1\downarrow\rangle - |1\downarrow, 1\uparrow\rangle)$, with $A = (\sqrt{n_b} + \sqrt{n_a})/2$ and $B = (\sqrt{n_b} - \sqrt{n_a})/2$ (see App. A and Ref. [95]). This means that for the noninteracting case ($n_b = 1$ and $n_a = 0$), each of the two electrons is equally distributed between the two sites, while increasing the interaction (n_b, $n_a \to 1/2$), double occupancies become less probable.

From Fig. 4.2, we see that the optimal occupation numbers for the Müller functional are the exact ones. The occupation numbers obtained using the CHF functional become quickly exact by increasing the interaction. Using the GU functional as well as varying α in the range 0.5-1 spoils this result. Again, G_0W_0 occupation numbers are very similar to the GU results. Note that G_0W_0 produces fractional occupation numbers with increasing U/t; eventually, they go to 1/2 at $t = 0$, but they go too slowly. This means that at strong interaction, G_0W_0 does not manage to well localize the two electrons, each on one site, and spurious double occupancies are still present.

Total energies are reported in the lower panel of Fig. 4.2. The total energy within the Müller approximation is exact. The CHF total energy is on top of the HF total

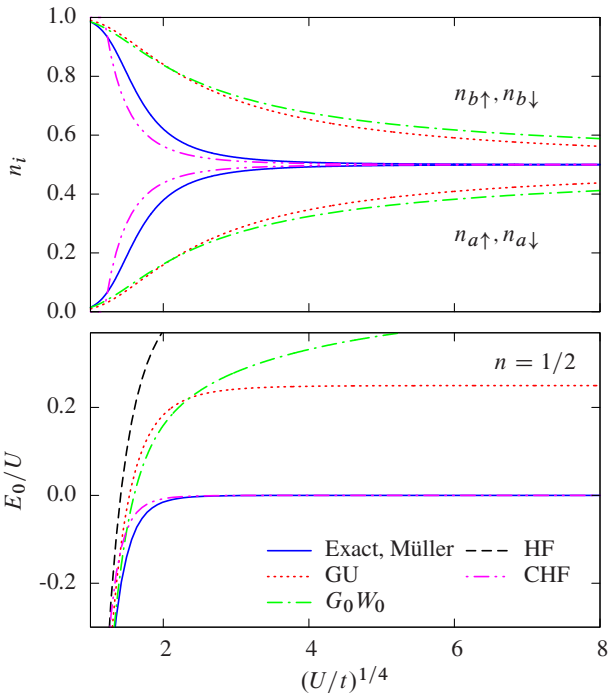

Figure 4.2: Occupation numbers (upper panel) and total energy (lower panel) as function of U/t at 1/2 filling: exact vs Müller functional, GU functional, CHF functional, and G_0W_0. The G_0W_0 total energies are obtained using the Galitskii-Migdal formula.

energy at weak interaction and merges with the exact result when increasing the interaction. The G_0W_0 result is similar to the result obtained using the GU functional below $(U/t)^{1/4} \simeq 3$; for stronger interaction, they differ, but both overestimate the total energy. Our G_0W_0 result is in line with previous GW calculations on the H_2 molecule [16, 102], which show GW to be very accurate close to equilibrium but to dramatically overestimate the total energy in the dissociation limit[3]. Comparison with recent total energy calculations on the Hubbard dimer [82] using the correlation energy expression obtained with the adiabatic-connection technique (see, *e.g.*, Ref. [93]) shows that RPA and beyond RPA approximations including excitonic effects give better results than G_0W_0 at strong interaction[4].

In conclusion, at one half filling, the Müller functional gives the exact occupation numbers. The CHF functional gives results similar to HF at weak interaction but rapidly similar to the exact results by increasing the interaction. G_0W_0 and the GU functional give similar occupation numbers, which merge with the exact ones at $t = 0$, but at a lower speed than the exact values. This reflects the fact that these two ap-

[3]Note that at 1/2 filling, we use the particle-hole form of the Hubbard Hamiltonian [94]. In the G_0W_0 removal/addition energies, the particle-hole symmetry is lost for $U \neq 0$ due to the lack of self-consistency; we restore this symmetry by absorbing the static part of the self-energy ($U/2$) into the chemical potential. This alignment of the chemical potential corrects for the lack of self-consistency [50, 90].

[4]Note that in Ref. [93], the authors chose $\epsilon_0 = 0$ and $V_0 = 0$ in the Hubbard Hamiltonian. A G_0W_0 calculation in this case gives a total energy better than the RPA total energy; in our calculations, instead, by restoring the particle-hole symmetry [94], the GW spectral properties are improved, but the total energy worsens.

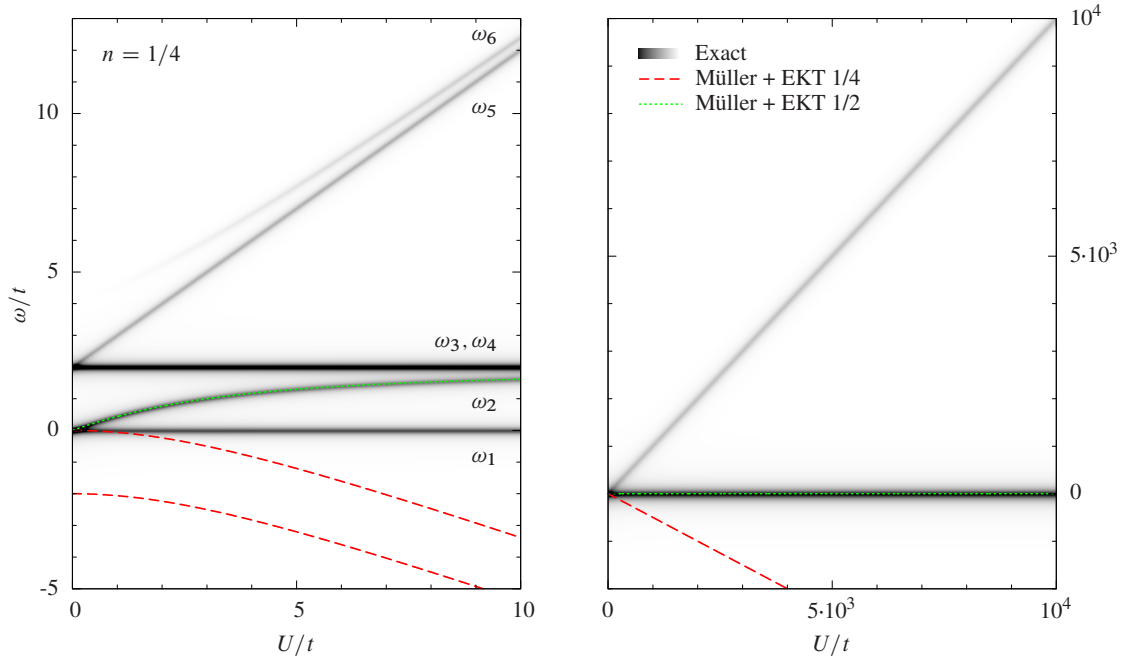

Figure 4.3: Removal and addition energies ω/t as function of U/t at 1/4 filling: exact *vs.* EKT method used with the Müller functional (the label "Müller+ EKT 1/4" refers to the removal energies, whereas "Müller+ EKT 1/2" to the lowest addition energy calculated from the highest removal energy of the system at 1/2 filling). The labels ω_i indicate the exact energies. The color gradient (from white to black) of the exact curves indicates increasing spectral weight; the energy ω_6 is hence a satellite, since it has vanishing spectral weight at vanishing interaction. The addition energy "Müller+ EKT 1/2" is on top of the exact energy ω_2, which goes to a constant at strong interaction (right panel).

proximations have difficulties to localize the two electrons, one on each site, missing the atomic physics of strongly correlated electrons. Concerning the total energy, both G_0W_0 and GU similarly overestimate the exact values, whereas the Müller functional gives the exact result. The CHF functional becomes rapidly exact with the interaction. Increasing α leads to higher total energies, with HF giving the worst agreement ($E_0/U = -2t/U + 1/2$).

4.4.2 Removal/addition energies and spectral function

Exact removal and addition energies are reported in Figs. 4.3, 4.4, 4.7, and 4.8. We analyze various ways to compute removal/addition energies within RDMFT, which elucidate the role played by an approximate exchange-correlation energy functional and by an approximate expression for the removal/addition energies. First, we test the Müller-like approximations to the xc functional by combining the latter with the method proposed by Pernal and Cioslowski (EKT) [88] for the calculation of removal energies. This method, based on the extended Koopmans theorem, gives the exact

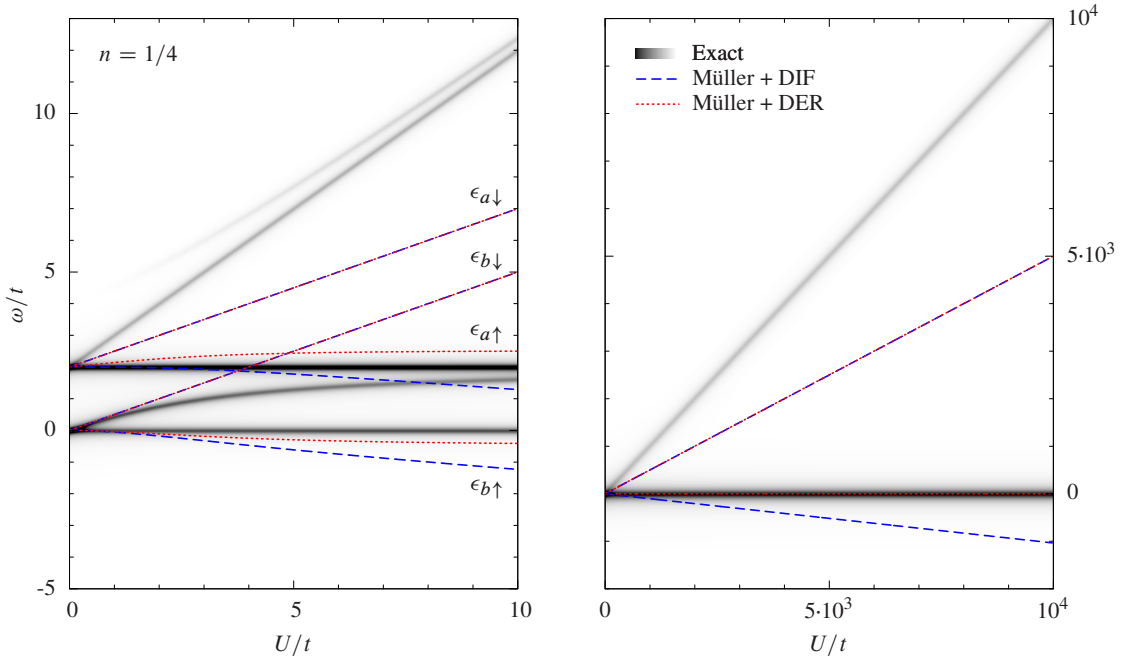

Figure 4.4: Removal and addition energies ω/t as function of U/t at 1/4 filling: exact *vs.* DIF and DER methods used with the Müller functional. The labels ϵ_i indicate the bonding/antibonding energies obtained using the DIF/DER methods. The color gradient of the exact curves has the same meaning as in Fig. 4.3. The energies $\epsilon_{b\downarrow}$ and $\epsilon_{a\downarrow}$ calculated with the DIF method are on top of those obtained with the DER method and go as $U/(2t)$ at strong interaction (right panel); the energies $\epsilon_{b\uparrow}$ and $\epsilon_{a\uparrow}$ calculated with the DER method reach a constant value at strong interaction (right panel).

removal energies of the Hubbard dimer at 1/4 and 1/2 fillings, when combined with the exact exchange-correlation energy functional. This allows us to study the accuracy of the xc functional approximations. Second we test the DIF/DER method for the calculation of removal/addition energies by combining it with the exact xc functional. We then test the combination of the DIF/DER method and the Müller-like approximations to the xc energy functional.

Finally we combine the DIF/DER method and the Müller-like functionals with the approximate expression for the spectral function given in Eq. (4.1). This is the approach used for the calculation of spectral functions of transition metal oxides already mentioned before [99].

Exact, G_0W_0, and DIF/DER (within the Müller functional) spectral functions are compared in Figs. 4.6 and 4.9.

The DER method is supposed to be a good approximation to the DIF method, provided the energy functional is nearly linear in the occupation number n_i. This is the case for extended systems as pointed out in Ref. [99] but it is not generally true for finite systems [123]. In the Hubbard dimer at 1/2 filling, for example, the total

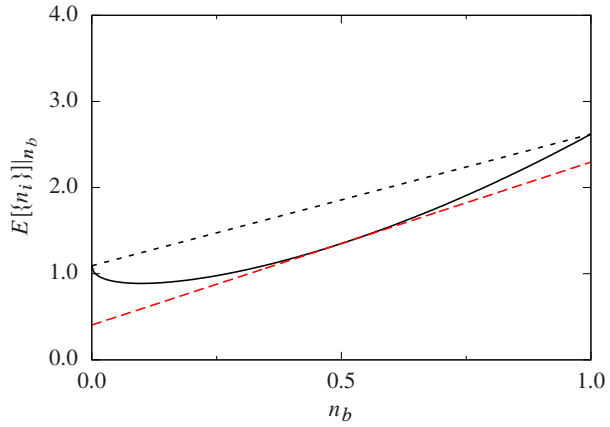

Figure 4.5: Total energy (black solid line) *vs.* occupation number n_b for the Hubbard dimer at 1/2 filling: the DIF energy ϵ_b is given by the slope of the black dashed line, while the DER energy by the slope of the tangent at $n_b = 1/2$ (red dashed line).

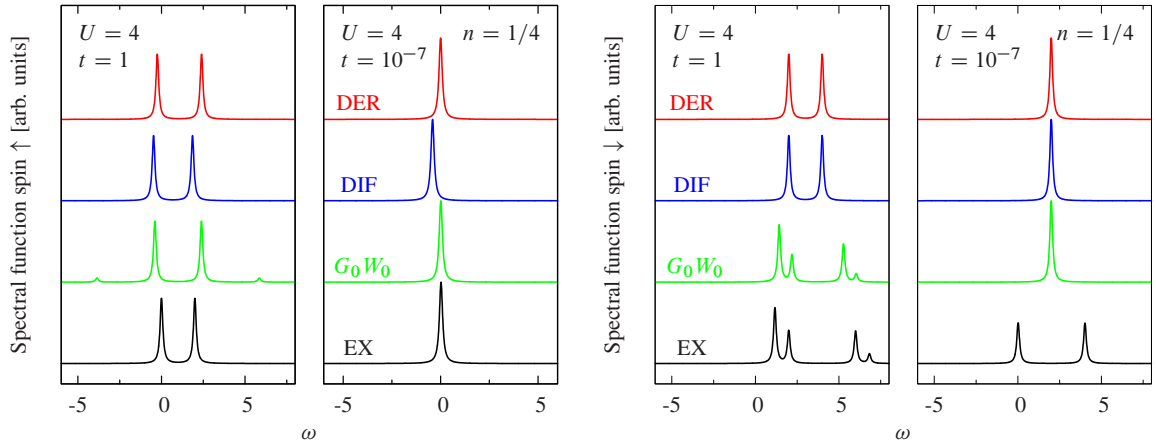

Figure 4.6: Spectral function at 1/4 filling: exact *vs.* G_0W_0, and DER and DIF methods using the Müller functional.

energy functional is not linear in n_i as can be seen in Fig. 4.5, where the total energy is reported as a function of the bonding occupation number n_b, while the antibonding occupation number n_a is held fixed to its optimal value. However, even if the functional is not linear, the DER method gives a good approximation of the DIF method.

1/4 filling

At 1/4 filling, the Hubbard dimer shows five quasiparticle energies (one removal, labeled ω_1 in Fig. 4.3, and four addition energies, labeled ω_2, ω_3, ω_4, ω_5) and one addition satellite energy (ω_6). Satellites are weak removal or addition energies which acquire spectral weight with increasing interaction, whereas the intensity of quasiparticles decreases or remains constant. If the exact energy functional is used (which, for one-electron, is just $E = E_{\text{kin}} + E_{\text{ext}}$), then the EKT method produces the exact removal energy $\epsilon_0 - t$ (ω_1 in Fig. 4.3). Using the Müller functional, instead, the EKT produces two removal energies (see result "Müller+ EKT 1/4" in Fig. 4.3). This is due to the fact that within this functional, the antibonding occupation number $n_{a\uparrow}$ is not

zero[5], and therefore more degrees of freedom are added to the problem. The energies do not match well with the exact results. In the limit $U/t \to \infty$, the two removal energies merge together at a value well off the exact one (see right panel of Fig. 4.3). In this limit, the exact energies merge towards ϵ_0 and $\epsilon_0 + U$: this reflects the fact that in this limit, the electron has equal probability to localize on one site or the other of the dimer; therefore one can have removal and addition energies (for a spin-down or a spin-up electron added to the empty site) at ϵ_0 and an addition energy at $\epsilon_0 + U$ (for a spin-down electron added to the site with one spin-up electron already present). We note that improvements are obtained changing α from 0.5 to 1 (Hartree-Fock) as the exact functional is approached. Hartree-Fock, indeed, gives the exact total energy at 1/4 filling, due to an exact cancellation between Hartree and exchange energies. If the lowest addition energy is calculated from the highest removal energy of the system at 1/2 filling, the EKT yields the exact result (see result "Müller+ EKT 1/2" in Fig. 4.3) but only because the Müller functional gives the exact total energy and occupation numbers at 1/2 filling ($(N+1)$-electron system).

The DIF/DER method (Eqs. (4.2) and (4.5)) performs as the EKT if the exact xc functional is used: it produces the exact removal energy and the exact second lowest addition energy. With the Müller functional, it gives four energies (see result "Müller+ DIF/DER" in Fig. 4.4): only two energies are in good agreement with the exact ones ($\epsilon_{b\uparrow}$ and $\epsilon_{a\uparrow}$, calculated from $n_{b\uparrow}$ and $n_{a\uparrow}$, respectively), whereas for the other two ($\epsilon_{b\downarrow}$ and $\epsilon_{a\downarrow}$), we observe that each is approximately an average of two exact ones, namely $\epsilon_{b\downarrow}$ is an average of ω_2 and ω_6[6] and $\epsilon_{a\downarrow}$ of ω_3 (or, equivalently, ω_4) and ω_5. This can be understood considering that the $G_{b\uparrow}$ and $G_{a\uparrow}$ components of the 1-GFs have only one pole, whereas $G_{b\downarrow}$ and $G_{a\downarrow}$ have two poles each; the corresponding occupation numbers (see Eq. (4.4)) hence reflect these features.

In general, the spectral function profile is in overall good agreement with the exact one at moderately strong interaction U/t. For the spin-down channel (right panel of Fig. 4.6), G_0W_0 is slightly superior. It shows a very weak spurious satellite due to self-screening [95] in the spin-up channel, but it correctly describes the spin-down satellite. In the atomic limit ($t \to 0$), both DIF and DER methods show the same failure as G_0W_0: for the spin-down spectral function, the poles merge at $\epsilon_0 + U/2$, unlike the exact result which shows a gap equal to U. We observe the same scenario increasing the number of sites (not shown). The GU functional does not add any significant improvement to the picture, whereas the CHF functional gives the HF result for any t. If the lowest addition energy (spin-down channel) is calculated from the highest removal energy of the $(N+1)$-electron system (1/2 filling), the method produces a gap, unlike the exact result, where the lowest addition energy coincides with the highest removal energy (ϵ_0). A similar error is found also in GW and it is a consequence of the self-screening error GW suffers from [95].

[5]Note that at $U = 0$, $n_{a\uparrow} = 0$ and the corresponding removal energy calculated with the EKT does not have a meaning. At $U = 0$ the EKT yields only the exact removal energy.

[6]Note that at $U = 0$, ω_6 has zero spectral weight.

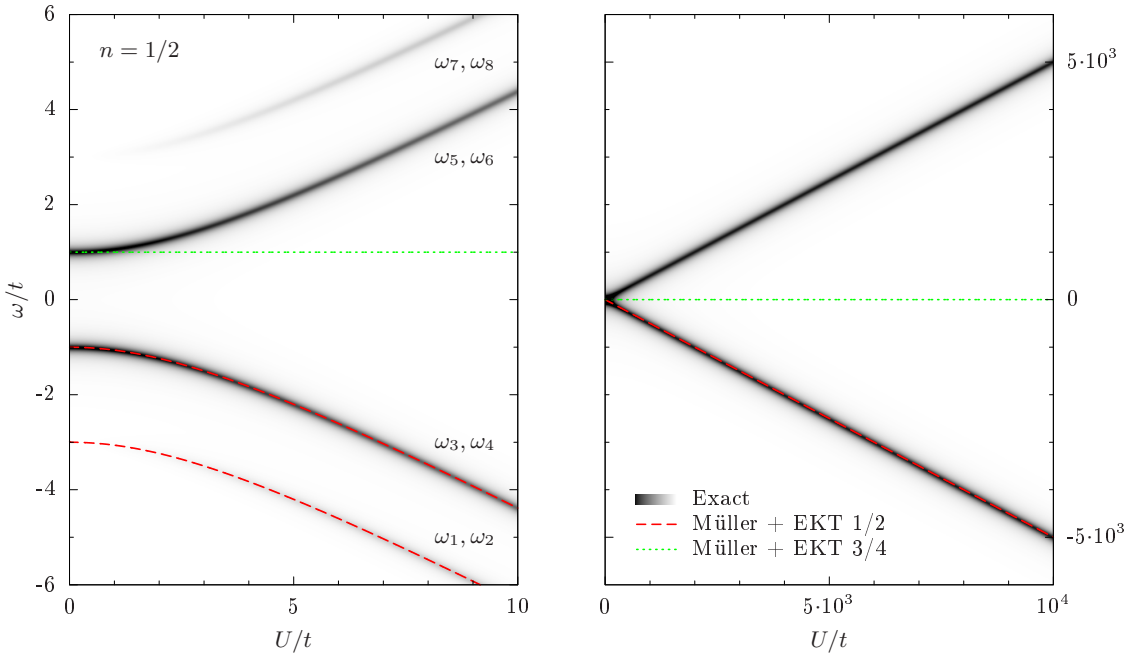

Figure 4.7: Removal and addition energies ω/t as function of U/t at 1/2 filling: exact *vs.* EKT method used with the Müller functional (the label "Müller+ EKT 1/2" refers to the removal energies, whereas "Müller+ EKT 3/4" to the lowest addition energy calculated from the highest removal energy of the system at 3/4 filling). The labels ω_i indicate the exact energies. The color gradient (from white to black) of the exact curves indicates increasing spectral weight; the energies ω_1, ω_2, ω_7, ω_8 are hence satellites, since they have vanishing spectral weight at vanishing interaction.

In conclusion, combining the Müller-like functionals with the DIF/DER method significantly improves electron addition and removal energies seen as poles in the spectral function with respect to the case where this functional is used with the more advanced EKT. This indicates that there is a cancellation of errors between the approximate Müller functional and the DIF/DER method, at least at 1/4 filling.

1/2 filling

At 1/2 filling, there are four quasiparticle energies (labeled ω_3, ω_4, ω_5, ω_6, in Fig. 4.7) and four satellites (ω_1, ω_2, ω_7, ω_8). Using the Müller functional, which, in this case, gives the exact total energy and occupation numbers, the EKT gives two doubly degenerate energies: these are the exact removal energies, including a satellite. To get the lowest addition energy, one has to look at the $(N+1)$-electron system (3/4 filling); in this case, the Müller functional does not reproduce the exact total energy and occupation numbers and, consequently, the EKT gives an addition energy that strongly departs from the exact one as U/t increases.

Both DIF and DER methods give only two energies per spin channel, but their

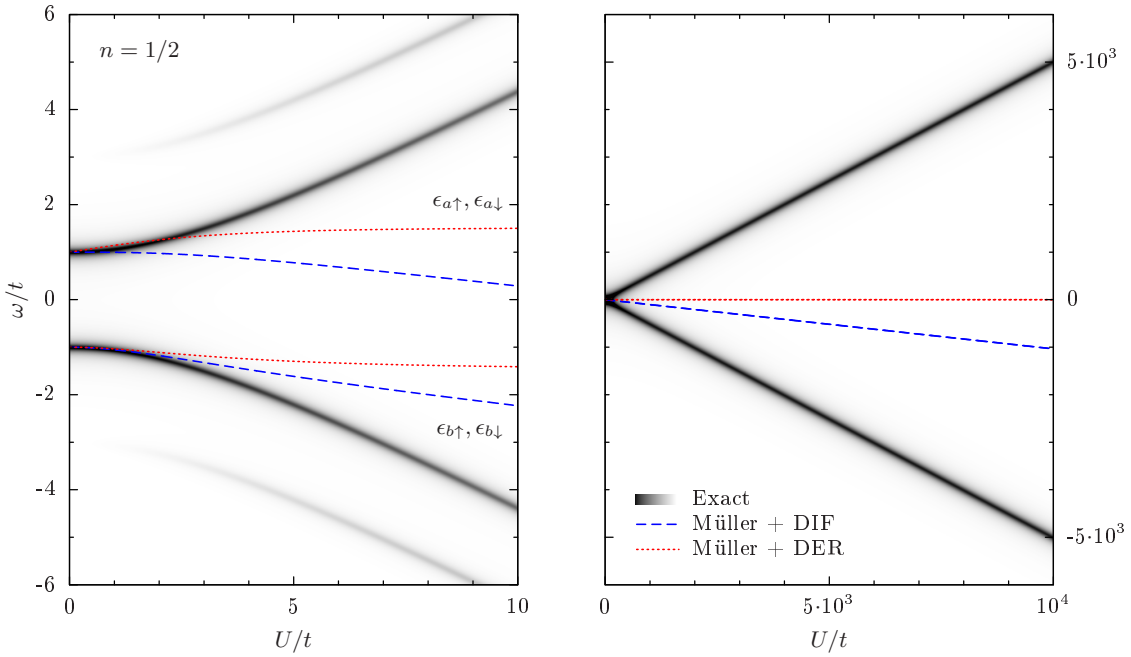

Figure 4.8: Removal and addition energies ω/t as function of U/t at 1/2 filling: exact *vs.* DIF and DER methods used with the Müller functional. The labels ϵ_i indicate the bonding/antibonding energies obtained using the DIF/DER methods. The color gradient of the exact curves has the same meaning as in Fig. 4.7.

nature is in fact a mixture of quasiparticle and satellite energies and of electron addition and removal; for example, we found that the energy $\epsilon_{b\uparrow}$ in Fig. 4.7 is roughly a weighted average of the satellite and quasiparticle energies ω_3 and ω_7, respectively. Again this can be understood by considering that the components $G_{b\sigma}$ and $G_{a\sigma}$ have two poles each, and therefore the corresponding occupation numbers reflect these features in the excitation energies $\epsilon_{b\sigma}$ and $\epsilon_{a\sigma}$. The results are quite different from the EKT, where one has both the removal quasiparticle and satellite energies. Since at 1/2 filling, the Müller functional is exact, there is not the same cancellation of error as observed at 1/4 filling, and the DER/DIF method introduces, hence, quite a large error.

In Fig. 4.9, we report the exact spectral function in comparison to the spectral functions obtained with G_0W_0 and DIF/DER using the Müller functional. Only two peaks appear in the DIF/DER spectra, which merge in the $t \to 0$ limit both for the DIF and DER methods. We note that the GU functional tends to open the gap, but it is not enough in the strongly correlated dissociation limit, whereas the CHF functional gives the HF results for any t. Changing α does not improve the situation. DIF and DER, therefore, perform as bad as G_0W_0 in the atomic limit, whereas G_0W_0 is significantly superior at moderately strong interaction. We note that this conclusion is not restricted to the Hubbard dimer; we find the same scenario by increasing the number of sites, as illustrated in Fig. 4.10 for a chain of 12 sites at 1/2

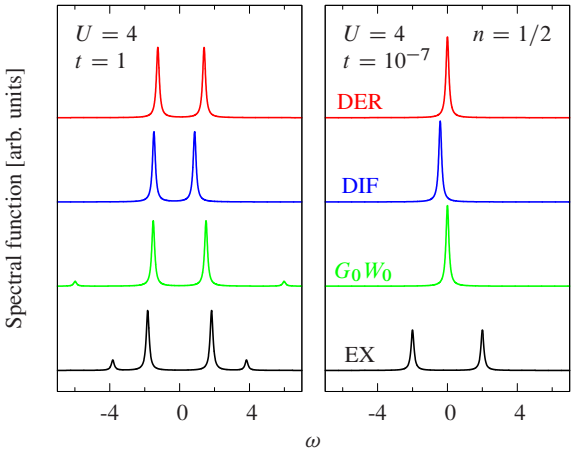

Figure 4.9: Spectral function at 1/2 filling: exact *vs.* G_0W_0, and DER and DIF methods using the Müller functional.

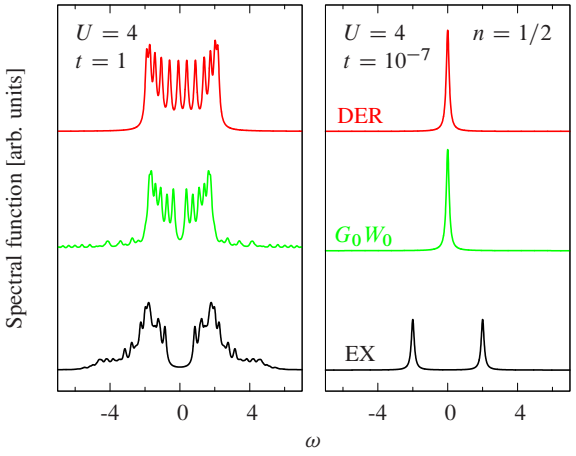

Figure 4.10: Spectral function for a chain of 12 sites at 1/2 filling: exact *vs.* G_0W_0, and DER method using the Müller functional.

filling. However, if the lowest addition energy is calculated from the highest removal energy of the $(N+1)$-electron system, the DIF/DER method yields a gap at best half of the exact one in the atomic limit.

In conclusion, using an exact xc functional, the method of Ref. [99] has a large deviation from the exact results, both in the values and nature of the removal and addition energies. For moderately strong interaction, G_0W_0 is clearly superior. In the atomic limit, no gap is observed, as in GW, unless the $(N+1)$-electron system is considered for the calculation of the lowest addition energy.

4.5 RDMFT for a spin-symmetry broken dimer

In the case of the spin-symmetry broken dimer at 1/2 filling, any Müller-like functional gives the exact result for the total energy, the occupation numbers and the spectral function calculated using the DIF method. Using the DER method, one gets the exact spectral function with $\alpha = 1$ and 1/2. This is due to the extreme simplicity of the system in presence of symmetry breaking. In this case, indeed, the ground-state wavefunction reads as $|\Psi_0\rangle = |1\uparrow, 2\downarrow\rangle$ (or, equivalently, $|\Psi_0\rangle = |1\downarrow, 2\uparrow\rangle$), the natural

orbitals are the site orbitals, and the occupation numbers are $n_{1\uparrow} = n_{2\downarrow} = 1$ and $n_{1\downarrow} = n_{2\uparrow} = 0$. The total energy, using a Müller-like functional, reads as

$$E[\{n_{i\sigma_i}\}] = \sum_{j,\sigma} h_j n_{j\sigma} + \frac{U}{2} \sum_{j,\sigma,\sigma'} n_{j\sigma} n_{j\sigma'} - \frac{U}{2} \sum_{j,\sigma} n_{j\sigma}^{2\alpha},$$

where $h_i = \epsilon_0$ and the sum runs over the sites. One can check that for the DIF method one gets

$$\epsilon_{i\sigma} = h_i + U n_{i\bar{\sigma}},$$

where $\bar{\sigma}$ is the spin opposite of σ, for any $1/2 \leq \alpha \leq 1$, from which $\epsilon_{1\uparrow} = \epsilon_{2\downarrow} = \epsilon_0$ and $\epsilon_{1\downarrow} = \epsilon_{2\uparrow} = \epsilon_0 + U$, as the exact result. For the DER method one gets

$$\epsilon_{i\sigma} = h_i + \left(U \sum_{\sigma'} n_{i\sigma'} - \alpha U n_{i\sigma}^{2\alpha-1} \right) \Bigg|_{n_{i\sigma}=1/2}.$$

For $\alpha = 1$ and $1/2$ the DER equation reduces to the DIF equation, which gives the exact spectral function. For other values of α, one gets $\epsilon_{1\uparrow} = \epsilon_{2\downarrow} = \epsilon_0 + U/2 - \alpha U/2^{2\alpha-1}$ and $\epsilon_{1\downarrow} = \epsilon_{2\uparrow} = \epsilon_{1\uparrow} + U$, which gives the exact band gap of U.

4.6 Occupation numbers and correlation

Occupation numbers are an indicator of correlation. However, what is observed is a result of measurements, and measurements change the system. One hence cannot look only at the occupation numbers of the initial system to understand observed correlation effects. For example, in Sec. 4.4.1, the Hubbard dimer at 1/4 filling has exact occupation numbers that are either zero or one. This is a clear example in which the occupation numbers indicate no correlation in the system, but there are correlation effects in the electron addition spectrum that one would measured, *e.g.*, in inverse photoemission. In this case, indeed, the spectrum shows, besides quasiparticle peaks, also a satellite (ω_6 in Fig. 4.3), which is a pure signature of correlation. Therefore whether a system "is" correlated or not depends on how one looks at it.

Let us examine this point further, by looking at the Hubbard dimer at 1/2 filling as example. In the atomic limit, the spin-singlet ground-state $|\Psi_0\rangle = 1/\sqrt{2}[|1\uparrow, 2\downarrow\rangle - |1\downarrow, 2\uparrow\rangle]$ becomes degenerate with the spin-symmetry broken state $|\Psi_0\rangle = |1\uparrow, 2\downarrow\rangle$ (or, equivalently, $|\Psi_0\rangle = |1\downarrow, 2\uparrow\rangle$), which is also an eigenstate of the system in this limit. We note that in the spin-symmetry broken case, both G_0W_0 and RDMFT within the Müller functional give the exact result for total energy, occupation numbers, and spectral function[7] (see Sec. 4.5). In this case the electrons have fixed positions and

[7]To be precise, RDMFT gives the exact total energy and occupation number for any Müller-like functional; the DIF method gives the exact spectral function for any Müller-like functional, whereas the DER method gives the exact results using Müller and HF

one does not need to consider explicitly the correlation between two particles. One can hence think that there is little correlation in this state. In reality, the system is correlated, but part of the correlation is included in the symmetry breaking.

4.6.1 Spectral function

Let us first focus on the spectral function. From Fig. 4.9 we see that the exact spectral function of the spin singlet (lowest right panel) shows two peaks, one at ϵ_0 and one at $\epsilon_0 + U$, both for spin-up and spin-down channels. For the spin-symmetry broken case, the components of the 1-GFs show the spin-symmetry breaking nature of the ground-state, *i.e.*, $G^{\uparrow}_{ii} \neq G^{\downarrow}_{ii}$ and $G^{\uparrow}_{11} = G^{\downarrow}_{22}$, $G^{\downarrow}_{11} = G^{\uparrow}_{22}$, and hence are different from the ones of the singlet case (all diagonal components are the same, all off-diagonal components are the same). However the spin-resolved total spectral function, *i.e.*,

$$A_\sigma(\omega) = \frac{1}{\pi} \sum_i \text{sign}(\mu - \omega) \, \text{Im} \, G^\sigma_{ii}(\omega),$$

is the same for the two spin structures: one can remove a spin-up or spin-down electron with energy ϵ_0, and can add a spin-up or spin-down electron with energy $\epsilon_0 + U$.[8]

4.6.2 Momentum distribution

Can the occupation numbers distinguish between the spin-singlet and spin-symmetry broken states? For the spin-singlet structure, the natural orbitals are the bonding/antibonding orbitals and the occupation numbers are $n_{b\uparrow} = n_{b\downarrow} = 1/2$ and $n_{a\uparrow} = n_{a\downarrow} = 1/2$ (see Fig. 4.2). For the spin-symmetry broken structure, characterized by a single Slater determinant, the natural orbitals are the site orbitals $\psi_{1\sigma/2\sigma} = (\phi_{b\sigma} \pm \phi_{a\sigma}) / \sqrt{2}$ with occupation numbers $n_{1\uparrow} = n_{2\downarrow} = 1$ and $n_{1\downarrow} = n_{2\uparrow} = 0$. Spin-resolved occupation numbers are, hence, different for the two spin structures. It is now interesting to examine whether this difference could be measured.

The most direct experimental route to access occupation numbers is Compton scattering. The Compton profile gives information about the momentum distribution, *i.e.*, the probability to observe a particle of momentum $\mathbf{p}$ (see, *e.g.*, Refs [56, 81]). This can be expressed in terms of the Fourier transform in momentum space of the density matrix, as

$$n(\mathbf{p}) \propto \int d\mathbf{r} d\mathbf{r}' e^{-i\mathbf{p}\cdot(\mathbf{r}-\mathbf{r}')} \gamma(\mathbf{r}, \mathbf{r}'), \tag{4.6}$$

where we defined $\gamma(\mathbf{r}, \mathbf{r}') = \sum_\sigma \sum_{ss'} \chi^*_\sigma(s) \gamma(\mathbf{x}, \mathbf{x}') \chi_\sigma(s')$, with $\chi_\sigma(s)$ the spin function, which is defined as $\chi_\uparrow(1/2) = \chi_\downarrow(-1/2) = 1$ and $\chi_\uparrow(-1/2) = \chi_\downarrow(1/2) = 0$. The Fourier

[8] In real materials, this is often observed. For example, in NiO no significant changes in the valence band structure are detected passing from the paramagnetic to the antiferromagnetc phase [108].

transform (4.6) gives the matrix elements of the density matrix in a basis of plane waves $\phi_{p\sigma}(\mathbf{r}, s) = 1/\sqrt{\Omega}\, e^{i\mathbf{p}\cdot\mathbf{r}}\chi_\sigma(s)$, which are the exact one-electron eigenfunctions of the free electron gas, *i.e.*, the perfectly translationally invariant system. The question is hence what one could observe looking at matrix elements of the density matrix in the basis of plane waves. The analogous basis for the Hubbard dimer which reflects the symmetry of the system is the bonding/antibonding basis $\{\phi_{b\sigma/a\sigma}\}$. Since this basis is the basis of natural orbitals for the spin-singlet system, in this case the analog of the Compton profile gives the occupation numbers $n_b = 1$ (with $n_{b\uparrow} = n_{b\downarrow} = 1/2$) and $n_a = 1$ (with $n_{a\uparrow} = n_{a\downarrow} = 1/2$). One gets the same result for the spin-symmetry broken structure. Note, however, that in this case, unlike for the spin-singlet structure, this distribution corresponds to density-matrix elements that are not occupation numbers. This is because the bonding/antibondig basis in which the density matrix is projected is not the basis of natural orbitals for the spin-symmetry broken structure. In fact, not even a spin-resolved "Compton profile" would distinguish between the two spin structures, since for the spin-broken symmetry structure, one gets the density-matrix elements $n_{b\sigma/a\sigma} = \int d\mathbf{x}d\mathbf{x}'\phi^*_{b\sigma/a\sigma}(\mathbf{x})\left[\sum_{i=1\uparrow,2\downarrow}\psi_i(\mathbf{x})\psi^*_i(\mathbf{x}')\right]\phi_{b\sigma/a\sigma}(\mathbf{x}') = 1/2$, as for the spin-singlet case. To distinguish between the two cases one should measure other aspects of the density matrix, for example, carry out a spin- and space-resolved measurement of the density matrix elements. In this case, the density matrix is projected in the site basis, which gives the density matrix elements $n_{1\uparrow} = n_{2\uparrow} = n_{1\downarrow} = n_{2\downarrow} = 1/2$ for the spin-singlet and the occupation numbers $n_{1\uparrow} = n_{2\downarrow} = 1$, $n_{1\downarrow} = n_{2\uparrow} = 0$ for the spin-symmetry broken case.

4.7 Conclusions

We analyzed the results for total energy, natural occupation numbers, removal/addition energies, and spectral function for the Hubbard dimer at 1/4 and 1/2 fillings by using Reduced Density-Matrix Functional Theory and Many-Body Perturbation Theory within standard approximations to electron correlation, namely Müller-like functionals and G_0W_0, respectively. In general, there is no Müller-like functional which works well at both one fourth and half filling: for the former the Hartree-Fock functional gives the exact total energy and occupation numbers, whereas for the latter the original Müller functional does the job. Other Müller-like functionals underestimate the total energy at 1/4 filling and overestimate it at 1/2 filling, like G_0W_0. The same behavior is found for the occupation numbers, which deviate in a similar way as G_0W_0 from the exact results.

We also analyzed various approximate methods to obtain removal/addition energies and spectral functions from RDMFT. Our results using the extended Koopmans theorem confirm its reliability for the calculation of removal energies and the lowest addition energy (for finite systems), if a good approximation to the two-body density matrix is used. However, the calculation of the addition energy relies on the $(N+1)$-

electron system; in this case, one has an anion, which might not be stable. Moreover, the EKT does not give higher addition energies nor the spectral function. These can be obtained using the approximate DIF/DER method. However, our results suggest a cancellation of errors between this method and Müller-like approximations to electron correlations. Moreover, we find that the spectral peaks are fewer than the exact ones and can have a mixed removal and addition nature as well as a mixed quasiparticle and satellite nature. These findings indicate that although an *ab initio* simulation of the spectral function of a real material using the DIF/DER method could be in agreement with experiment, the underlying physics is not correct.

At moderately strong interaction, the G_0W_0 method is superior. In the strongly correlated electron regime, which is obtained by stretching the dimer (atomic limit), we found that both the DIF/DER method and G_0W_0 fail for a spin-singlet ground-state, whereas they give the exact results for the spin-symmetry-broken case.

Our analysis shows that the failure of the DIF/DER method is mainly due to the approximation of removal/addition energies, rather than to the approximation of the spectral function itself. Therefore one should focus on better approximations to these energies, to improve the description of photoemission spectra. This will be the subject of Chap. 5

Because the Hubbard dimer is a simple test case, it shines light on the content, successes and limits of current RDMFT approaches and we believe that arguments like those based on symmetry and symmetry breaking can be safely generalized to improve our understanding of real systems.

Chapter 5

Photoemission spectra from reduced density matrices

We present a method for the calculation of photoemission spectra in terms of reduced density matrices. We start from the spectral representation of the 1-GF, whose imaginary part is related to photoemission spectra, and we introduce an effective energy that accounts for all the poles of the 1-GF. Simple approximations to this effective energy give accurate spectra in model systems in the weak as well as strong correlation regimes. To illustrate our method on real materials we apply it here to Reduced Density-Matrix Functional Theory, which is an efficient method to calculate one- and two-body reduced density matrices. We calculate the photoemission spectrum of bulk NiO, which is a paradigmatic example of strongly correlated materials: our method yields a qualitatively correct picture both in the antiferromagnetic and in the paramagnetic phases, contrary to currently used mean-field methods, which give a metal in the latter case.

5.1 Introduction

Photoemission is a powerful tool to obtain insight into the electronic structure of materials. The interpretation of the experimental data is, however, a complicated task. Theory represents, hence, an essential tool for the analysis of the experiments as well as the prediction of material properties. One of the most popular approaches in condensed-matter physics is Many-Body Perturbation Theory (MBPT) based on Green's functions. Within the so-called *GW* approximation [50] to electron correlation, MBPT has become, over the last two decades, the method of choice for the calculations of quasiparticle band structures [6, 7, 79, 113, 114, 117] and direct and inverse photo-emission spectra [17, 30, 37, 67, 84] of many materials, improving substantially over the results obtained with static mean-field electronic structure methods. However *GW* suffers from some fundamental shortcomings [15, 80, 91, 95, 102, 112], and, in particular, it does not describe strong correlation (without imposing a magnetic

ordering). A deep problem is, indeed, the description of the paramagnetic phase. A paradigmatic example is the case of paramagnetic NiO, which is described as a metal by *GW* (and by standard band structure theory). Qualitatively new approaches are hence needed and much effort is devoted to this goal both by going beyond standard methods [47–49, 68, 94, 100, 124] and by exploring novel routes to calculate Green's functions [11, 61]. In this context, promising results for solids have been reported using Reduced Density-Matrix Functional Theory (RDMFT) [99], which allows for the calculation of all the ground-state expectation values as functionals of the one-body reduced density matrix (1-RDM), provided that the functional is known. This is not the case for photoemission spectra, for which approximations are used. The RDMFT framework offers the advantage of being computationally more efficient than MBPT. However a systematic analysis of the currently used approximations for the calculation of photoemission spectra showed that the underlying physics is not correct, in particular in the strong correlation regime (see Chap. 4).

Describing strongly correlated systems with no magnetic ordering is beyond the state-of-the-art approximations employed in RDMFT and MBPT and it is nowadays one of the greatest challenge for condensed matter theory. In this work we derive an expression for the spectral function, which is related to photoemission spectra, in terms of reduced density matrices (RDMs). These latter can be very accurately calculated in quantum Monte Carlo (see, *e.g.*, [13, 83]). We show that simple approximations, which require the knowledge of the lowest n-RDMs only, can provide accurate photoemission spectra in model systems at moderate as well as at strong electron correlation. With the realistic example of bulk NiO we show that our method opens a gap both in the antiferromagnetic and paramagnetic phases.

This chapter is organized as follows. In Sec. 5.2 we derive a method to calculate the spectral function in terms of RDMs; the physical meaning and some general aspects of the method are discussed in Sec. 5.3. The method is applied to Hubbard rings in Sec. 5.4 and to bulk NiO, as an example of a strongly correlated real material, in Sec. 5.5.

5.2 The effective-energy technique for the spectral function

The spectral function can be expressed in terms of the imaginary part of the 1-GF as $A(\omega) = \mathrm{sign}(\mu - \omega)\,\mathrm{Im}\,G(\omega)/\pi$ (see Sec. 3.1.3). Our goal is to derive an expression for $A(\omega)$ in terms of RDMs only. We start from the spectral representation of G at zero temperature, which reads as (see Sec. 3.1.2)

$$G_{ij}(\omega) = \sum_k \frac{B_{ij}^{k,R}}{\omega - \epsilon_k^R - \mathrm{i}\eta} + \sum_k \frac{B_{ij}^{k,A}}{\omega - \epsilon_k^A + \mathrm{i}\eta}, \tag{5.1}$$

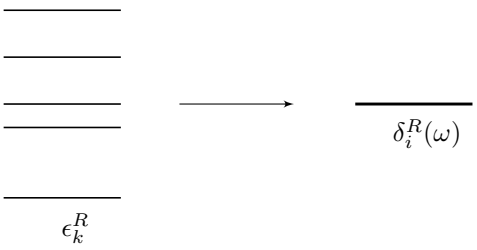

Figure 5.1: A pictorial representation of the idea of the effective-energy technique: the frequency-dependent effective energy $\delta_i^R(\omega)$ is introduced to account for all the poles ϵ_k^R of the removal part of the 1-GF.

where $\epsilon_k^R = E_0 - E_k^{N-1}$, $\epsilon_k^A = E_k^{N+1} - E_0$, $B_{ij}^{k,R} = \langle\Psi_0|\hat{c}_j^\dagger|\Psi_k^{N-1}\rangle\langle\Psi_k^{N-1}|\hat{c}_i|\Psi_0\rangle$, $B_{ij}^{k,A} = \langle\Psi_0|\hat{c}_i|\Psi_k^{N+1}\rangle\langle\Psi_k^{N+1}|\hat{c}_j^\dagger|\Psi_0\rangle$, with E_0 and Ψ_0 the ground-state energy and wavefunction of the N-electron system and $E_k^{N\pm1}$ and $\Psi_k^{N\pm1}$ the energies and wavefunctions of the $N \pm 1$-electron system. Here $\hat{c}_i^\dagger$ and $\hat{c}_i$ are the creation and annihilation operators. The subscripts i and j combine both space and spin indices. The superscripts 'R' and 'A' in (5.1) indicate the removal and addition parts of G, respectively.

In the following we concentrate on the diagonal elements of G, which are needed to calculate photoemission spectra. We choose to work in the basis of natural orbitals ϕ_i, *i.e.*, the orbitals which diagonalize the 1-RDM, $\gamma(\mathbf{x},\mathbf{x}') = \sum_i n_i\phi_i(\mathbf{x})\phi_i^*(\mathbf{x}')$, where n_i are the occupation numbers. In this basis $\sum_k B_{ii}^{k,R} = n_i$ and $\sum_k B_{ii}^{k,A} = (1 - n_i)$.

Let us first concentrate on the removal part. Inspired by the effective-energy technique (EET) proposed in Refs [9, 10] to get rid of the infinite sum over unoccupied states in the self-energy, we introduce an effective energy $\delta_i^R(\omega)$ such that

$$\sum_k \frac{B_{ii}^{k,R}}{\omega - \epsilon_k^R} = \frac{\sum_k B_{ii}^{k,R}}{\omega - \delta_i^R(\omega)} = \frac{n_i}{\omega - \delta_i^R(\omega)}. \tag{5.2}$$

The diagonal part of the 1-GF is thus given by

$$G_{ii}^R(\omega) = \frac{n_i}{\omega - \delta_i^R(\omega)}. \tag{5.3}$$

The effective energy $\delta_i^R(\omega)$ accounts for all the poles of the removal part of G_{ij} (see Fig. 5.1 for an illustration of this idea).

If we know $\delta_i^R(\omega)$ we can get all the (removal) poles of G. How can we determine $\delta_i^R(\omega)$? From Eq. (5.2) we have

$$\sum_k B_{ii}^{k,R}\left[\frac{1}{\omega - \epsilon_k^R} - \frac{1}{\omega - \delta_i^R(\omega)}\right] = 0.$$

After putting everything on common denominator we arrive at

$$\begin{aligned}\overbrace{\sum_k \frac{B_{ii}^{k,R}}{\omega-\epsilon_k^R}}^{G_{ii}^R(\omega)}\delta_i^R(\omega) &= \sum_k \frac{B_{ii}^{k,R}}{\omega-\epsilon_k^R}\epsilon_k^R \\ &= \sum_k \frac{\langle\Psi_0|\hat{c}_i^\dagger|\Psi_k^{N-1}\rangle\langle\Psi_k^{N-1}|\hat{c}_i|\Psi_0\rangle}{\omega-\epsilon_k^R}\epsilon_k^R \\ &= \sum_k \frac{\langle\Psi_0|\hat{c}_i^\dagger|\Psi_k^{N-1}\rangle\langle\Psi_k^{N-1}|[\hat{c}_i,\hat{H}]|\Psi_0\rangle}{\omega-\epsilon_k^R},\end{aligned} \tag{5.4}$$

where we introduced the Hamiltonian operator $\hat{H}$, and from its action on the $(N-1)$-electron and N-electron wavefunctions we get $E_0 - E_k^{N-1} = \epsilon_k^R$. From Eq. (5.4) we get

$$\delta_i^R(\omega) = \frac{1}{G_{ii}^R(\omega)}\sum_k \frac{\langle\Psi_0|\hat{c}_i^\dagger|\Psi_k^{N-1}\rangle\langle\Psi_k^{N-1}|[\hat{c}_i,\hat{H}]|\Psi_0\rangle}{\omega-\epsilon_k^R}. \tag{5.5}$$

We note that Eq. 5.5 is an exact expression for $\delta_i^R(\omega)$.

Similarly for the addition energies one gets

$$\begin{aligned}\overbrace{\sum_k \frac{B_{ii}^{k,A}}{\omega-\epsilon_k^A}}^{G_{ii}^A(\omega)}\delta_i^A(\omega) &= \sum_k \frac{B_{ii}^{k,A}}{\omega-\epsilon_k^A}\epsilon_k^A \\ &= \sum_k \frac{\langle\Psi_0|\hat{c}_i|\Psi_k^{N+1}\rangle\langle\Psi_k^{N+1}|\hat{c}_i^\dagger|\Psi_0\rangle}{\omega-\epsilon_k^A}\epsilon_k^A \\ &= \sum_k \frac{\langle\Psi_0|[\hat{c}_i,\hat{H}]|\Psi_k^{N+1}\rangle\langle\Psi_k^{N+1}|\hat{c}_i^\dagger|\Psi_0\rangle}{\omega-\epsilon_k^A}.\end{aligned} \tag{5.6}$$

From Eq. (5.6) we get

$$\delta_i^A(\omega) = \frac{1}{G_{ii}^A(\omega)}\sum_k \frac{\langle\Psi_0|[\hat{c}_i,\hat{H}]|\Psi_k^{N+1}\rangle\langle\Psi_k^{N+1}|\hat{c}_i^\dagger|\Psi_0\rangle}{\omega-\epsilon_k^A}. \tag{5.7}$$

Note that $\delta_i^R \neq \delta_i^A$, so that we have an effective energy for the removal part and an effective energy for the addition part.

Using Eq. (3.12) together with Eq. (5.3) (and an analogous expression for the addition part), the spectral function can then be written as

$$A_{ii}(\omega) = n_i\delta(\omega-\delta_i^R(\omega)) + (1-n_i)\delta(\omega-\delta_i^A(\omega)), \tag{5.8}$$

which satisfies the well-known sum rule $\int_{-\infty}^{\infty} A_{ii}(\omega)d\omega = 1$ (see Sec. 3.1.3). We note that this expression is similar to the one obtained by Sharma *et al.* [99] through a

different derivation in the context of RDMFT. What is different in our approach is the way to determine the removal and addition energies. In the approach of Ref. [99] they are calculated in an approximate way as functional derivatives of the ground-state total energy with respect to the occupation numbers, so that one has as many energies as occupation numbers, which, in general, are less than the true number of energies (see Chap. 4). In the following we will refer to this approach as the DER method. Our approach is based on Eqs (5.5) and (5.7), which are exact, but not very useful in practice because one needs $|\Psi_0\rangle$, $\left|\Psi_k^{N\pm1}\right\rangle$ and $G_{ii}^{R/A}(\omega)$. Approximations to $\delta_i^{R/A}(\omega)$ are therefore needed. In the following we show how to find them.

5.2.1 The method

Here we derive approximate expressions for $\delta_i^R(\omega)$ and $\delta_i^A(\omega)$ and we relate them to RDMs.

A. Approximations for $\delta_i^R(\omega)$

Equation (5.5) can be rewritten as

$$\delta_i^R(\omega) = \frac{\tilde{G}_{ii}^R(\omega)}{G_{ii}^R(\omega)}, \tag{5.9}$$

where we introduced the quantity

$$\tilde{G}_{ii}^R(\omega) = \sum_k \frac{\langle\Psi_0|\hat{c}_i^\dagger|\Psi_k^{N-1}\rangle\langle\Psi_k^{N-1}|[\hat{c}_i,\hat{H}]|\Psi_0\rangle}{\omega-\epsilon_k^R}.$$

We also define the following quantity

$$\tilde{n}_i^R = \sum_k \langle\Psi_0|\hat{c}_i^\dagger|\Psi_k^{N-1}\rangle\langle\Psi_k^{N-1}|[\hat{c}_i,\hat{H}]|\Psi_0\rangle = \langle\Psi_0|\hat{c}_i^\dagger[\hat{c}_i,\hat{H}]|\Psi_0\rangle, \tag{5.10}$$

where we used the completeness relation $\sum_k \left|\Psi_k^{N-1}\right\rangle\left\langle\Psi_k^{N-1}\right| = \hat{1}$. We can now use the same trick for $\tilde{G}_{ii}^R(\omega)$, by introducing another effective energy $\tilde{\delta}_i^R(\omega)$. We get

$$\tilde{G}_{ii}^R(\omega) = \frac{\tilde{n}_i^R}{\omega-\tilde{\delta}_i^R(\omega)}, \tag{5.11}$$

from which it follows that

$$\tilde{G}_{ii}^R(\omega)\tilde{\delta}_i^R(\omega) = \sum_k \frac{\langle\Psi_0|[\hat{H},\hat{c}_i^\dagger]|\Psi_k^{N-1}\rangle\langle\Psi_k^{N-1}|[\hat{c}_i,\hat{H}]|\Psi_0\rangle}{\omega-\epsilon_k^R}. \tag{5.12}$$

From Eq. (5.12) we obtain the relation

$$\tilde{\delta}_i^R(\omega) = \frac{\tilde{\tilde{G}}_{ii}^R(\omega)}{\tilde{G}_{ii}^R(\omega)}, \tag{5.13}$$

with

$$\tilde{\tilde{G}}^R_{ii}(\omega) = \sum_k \frac{\langle\Psi_0|[\hat{H},\hat{c}_i^\dagger]|\Psi_k^{N-1}\rangle\langle\Psi_k^{N-1}|[\hat{c}_i,\hat{H}]|\Psi_0\rangle}{\omega-\epsilon_k^R} = \frac{\tilde{\tilde{n}}_i^R}{\omega-\tilde{\tilde{\delta}}_i^R(\omega)}.$$

In the last step we introduced the the effective energy $\tilde{\tilde{\delta}}_i^R(\omega)$ and the term

$$\begin{aligned}\tilde{\tilde{n}}_i^R &= \sum_k \big\langle\Psi_0\big|[\hat{H},\hat{c}_i^\dagger]\big|\Psi_k^{N-1}\big\rangle\big\langle\Psi_k^{N-1}\big|[\hat{c}_i,\hat{H}]\big|\Psi_0\big\rangle \\ &= \langle\Psi_0|[\hat{H},\hat{c}_i^\dagger][\hat{c}_i,\hat{H}]|\Psi_0\rangle, \end{aligned} \tag{5.14}$$

where we used again the completeness relation. Combining Eqs (5.3), (5.9), (5.11) and (5.13) we arrive at

$$\delta_i^R(\omega) = \frac{\frac{\tilde{n}_i^R}{\omega-\tilde{\delta}_i^R(\omega)}}{\frac{n_i}{\omega-\delta_i^R(\omega)}} = \frac{\frac{\tilde{n}_i^R}{\omega-\frac{\tilde{\tilde{G}}_{ii}^R(\omega)}{\tilde{G}_{ii}^R(\omega)}}}{\frac{n_i}{\omega-\frac{\tilde{G}_{ii}^R(\omega)}{G_{ii}^R(\omega)}}} = \frac{\tilde{n}_i^R}{n_i}\frac{\omega-\frac{\tilde{G}_{ii}^R(\omega)}{G_{ii}^R(\omega)}}{\omega-\frac{\tilde{\tilde{G}}_{ii}^R(\omega)}{\tilde{G}_{ii}^R(\omega)}}.$$

In principle, one can continue this procedure *ad infinitum*. In practice, however, one would like to truncate this series to have something that is simple to calculate. This can be done in various ways. Here we choose a truncation similar, but not the same, to the one adopted in the original paper on the effective energy technique [9],[1] which guarantees the exact result for the Hubbard dimer at all orders $n \geq 1$, as we will discuss in Sec. 5.4. Here we give the first two approximations to $\delta_i^R(\omega)$, which read as

$$\delta_i^{R,(1)} = \frac{\tilde{n}_i^R}{n_i}, \tag{5.15}$$

$$\delta_i^{R,(2)}(\omega) = \frac{\tilde{n}_i^R}{n_i}\frac{\omega-\frac{\tilde{n}_i^R}{n_i}}{\omega-\frac{\tilde{\tilde{n}}_i^R}{\tilde{n}_i^R}}. \tag{5.16}$$

B. Approximations for $\delta_i^A(\omega)$

One can derive similar relations for $\delta_i^A(\omega)$:

$$\delta_i^A(\omega) = \frac{\tilde{n}_i^A}{1-n_i}\frac{\omega-\frac{\tilde{G}_{ii}^A(\omega)}{G_{ii}^A(\omega)}}{\omega-\frac{\tilde{\tilde{G}}_{ii}^A(\omega)}{\tilde{G}_{ii}^A(\omega)}},$$

[1] In the original paper the various commutators with the Hamiltonian are worked out to separate the one-particle part. For example $[\hat{c}_i,\hat{H}] = h_{ii}\hat{c}_i + [\hat{c}_i,\hat{V}]$, where $\hat{V}$ is the two-particle interaction operator. For $\delta^{R,(1)}$, this is equivalent to our formulation, but it gives a different expression for $\delta^{R,(n)}$ with $n \geq 2$. We found that the formulation adopted in this chapter gives a simpler physical meaning to the approximate $\delta^{R,(n)}$. This is discussed in Sec. 5.3.

with

$$\tilde{G}^A_{ii}(\omega) = \sum_k \frac{\langle\Psi_0|[\hat{c}_i, \hat{H}]|\Psi^{N+1}_k\rangle\langle\Psi^{N+1}_k|\hat{c}^\dagger_i|\Psi_0\rangle}{\omega - \epsilon^A_k} = \frac{\tilde{n}^A_i}{\omega - \tilde{\delta}^A_{i\sigma}(\omega)},$$

and

$$\tilde{n}^A_i = \sum_k \langle\Psi_0|[\hat{c}_i, \hat{H}]|\Psi^{N+1}_k\rangle\langle\Psi^{N+1}_k|\hat{c}^\dagger_i|\Psi_0\rangle = \langle\Psi_0|[\hat{c}_i, \hat{H}]\hat{c}^\dagger_i|\Psi_0\rangle, \tag{5.17}$$

where we used the completeness relation $\sum_k |\Psi^{N+1}_k\rangle\langle\Psi^{N+1}_k| = \hat{1}$. At the second order we have

$$\tilde{\tilde{G}}^A_{ii}(\omega) = \sum_k \frac{\langle\Psi_0|[\hat{c}_i, \hat{H}]|\Psi^{N+1}_k\rangle\langle\Psi^{N+1}_k|[\hat{H}, \hat{c}^\dagger_i]|\Psi_0\rangle}{\omega - \epsilon^A_k} = \frac{\tilde{\tilde{n}}^A_i}{\omega - \tilde{\tilde{\delta}}^A_{i\sigma}(\omega)},$$

with

$$\tilde{\tilde{n}}^A_i = \sum_k \langle\Psi_0|[\hat{c}_i, \hat{H}]|\Psi^{N+1}_k\rangle\langle\Psi^{N+1}_k|[\hat{H}, \hat{c}^\dagger_i]|\Psi_0\rangle = \langle\Psi_0|[\hat{c}_i, \hat{H}][\hat{H}, \hat{c}^\dagger_i]|\Psi_0\rangle, \tag{5.18}$$

where we used again the completeness relation. Several approximations to $\delta^A_i(\omega)$ can be obtained. The first two read as

$$\delta^{A,(1)}_i = \frac{\tilde{n}^A_i}{1 - n_i}, \tag{5.19}$$

$$\delta^{A,(2)}_i(\omega) = \frac{\tilde{n}^A_i}{1 - n_i} \frac{\omega - \frac{\tilde{n}^A_i}{1-n_i}}{\omega - \frac{\tilde{\tilde{n}}^A_i}{\tilde{n}^A_i}}. \tag{5.20}$$

C. $\delta^R_i(\omega)$ and $\delta^A_i(\omega)$ in terms of reduced density matrices

In the following we express $\delta^{R/A}_i(\omega)$ in terms of RDMs. Let us consider the following many-body Hamiltonian

$$\hat{H} = \hat{H}_0 + \hat{V} = \sum_{ij} h_{ij}\hat{c}^\dagger_i\hat{c}_j + \frac{1}{2}\sum_{ijkl} V_{ijkl}\hat{c}^\dagger_i\hat{c}^\dagger_j\hat{c}_l\hat{c}_k \tag{5.21}$$

where $\hat{c}^\dagger_i$ and $\hat{c}_i$ are the creation and annihilation operators in the basis of natural orbitals $\phi_i(\mathbf{x})$. Here $h_{ij} = \int d\mathbf{x}\phi^*_i(\mathbf{x})h(\mathbf{r})\phi_j(\mathbf{x})$ are the matrix elements of the one-particle noninteracting Hamiltonian $h(\mathbf{r}) = -\nabla^2/2 + v_{\text{ext}}(\mathbf{r})$, and

$$V_{ijkl} = \int d\mathbf{x}d\mathbf{x}'\phi^*_i(\mathbf{x})\phi^*_j(\mathbf{x}')v_c(\mathbf{r}, \mathbf{r}')\phi_k(\mathbf{x})\phi_l(\mathbf{x}'),$$

are the matrix elements of the Coulomb interaction v_c. Using the Hamiltonian (5.21), we can evaluate the commutators in Eqs (5.10), (5.14), (5.17), and (5.18) (see App. D) obtaining the following relations

$$\tilde{n}^R_i = h_{ii}n_i + \sum_{jkl} V_{ijkl}\Gamma^{(2)}_{klji}, \tag{5.22}$$

$$\tilde{\tilde{n}}_i^R = h_{ii}^2 n_i + h_{ii} \sum_{jkl} \left(V_{ijkl}\Gamma^{(2)}_{klji} + V_{klij}\Gamma^{(2)}_{ijlk} \right) + \sum_{jklqs} V_{klij}V_{ijqs}\Gamma^{(2)}_{qslk} + \sum_{jklpqs} V_{klij}V_{ipqs}\Gamma^{(3)}_{qjsplk}, \tag{5.23}$$

$$\tilde{n}_i^A = h_{ii}(1-n_i) + \sum_j V_{ijij}n_j - \sum_j V_{ijji}n_j - \sum_{jkl} V_{ijkl}\Gamma^{(2)}_{klji}, \tag{5.24}$$

$$\begin{aligned}\tilde{\tilde{n}}_i^A = {} & h_{ii}^2(1-n_i) + 2h_{ii}\sum_j (V_{ijij}n_j - V_{jiij}n_j) - \sum_{jlk} V_{klij}\Gamma^{(2)}_{ijlk} - \sum_{jlk} V_{ijkl}\Gamma^{(2)}_{klji} \\ & + \sum_{jkl} V_{ijkl}V_{klij}n_j - \sum_{jkl} V_{ijkl}V_{lkij}n_j + \sum_{jklspq} \delta_{kp}V_{ijkl}V_{pqis}\Gamma^{(2)}_{lsqj} \\ & - \sum_{jklspq} V_{ijkl}V_{pqis}\left(\delta_{lp}\Gamma^{(2)}_{ksqj} + \delta_{kq}\Gamma^{(2)}_{sljp} + \delta_{lq}\Gamma^{(2)}_{ksjp} \right) \\ & - \sum_{jklspq} V_{ijkl}V_{pqis}\Gamma^{(3)}_{klsqjp}.\end{aligned} \tag{5.25}$$

where $\Gamma^{(2)}_{ijkl} = \langle\Psi_0|\, \hat{c}_l^\dagger \hat{c}_k^\dagger \hat{c}_j \hat{c}_i \,|\Psi_0\rangle$ and $\Gamma^{(3)}_{ijklmn} = \langle\Psi_0|\hat{c}_n^\dagger \hat{c}_m^\dagger \hat{c}_l^\dagger \hat{c}_k \hat{c}_j \hat{c}_i|\Psi_0\rangle$ are the matrix elements of the 2-RDM and 3-RDM, respectively. Using Eqs (5.22)-(5.25) in Eqs (5.15),(5.16) and (5.19), (5.20), we get the expressions of $\delta_i^{R/A,(1)}$ and $\delta_i^{R/A,(2)}$ in terms of RDMs. Here for simplicity we give only the expressions of $\delta_i^{R/A,(1)}$, they read as

$$\delta_i^{R,(1)} = h_{ii} + \frac{1}{n_i}\sum_{jkl} V_{ijkl}\Gamma^{(2)}_{klji}, \tag{5.26}$$

$$\delta_i^{A,(1)} = h_{ii} + \frac{1}{1-n_i}\left(\sum_j V_{ijij}n_j - \sum_j V_{ijji}n_j - \sum_{jkl} V_{ijkl}\Gamma^{(2)}_{klji} \right). \tag{5.27}$$

Using Eq. (5.8) together with $\delta^{R/A,(n)}$ we can finally express the spectral function in terms of RDMs.

Before showing how these approximations perform in Sec. 5.4, in the next section we will discuss some general aspects of the method and its physical meaning.

5.3 General aspects and physical meaning

It would be interesting to understand the physical content of the effective energy $\delta_i^{R/A,(n)}$. In the following we get some insight into this aspect.

5.3.1 Relation between approximate and exact poles

Let us first show how the approximate poles of the 1-GF obtained using $\delta_i^{R/A,(n)}$ are related to the exact poles $\epsilon_k^{R/A}$. Let us start looking at and $\delta_i^{R/A,(1)}$. Using Eq. (5.10)

one can rewrite Eq. (5.15) in the following way

$$\begin{aligned}\delta_i^{R,(1)} &= \frac{1}{n_i}\sum_k \langle\Psi_0|\hat{c}_i^\dagger|\Psi_k^{N-1}\rangle\langle\Psi_k^{N-1}|[\hat{c}_i,\hat{H}]|\Psi_0\rangle \\ &= \frac{1}{n_i}\sum_k \langle\Psi_0|\hat{c}_i^\dagger|\Psi_k^{N-1}\rangle\langle\Psi_k^{N-1}|\hat{c}_i|\Psi_0\rangle\epsilon_k^R \\ &= \frac{\sum_k B_{ii}^{k,R}\epsilon_k^R}{\sum_k B_{ii}^{k,R}},\end{aligned}$$

where in the first step we used the fact that from the action of the Hamiltonian in the commutator on the $(N-1)$-electron and N-electron wavefunctions we get $E_0 - E_k^{N-1} = \epsilon_k^R$. Therefore, for each component G_i^R, $\delta_i^{R,(1)}$ gives a weighted average of all exact removal poles ϵ_k^R. In other words $\delta_i^{R,(1)}$ is equal to the first moment of the spectral function, which we defined as $\mu_{1,i}^R = \sum_k F_i^{k,R}\epsilon_k$, with $F_i^{k,R} = B_{ii}^{k,R}/n_i$. A similar relation can be derived for $\delta_i^{A,(1)}$.

These considerations can be extended to $\delta_i^{R/A,(2)}$. We found that that the first and second moments of the approximate spectral function generated by $\delta_i^{(2),R/A}$ are equal to the first and second moments of the exact spectral function. Here by second moment we mean the quantity $\mu_{2,i}^R = \sum_k F_i^{k,R}(\epsilon_k^R)^2$. For $\delta^{R/A,(n)}$ with $n > 2$ higher moments are involved.[2]

5.3.2 Total energy

We will now show that, thanks to the fact that the first moment $\mu_{1,i}^R$ of the approximate spectral function is equal to the exact one, the total energy calculated using the 1-GF (5.3) is exact, provided that the exact RDMs are used. Indeed, using the Galitski-Migdal formula (3.15) together with the exact 1-GF, the total energy can be expressed in terms of $\mu_{1,i}^R$ and n_i

$$E_0 = \frac{1}{2}\sum_i \left(\sum_k B_{ii}^{k,R}\epsilon_k + n_i h_{ii}\right) = \frac{1}{2}\sum_i n_i\left(\mu_{1,i}^R + h_{ii}\right).$$

Here we used the fact that Eq. (3.15) does not depend on the basis set, so we chose the natural orbital basis. Since the approximate $\delta_i^{R/A,(n)}$ $(n \geq 1)$ produces the exact first moment, the total energy obtained from the corresponding approximate 1-GF is exact.

5.3.3 Relation to the self-energy

At the level of Hartree-Fock (HF), $\delta_i^{R/A,(1)}$ yield the same removal/addition energies as the HF self-energy. In this case, indeed, $\delta_i^{R,(1)} = \delta_i^{A,(1)}$ (as it can be checked using

[2]We verified numerically that similar expressions are satisfied for $n > 2$, at least up to $n = 4$.

the HF 2-RDM, $\Gamma^{(2)}_{ijkl} = n_i n_j(\delta_{il}\delta_{jk} - \delta_{ik}\delta_{jl})$, in Eqs (5.26) and (5.27)) and

$$\delta_i^{R/A,(1)} = h_{ii} + \sum_j \left[V_{ijij} n_j - V_{ijji} n_j\right],$$

(as it can be seen from Eqs (5.15) and (5.22)), which corresponds to the poles of G obtained using the HF self-energy. Beyond HF the link with the self-energy is not straightforward. However, using the Dyson equation $G = G_0 + G_0 \Sigma G$ for G^R and G^A separately, with G_0 the non-interacting G and $\Sigma = -\mathrm{i} v_c G^{(2)} G^{-1}$ the self-energy ($G^{(2)}$ being the two-particle Green's function), one can derive $\delta^{R/A,(1)}$ assuming the non-interacting Green's function diagonal in the basis of natural orbitals and $G^{(2)}$ and G instantaneous.

5.4 Application to Hubbard rings

First we use the Hubbard model as a test system. Sufficiently small Hubbard clusters can be solved with exact diagonalization methods [3, 24] and, in particular, we can calculate the exact n-RDM. In the following we will test the EET method, both with exact and approximate RDMs.

5.4.1 Hubbard rings: exact reduced density matrices

For the Hubbard dimer at 1/2 filling the method is exact for all $\delta^{R/A(n)}$ with $n \geq 1$ (see App. E). Note that a similar result has been found for the HEG in Ref. [9] where the effective energy technique is applied in another context. The case with more sites at 1/2 filling is highly non trivial. However, for small chains, the simple approximation $\delta^{R/A,(1)}$ suffices to give an accurate spectrum at any interaction strength. As illustration we report the results for a four-site ring at 1/2 filling in Fig. 5.2. There are two striking features of the results obtained with our method: (i) the appearance of satellites, even with a static approximation ($\delta^{(1)}$), *i.e.*, more energies than the number of occupation numbers; (ii) the description of the gap in the atomic limit without breaking the symmetry of the system (*i.e.*, without localizing the electrons each on a site). The first feature can be understood by looking at the spectral weights in the spectral function (5.8), which are n_i for the removal energies and $1 - n_i$ for the addition energies. As long as the occupation numbers are 0 or 1, as in the noninteracting case, for each n_i one gets either a removal quasiparticle energy or an addition quasiparticle energy. When, instead, $0 < n_i < 1$, then, for each n_i one gets both a removal and an addition energy. It is essential to have two different expressions for $\delta^{R,(1)}$ and $\delta^{A,(1)}$ for each orbital in order to get two energies. These two energies are related by

$$\delta_i^{A,(1)} = \delta_i^{R,(1)} + \frac{1}{n_i(n_i-1)} \sum_{jkl} V_{ijkl} \Gamma^{(2),}_{c,klji}, \tag{5.28}$$

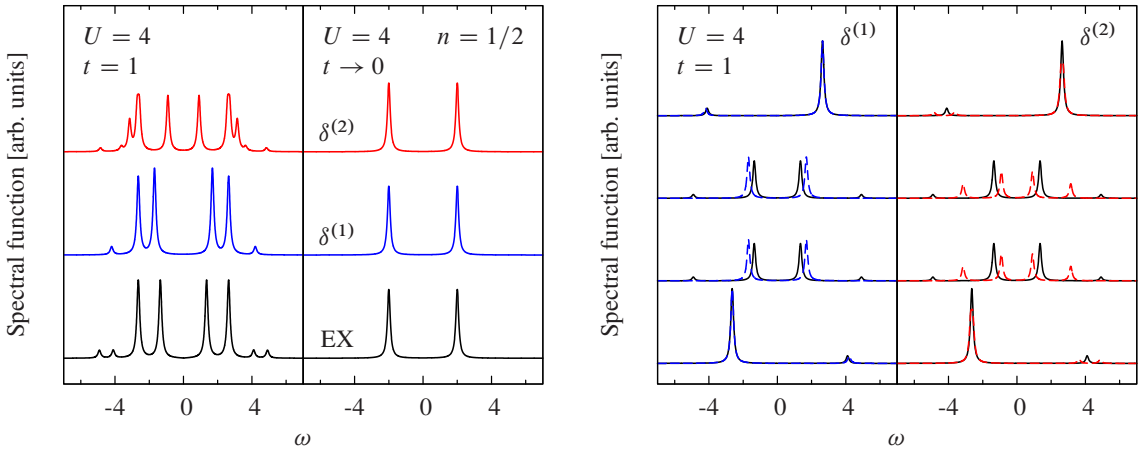

Figure 5.2: Spectral function for a 4-site Hubbard ring at 1/2 filling: (left) exact (lower panel) *vs.* EET ($\delta^{(1)}$ and $\delta^{(2)}$, with exact 1-, 2- and 3-RDMs) (middle and upper panels, respectively); (right) the spectral function is resolved by components in the natural orbitals basis set; for each component $\delta^{(1)}$ (dashed blue lines) and $\delta^{(2)}$ (dashed red lines) are compared with the exact spectral function (black solid lines).

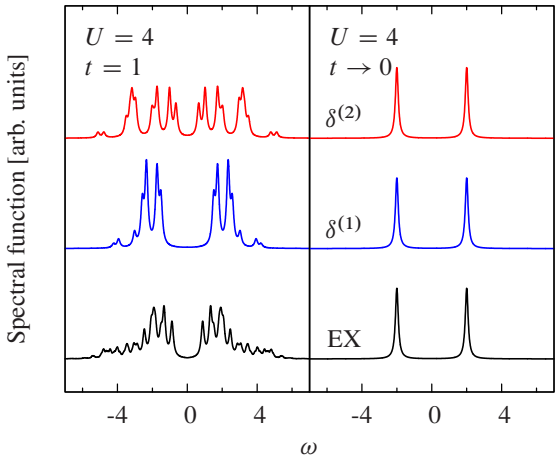

Figure 5.3: Spectral function for a 12-site Hubbard ring at 1/2 filling: exact (lower panel) *vs.* EET ($\delta^{(1)}$ and $\delta^{(2)}$, with exact 1-, 2- and 3-RDMs) (middle and upper panels, respectively).

where $\Gamma^{(2)}_{c,klji}$ is the correlation contribution to the 2-RDM. In the Hubbard dimer at 1/2 filling (see App. E), for example, $\sum_{jkl} V_{ijkl}\Gamma^{(2)}_{c,klji} = -Un_i$, which, when used in Eq. (5.28), opens a gap of U in the atomic limit (in this limit the occupation numbers tend to 1/2, as shown in Fig. 4.2).

As already discussed in Sec. 5.3 for each component G^R_i (G^A_i), $\delta^{R,(1)}_i$ ($\delta^{A,(1)}_i$) gives a weighted average of all exact removal (addition) poles; at 1/2 filling this produces a slight overestimation of the band gap, however the spectral shape is in good agreement with the exact one as a consequence of the fact that these averages, in this case, are close to the predominant poles for any U.

When we consider larger chains, at the level of $\delta^{(1)}$, the spectral shape is still acceptable, however the overestimation of the band gap is more evident, as can be seen in Fig. 5.3, where we present the case of a 12-site ring. For extended real systems

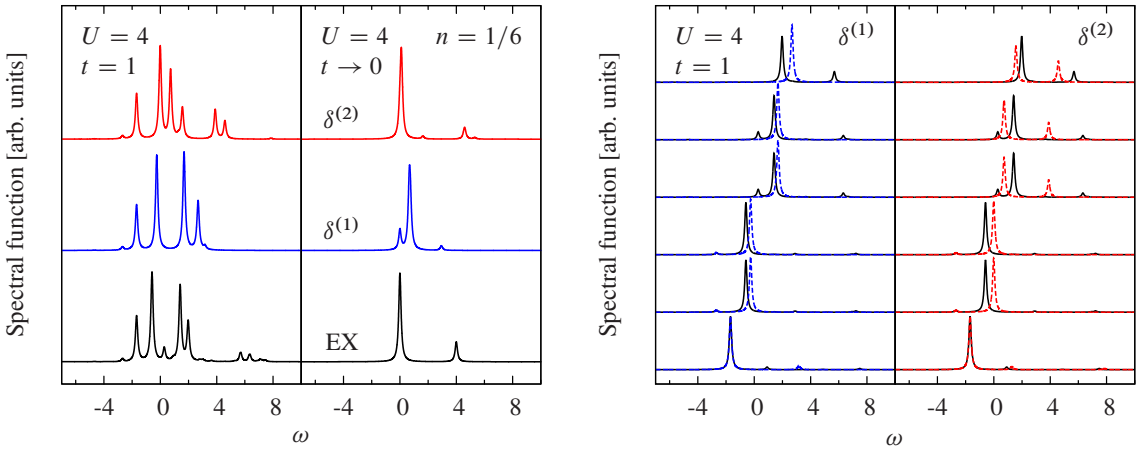

Figure 5.4: Spectral function for a 6-site Hubbard ring at 1/6 filling: (left) exact (lower panel) *vs.* EET ($\delta^{(1)}$ and $\delta^{(2)}$, with exact 1-, 2- and 3-RDMs) (middle and upper panels, respectively); (right) the spectral function is resolved by components in the natural orbitals basis; for each component $\delta^{(1)}$ and $\delta^{(2)}$ are compared with the exact spectral function.

one may expect a similar trend. One has to go to $\delta^{(2)}$, which requires the knowledge of the 3-RDM as well, to correct this overestimation (there is in fact a slight tendency to underestimate the gap). In this case the spectral shape improves in the gap region (see the range $-2 < \omega < 2$ in Fig. 5.3). However two structures appear (around $\omega = \pm 3$) which are not present in the exact spectrum, in which the spectral weight is distributed more uniformly in this region.

Away from 1/2 filling, one has to go to $\delta^{(2)}(\omega)$ to have good spectra in the atomic limit (see Fig. 5.4). Indeed, in this limit, $\delta^{(1)}$ opens a band gap around $\omega = 0$; in the exact case there is only one peak which is a superposition of a removal and addition peak. This indicates that $\delta^{(1)}$ is not a good approximation in metallic systems, because it tends to open a gap, unless $\alpha = 1$. Using $\delta^{(2)}(\omega)$ tends to correct these errors.

5.4.2 Hubbard rings: approximate reduced density matrices

We now see how the EET method performs with approximate RDMs. Here we concentrate on $\delta^{(1)}$ and we use the power functional to approximate the 2-RDM, both in the total energy functional and in the expression for $\delta^{(1)}$. Total energy minimization provides us with the occupation numbers to feed into $\delta^{(1)}$.

In Fig. 5.5 we illustrate the results of the EET method at the level of $\delta^{(1)}$, with approximate RDMs using the Müller functional both at 1/2 and 1/6 filling. When used with our method this approximation gives good results for the Hubbard model at 1/2 filling, and, in particular, it opens the gap in the atomic limit (for $\alpha = 0.5$ we retrieve the correct gap), without recurring to any symmetry breaking (see Chap. 4). However we observe that the gap width strongly depends on the value of α, being maximal at $\alpha = 0.5$ and disappearing at $\alpha = 1$. The maximum gap, obtained for

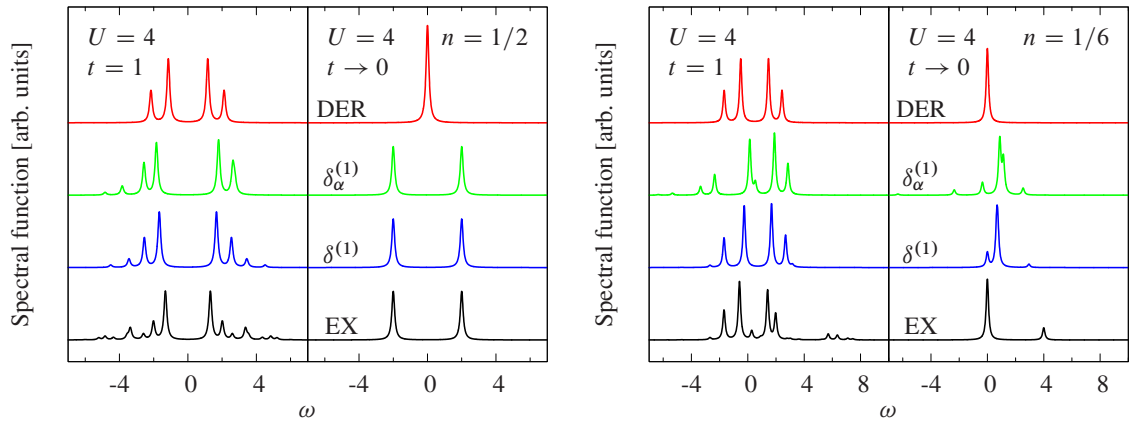

Figure 5.5: Spectral function for a 6-site Hubbard ring at 1/2 filling (left) and 1/6 filling (right): exact (lower panel) *vs.* EET ($\delta^{(1)}$) with exact 1- and 2-RDMs, EET ($\delta^{(1)}_\alpha$, $\alpha = 0.5$) with approximate 1- and 2-RDMs, and DER method ($\alpha = 0.5$).

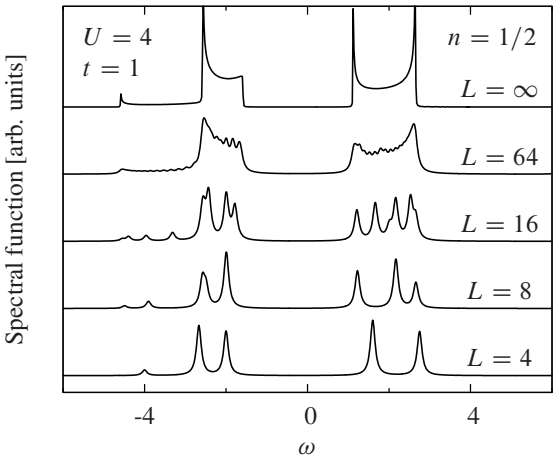

Figure 5.6: Spectral function with EET ($\delta^{(1)}$) method and approximate RDMs ($\alpha = 0.5$) for the Hubbard ring at 1/2 filling for various ring sizes L: the fundamental gap only slightly depends on the ring size.

$\alpha = 0.5$, is comparable to the gap obtained using the exact RDMs. For comparison in Fig. 5.5 we report also the results obtained using the DER method: in the atomic limit this method does not open any gap (unless the symmetry of the system is broken, as we saw in Chap. 4). At 1/6 filling (see right panel of Fig. 5.5), as in the case of exact RDMs, our method opens a gap around $\omega = 0$ in the atomic limit. We observe similar trends for longer rings and the fundamental gap at 1/2 filling depends only slightly on the ring length as can be seen in Fig. 5.6.

Finally, in Fig. 5.7 the ground-state energy per site $E_0/(tN_s)$ and the fundamental gap ΔE_g, calculated using the EET method, are given as a function of the Coulomb repulsion strength U for the half-filled Hubbard model on infinite 1D, 2D square and 3D simple cubic lattices (see App. F). Results are given for different values of α. For the 1D Hubbard model, the EET results are compared to the exact Bethe-Ansatz solution [66]. For 2D the EET results are compared with exact results for finite-size

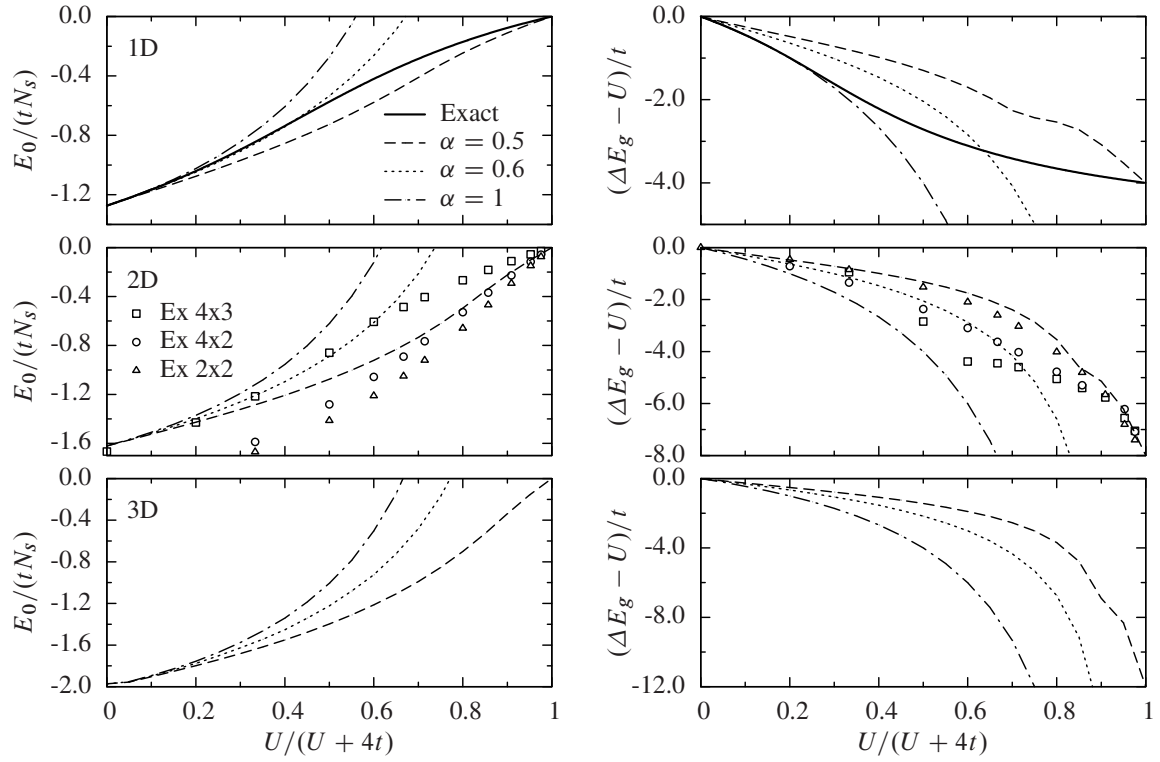

Figure 5.7: Ground-state energy per site $E_0/(tN_s)$ (left) and fundamental gap ΔE_g (right) of the half-filled Hubbard model as a function of the Coulomb repulsion U: 1D lattice (top), 2D square lattice (center), and 3D simple cubic lattice (bottom). Solid lines with markers are obtained from RDMFT, with different values of α, and $\delta^{(1)}$ for the band gap. The black solid line in the upper panel is the exact result derived from the Bethe-ansatz solution [66]. The triangles, circles, and squares in the middle panel are finite-size exact calculations for the 2x2, 4x2, and 4x3 2D Hubbard clusters, respectively.

2D Hubbard clusters. In 2D and 3D, in absence of long range magnetic order and small U, the system is a metal (the HF solution, $\alpha = 1$) up to a critical interaction strength U where a metal-insulator transition, characterized by a typical three-peak structure in the spectral function, occurs (see, e.g., [35, 116]). For large U the exact band gap goes as U.

We see that for each value of U the EET method can produce the correct band gap by properly tuning α. Of course, in a real system, in absence of experimental results, one could risk to use the wrong value of α, which would make the theory non-predictive. Similar trends of the EET results are observed for the 3D system. In this case finite-size exact calculations are not reported, since they are computationally very demanding.

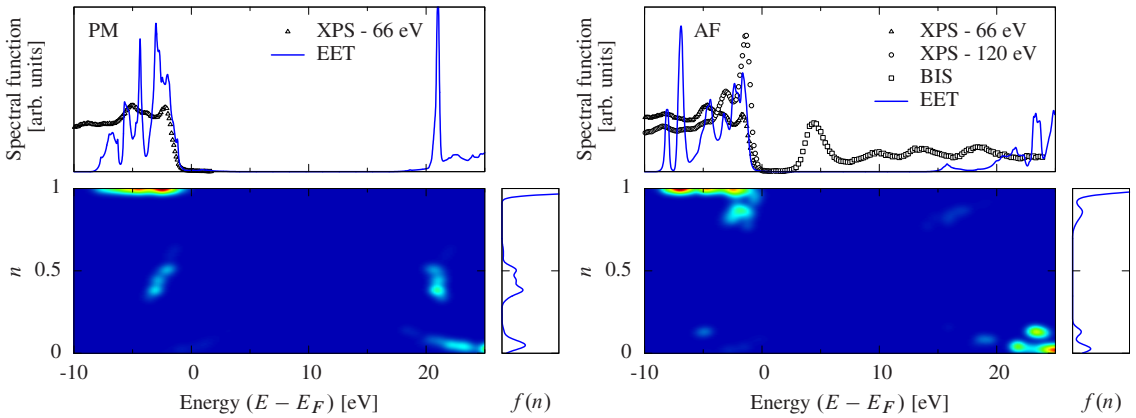

Figure 5.8: Paramagnetic (left panel) and antiferromagnetic (right panel) bulk NiO: experimental photoemission spectrum *vs.* EET spectrum ($\delta^{(1)}$, with power functional, α=0.65). The color map and the distribution $f(n) = \beta \sum_k N_k \delta(n_k - n)$, with N_k the occurrence of n_k, and $\beta = n$ for the removal and $\beta = 1 - n$ for the addition part, illustrate the occupation numbers $0 \leq n \leq 1$ which play a role into the spectrum for the reported energy range.

5.5 Real systems: the example of NiO

In the following we illustrate our method together with RDMFT in real gapped materials using $\delta^{R/A(1)}$. We implemented our approach in a modified version of the full-potential linearized augmented plane wave (FP-LAPW) code ELK [28] and we apply it to bulk NiO. This system shows antiferromagnetic behavior below the Néel temperature, and the photoemission spectrum is very similar for the paramagnetic and the antiferromagnetic phases, with a band gap of about 4.3 eV [96, 107]. Whereas the spectrum in the antiferromagnetic phase can be well described by *GW* [31] as well as RDMFT using the DER method [99], the paramagnetic phase is more problematic, and these methods produce a metallic spectrum. Our method produces qualitatively good spectra and opens a gap, although too large, even in the paramagnetic phase. The results are reported in Fig. 5.8. For the calculations we used the experimental lattice constants and the power functional ($\alpha = 0.65$) with the self-interaction correction proposed by Goedecker and Umrigar [45]. From the analysis of the occupation numbers it emerges that the physics underlying the band gap opening in the two phases is different: in the antiferromagnetic case it is mainly due to occupation numbers around one or zero, whereas in the paramagnetic phase the occupation numbers around 0.5 play a crucial role. This is in line with an analogous analysis on the Hubbard dimer (see Chap. 4). It still remains to improve the band gap, which is now largely overestimated in our method. This finding is in line with the results on long Hubbard rings, which indicate that this overestimation is due to the use of $\delta^{(1)}$. The use of $\delta^{(2)}$ could improve significantly the spectrum and reduce the band gap.

For comparison in Fig. 5.9 we report the results obtained with the DER method. The spectrum of the antiferromagnetic NiO is in good agreement with the experiments;

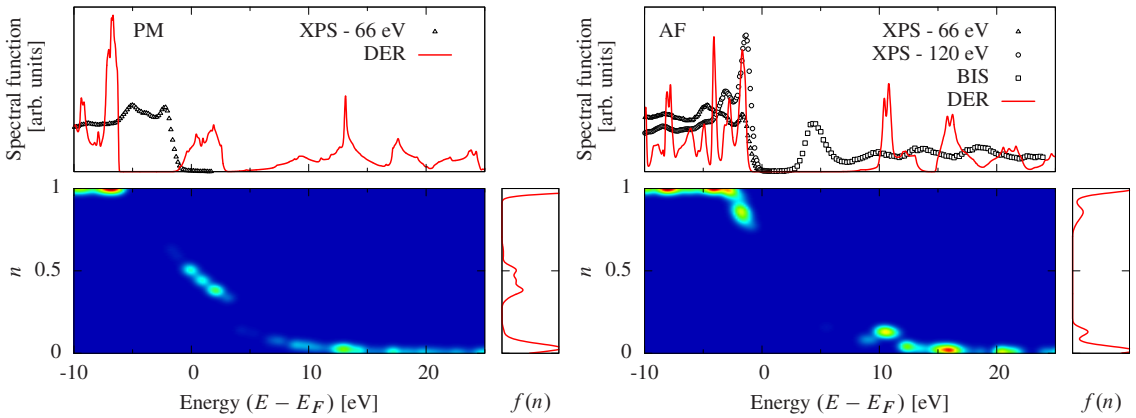

Figure 5.9: Paramagnetic (left panel) and antiferromagnetic (right panel) bulk NiO: experimental photoemission spectrum *vs.* DER spectrum (with power functional, α=0.65). (see caption of Fig. 5.8 for the explication of the color map and the distribution $f(n)$.)

although the physics is similar as in our method, the band gap is better reproduced. This can be understood by inspecting the expression for removal/addition energies in the DER method [99]. Using the power functional these energies are obtained as

$$\begin{aligned}\epsilon_i^R = -\epsilon_i^A &= \left.\frac{\partial E_0[\{n_k\},\{\phi_k\}]}{\partial n_i}\right|_{n_i=1/2} \\ &= h_{ii} + \left[\sum_j V_{ijij} n_j - \alpha n_i^{\alpha-1} \sum_j V_{ijji} n_j^\alpha\right]_{n_i=1/2} . \end{aligned} \tag{5.29}$$

This expression, which is the same for both removal and addition energies, is similar to the expression for the removal energies $\delta_i^{R,(1)}$, which, with the power functional, reads

$$\delta_i^{R,(1)} = h_{ii} + \sum_j V_{ijij} n_j - n_i^{\alpha-1} \sum_j V_{ijji} n_j^\alpha . \tag{5.30}$$

The difference between the two expressions resides in the prefactor α in the last term on the right-hand side of Eq. (5.29), which is one in Eq. (5.30), and the use of $n_i = 1/2$ in Eq. (5.29) instead of the value which minimizes the total energy E_0,[3] as in Eq. (5.30). This tends to reduce the band gap width with respect to our method by carefully choosing α. We also note that with $\alpha = 1$ (HF), the two methods coincide. In this case, indeed, $\delta_i^{R,(1)} = \delta_i^{A,(1)}$, as one can see from Eq. (5.28), and $\delta_i^{R,(1)} = \epsilon_i^R$, as it is clear from Eqs (5.29) and (5.30) using $\alpha = 1$.

In the paramagnetic phase, instead, the DER method does not open any gap. The occupation numbers mainly involved in the band gap region are again those around 0.5, however they accumulate in the band gap region, whereas our method separates them and opens a gap.

[3]Note that in practice in the ELK code only the exchange-correlation contribution in (5.29) is evaluated at $n_i = 1/2$.

5.6 Conclusions and outlooks

We derived an expression for the spectral function in terms of RDMs. Simple approximations can give accurate spectra for model systems in the weak as well as in the strong correlation regime. In particular the method correctly reproduces the atomic limit without breaking the symmetry of the system. This is an exceptional result, since state-of-the-art methods such as *GW* fail in this regime. We applied a simple approximation depending only on the one-body and two-body RDMs to bulk NiO within the computationally efficient Reduced Density-Matrix Functional Theory. Our method produces qualitatively good photoemission spectra for the antiferromagnetic and paramagnetic phases, although the band gap is largely overestimated. Our results on the Hubbard model indicate that this is due to the use of $\delta^{(1)}$. To improve the spectrum one should use $\delta^{(2)}$; in this case, however, an approximation for the 3-RDM should be introduced. If, instead, one wants to remain at the level of $\delta^{(1)}$ one could introduce some effective screening to take into account higher order terms in the approximation of $\delta(\omega)$. Preliminary tests on NiO with a modified approximation $\Gamma^{(2)}(\mathbf{x},\mathbf{x}';\mathbf{x},\mathbf{x}') = \gamma(\mathbf{x},\mathbf{x})\gamma(\mathbf{x}',\mathbf{x}') - \beta\gamma^{\alpha}(\mathbf{x},\mathbf{x}')\gamma^{\alpha}(\mathbf{x}',\mathbf{x})$, with an effective screening $0 < \beta < 1$, show a global improvement of the spectrum.

One could also explore other ways to truncate the $\delta^{R/A}$ series. Work in these directions is in progress. We think that this method has a great potential and opens the way to a more accurate and computationally efficient description of strongly correlated materials.

Chapter 6

Time-Dependent Reduced Density-Matrix Functional Theory: an exploration of memory effects and strong correlation

This last chapter is more explorative and deals with time-dependent phenomena within Reduced Density-Matrix Functional Theory (RDMFT). In general the time evolution of the reduced density matrices is given by the Bogoliubov-Born-Green-Kirkwood-Yvon (BBGKY) hierarchy of equations, in which the equation of motion of the n-body reduced density matrix is given in terms of the $(n+1)$-body reduced density matrix. The first equation of the hierarchy relates the one-body to the two-body reduced density matrix. The difficult task is to find approximations to the two-body reduced density matrix. Commonly used approximations are adiabatic extensions of ground-state approximations. We explore this issue by looking at new approximations derived from Many-Body Perturbation Theory (MBPT) based on Green's functions as well as from the exact solution of the two-level Anderson impurity model in its ground state. Our first results on the two-level Anderson model subject to various external potentials show some interesting, although contradictory, features, which might be a pathology of the small test model used. This indicates to explore these approximations also for larger model systems.

6.1 Introduction

Advances in experimental techniques offer the opportunity to explore properties and phenomena of increasing complexity. For example, the progress in laser technologies opens the way to the investigation of a broad spectrum of dynamical phenomena that are far beyond the mere analysis of the ground-state properties, such as photoionization, excited-state relaxation, structural modifications, violent collective electron

motion and Coulomb explosion. Complementing experiments with theory can provide a profound understanding of the fundamental mechanism of these phenomena. However, modelling these complex phenomena becomes a difficult task, since the theory has to describe many complicated physical processes. Besides the increasing demands, theoretical treatments are limited also by practical aspects like numerical costs. In this situation Reduced Density-Matrix Functional Theory (RDMFT) offers a promising framework to treat dynamics. RDMFT has been used to overcome some problems of Density Functional Theory (DFT) related to electron correlation, such as the dissociation of diatomic molecules. It has also been applied to the calculation of the fundamental gap [98] and photoemission spectra [99] in solids. Within RDMFT the central variable is the one-body reduced density matrix (1-RDM), $\gamma(\mathbf{x}, \mathbf{x}')$, instead of the density $\rho(\mathbf{x}) = \gamma(\mathbf{x}, \mathbf{x})$ as in DFT. As a consequence the functional form of the kinetic and exchange energies are known exactly in terms of the 1-RDM, unlike in DFT, and one has to find approximations to the correlation part only. The exact 1-RDM minimizes the ground-state energy functional of the many-body system, and, thanks to the one-to-one mapping between γ and the (non-degenerate) ground-state wave function [44], all the ground-state expectation values of the system can in principle be obtained from the 1-RDM. RDMFT has been recently extended to time domain and successful applied to treat double excitations in the linear response of finite systems [41]. Here we go beyond the linear response. In general the time evolution of the RDMs is given by the Bogoliubov-Born-Green-Kirkwood-Yvon (BBGKY) hierarchy of equations, in which the equation of motion (EoM) of the n-RDM is given in terms of the $(n+1)$-RDM. The first equation of the hierarchy reads

$$\mathrm{i}\,\frac{\partial}{\partial t}\gamma(\mathbf{x}_1, \mathbf{x}_1'; t) - \left[h(\mathbf{x}_1, t) - h(\mathbf{x}_1', t^+)\right]\gamma(\mathbf{x}_1, \mathbf{x}_1'; t) = \\ + \int d\mathbf{x}_2 \left[v_c(\mathbf{x}_1, \mathbf{x}_2) - v_c(\mathbf{x}_1', \mathbf{x}_2)\right]\Gamma^{(2)}(\mathbf{x}_1, \mathbf{x}_2; \mathbf{x}_1', \mathbf{x}_2; t), \qquad (6.1)$$

where we indicate with γ and $\Gamma^{(2)}$ the 1- and 2-RDMs, respectively (see Sec. 6.2 for the definitions). Here $h(\mathbf{x}, t) = -\nabla^2/2 + v_{\mathrm{ext}}(\mathbf{x}, t)$ is the one-body Hamiltonian, with v_{ext} a general local time-dependent external potential, and v_c is the Coulomb potential. The coordinates are written as combined space-spin variables, $\mathbf{x} \equiv (\mathbf{r}, s)$. A similar equation exists for $\Gamma^{(2)}$ and higher-order RDMs. To solve Eq. (6.1) we hence need to know all the higher-order reduced density matrices. In practice the BBGKY hierarchy is truncated, and approximations are introduced in order to have a closed set of equations to solve. However, how to truncate the hierarchy is not trivial and the truncated set of equations can lead to instabilities or violation of sum rules [2]. One could also extend ground-state approximations for the 2-RDM to the time-domain in the same spirit as the adiabatic approximations used in Time-Dependent Density Functional Theory (TDDFT) [121, 122]. However the lack of memory effects (caused by the adiabatic approximation) causes some shortcomings, such as static occupation numbers [5]. This can be easily understood by project-

ing Eq. (6.1) onto the set of (time-dependent) natural orbitals $\{\phi_i(\mathbf{x},t)\}$, *i.e.*, the orbitals which diagonalize the 1-RDM (where the eigenfunctions $\phi_i(\mathbf{x},t)$ form a complete set at each point in time).[1] For simplicity, in the following the index i condensates both space and spin indices; they will be explicitly indicated only when necessary. Inserting the spectral representation of $\gamma(\mathbf{x}_1,\mathbf{x}_1';t)=\sum_i n_i(t)\phi_i(\mathbf{x}_1t)\phi_i^*(\mathbf{x}_1't)$ and $\Gamma^{(2)}(\mathbf{x}_1,\mathbf{x}_2;\mathbf{x}_1',\mathbf{x}_2';t)=\sum_{ijkl}\Gamma^{(2)}_{ijkl}(t)\phi_i(\mathbf{x}_2t)\phi_j(\mathbf{x}_1t)\phi_k^*(\mathbf{x}_1't)\phi_l^*(\mathbf{x}_2't)$ in (6.1) we arrive at

$$\mathrm{i}\,\dot{n}_i(t)=\sum_{jkl}\Gamma^{(2)}_{jkil}(t)V_{ilkj}(t)-\text{c.c.} \tag{6.2}$$

where $V_{ijkl}(t)=\int d\mathbf{x}_1 d\mathbf{x}_2\phi_i^*(\mathbf{x}_1t)\phi_j^*(\mathbf{x}_2t)v_c(\mathbf{r}_1\mathbf{r}_2)\phi_k(\mathbf{x}_1t)\phi_l(\mathbf{x}_2t)$. Most of the ground-state approximations to $\Gamma^{(2)}$ have the same structure of the Hartree-Fock approximation (as discussed in Sec. 2.6)

$$\Gamma^{(2)}_{ijkl}=n_in_j\left(\delta_{il}\delta_{jk}-\delta_{ik}\delta_{jl}\right).$$

If we consider the time domain the occupation numbers on the right-hand side acquire a time-dependence. One can verify that this kind of structure for the $\Gamma^{(2)}$, when used in Eq. (6.2), leads to static occupation numbers (the first term on the right-hand side is exactly canceled by its complex conjugate [5]). Besides memory effects, which in general become important in case of highly non-adiabatic external potentials, another important aspect to consider is the description of strong electron correlation, which is already a difficult task at equilibrium.

In this work we will explore these two issues from a specific perspective, *i.e.*, using lattice model systems. These models occupy a special place in condensed matter physics, due to their simplicity and to the fact that many of them can be solved exactly, hence providing exact data for benchmarking. Here we will focus on the Anderson impurity model [4], as a particularly interesting example for applications. We will first combine Time-Dependent Reduced Density-Matrix Functional Theory (TDRDMFT) with Many-Body Perturbation Theory (MBPT) based on Green's functions, and we will derive approximations to $\Gamma^{(2)}$ from commonly-used many-body approximations, namely *GW*, second Born, and T matrix. The advantage of using many-body approximations is that they have memory effects already built-in. We will study how these approximations perform for the case of slow varying external potentials as well as strongly nonadiabatic external potentials, and in case of weak and strong correlation regimes. There are two main drawbacks of these MBPT-based approximations to $\Gamma^{(2)}$: (i) they depend on the non-equilibrium one-body Green's function; (ii) since they are based on perturbation schemes, they may break down in case of strong electron correlations. We, therefore, explore also another approximation: along the same line followed in Ref. [109] for the ground state, we derive an adiabatic approximation to $\Gamma^{(2)}$ from the exact ground-state functional of the two-level Anderson model. It is

[1] Note that the set of orbitals which diagonalize the reduced density matrix γ is not the same at each point in t, that is why the natural orbitals depend on time.

clear that within this approximation the occupation numbers will not change in time; however, one can explore how the site densities are described.

This chapter is organized in the following way. In Sec. 6.2 we show the link between the EoM of the 1-RDM and the non-equilibrium one-body Green's function, and how approximations to $\Gamma^{(2)}$ can be obtained from common many-body approximations. Next we derive a new approximation to $\Gamma^{(2)}$, based on the two-site Anderson impurity model, along the same line of Ref. [109] for the ground state. In Sec. 6.3 we illustrate how these new approximations perform for the two-level Anderson impurity model, for various external potentials and strengths of the electron-electron interaction. We finally summarize our findings in Sec. 6.4.

6.2 Theory

We consider a N-electron system described by the time-dependent Hamiltonian (in second quantization)

$$\hat{H}(t) = \int d\mathbf{x}\hat{\psi}^\dagger(\mathbf{x})h(\mathbf{x},t)\hat{\psi}(\mathbf{x}) + \frac{1}{2}\int d\mathbf{x}'d\mathbf{x}'\hat{\psi}^\dagger(\mathbf{x})v_c(\mathbf{r},\mathbf{r}')\hat{\psi}^\dagger(\mathbf{x}')\hat{\psi}(\mathbf{x}')\hat{\psi}(\mathbf{x}).$$

We can define the time-dependent p-RDM, $\Gamma^{(p)}$, for such a system as

$$\Gamma^{(p)}(\mathbf{x}_1,...,\mathbf{x}_p;\mathbf{x}'_1,...,\mathbf{x}'_p;t) \equiv \langle\Psi(t)|\,\hat{\psi}^\dagger(\mathbf{x}'_p)...\hat{\psi}^\dagger(\mathbf{x}'_1)\hat{\psi}(\mathbf{x}_1)...\hat{\psi}(\mathbf{x}_p)\,|\Psi(t)\rangle\,,$$

where $|\Psi(t)\rangle$ is the normalized wave function of the system. In particular in the following we will deal with the one-body ($\gamma \equiv \Gamma^{(1)}$) and the two-body ($\Gamma^{(2)}$) reduced density matrices. The equation of motion of the 1-RDM, Eq. (6.1), is obtained from the commutator $[\hat{\gamma}, \hat{H}]$, where $\hat{\gamma} \equiv \hat{\psi}^\dagger(\mathbf{x}'_1)\hat{\psi}(\mathbf{x}_1)$ is the 1-RDM operator.

We consider the following spectral representation of

$$\gamma(\mathbf{x}_1,\mathbf{x}'_1;t) = \sum_{ij}\gamma_{ij}(t)\varphi_i(\mathbf{x}_1)\varphi^*_j(\mathbf{x}'_1),$$

where the stationary eigenfunctions φ_i form a complete set. We further consider the following spectral representation for the 2-RDM

$$\Gamma^{(2)}(\mathbf{x}_1,\mathbf{x}_2;\mathbf{x}'_1,\mathbf{x}'_2;t) = \sum_{ijkl}\Gamma^{(2)}_{ijkl}(t)\varphi_i(\mathbf{x}_1)\varphi_j(\mathbf{x}_2)\varphi^*_k(\mathbf{x}'_2)\varphi^*_l(\mathbf{x}'_1).$$

Note that $\gamma_{ij}(t) = \langle\Psi(t)|\hat{c}^\dagger_j\hat{c}_i|\Psi(t)\rangle$ and $\Gamma^{(2)}_{ijkl}(t) = \langle\Psi(t)|\hat{c}^\dagger_l\hat{c}^\dagger_k\hat{c}_j\hat{c}_i|\Psi(t)\rangle$. Inserting the spectral representation of γ and $\Gamma^{(2)}$, respectively, in (6.1), multiplying both sides by $\varphi^*_k(\mathbf{x}_1)\varphi_l(\mathbf{x}'_1)$ and integrating over $\mathbf{x}_1$ and $\mathbf{x}'_1$ we arrive at

$$\begin{aligned}\mathrm{i}\,\dot{\gamma}_{ij}(t) =& \sum_k h_{ik}(t)\gamma_{kj}(t) - \sum_k h_{kj}(t)\gamma_{ik}(t) \\ &- \sum_{lkm} V_{iklm}\Gamma^{(2)}_{lmjk}(t) + \sum_{klm} V_{lmjk}\Gamma^{(2)}_{iklm}(t),\end{aligned} \tag{6.3}$$

where $V_{ijkl}(t) = \int d\mathbf{r}_1 d\mathbf{r}_2 \varphi_i^*(\mathbf{x}_1)\varphi_j^*(\mathbf{x}_2)v_c(\mathbf{x}_1,\mathbf{x}_2)\varphi_k(\mathbf{x}_1)\varphi_l(\mathbf{x}_2)$. The question now is how to get approximations to $\Gamma^{(2)}(t)$, which appears on the right-hand side of (6.3). Two ways are discussed in the following sections.

6.2.1 Approximations from Many-Body Perturbation Theory

One can also get the EoM (6.1) by subtracting the two following EoM of the 1-GF

$$\left[\mathrm{i}\frac{\partial}{\partial t_1} - h(1)\right] G(1,1') + \mathrm{i}\int d2 v_c(1,2) G^{(2)}(1,2^+;1',2^{++}) = \delta(1-1'),$$
$$\left[-\mathrm{i}\frac{\partial}{\partial t_1'} - h(1')\right] G(1,1') + \mathrm{i}\int d2 v_c(1',2) G^{(2)}(1,2^{--};1',2^-) = \delta(1-1'),$$

and then taking the limit $t_1' \to t_1^+$. One gets

$$\left[\mathrm{i}\frac{\partial}{\partial t_1} + \mathrm{i}\frac{\partial}{\partial t_1'}\right] G(1,1') - [h(1) - h(1')]\, G(1,1')$$
$$+ \mathrm{i}\int d2 v_c(1,2) G^{(2)}(1,2^+;1',2^{++}) - \mathrm{i}\int d2 v_c(1',2) G^{(2)}(1,2^{--};1',2^-) = 0, \quad (6.4)$$

which for $t_1' \to t_1^+$ becomes (6.1), where

$$\Gamma^{(2)}(\mathbf{x}_1,\mathbf{x}_2;\mathbf{x}_1',\mathbf{x}_2;t_1) = -G^{(2)}(\mathbf{x}_1 t_1, \mathbf{x}_2 t_1^+; \mathbf{x}_1' t_1^{+++}, \mathbf{x}_2 t_1^{++}).$$

We can hence derive approximations to $\Gamma^{(2)}$ from common MBPT approximations to $G^{(2)}$. For example, within the well-known GW approximation, $G^{(2)}$ reads as

$$G^{(2)}(1,2;1',2^+) \approx G(1,1')G(2,2^+) - \int d3 G(1,3)\varepsilon^{-1}(3,2)G(3,1'), \quad (6.5)$$

where $\varepsilon^{-1} = 1 + v_c\chi$, with χ the (reducible) polarizability, is the time-ordered inverse dielectric matrix. Using Eq. (6.5) in (6.4) and taking the limit $t_1' \to t_1^+$ we arrive at

$$\mathrm{i}\frac{\partial}{\partial t_1}\gamma(\mathbf{x}_1,\mathbf{x}_1';t_1) - [h_H(\mathbf{x}_1,t_1) - h_H(\mathbf{x}_1',t_{1+})]\,\gamma(\mathbf{x}_1,\mathbf{x}_1';t_1) =$$
$$\int d2 \left[W(1^+,2) - W(\mathbf{x}_1' t_1, 2)\right] G(1,2)G(2,\mathbf{x}_1' t_1^+), \quad (6.6)$$

where in h_H we have included also the Hartree potential. From this equation we get the following EoM for the occupation numbers

$$\mathrm{i}\,\dot{n}_i(t_1) = \sum_{jnm}\int dt_2 \,[W_{ijmn}(t_1,t_2)G_{mj}(t_1,t_2^+)G_{ni}(t_2,t_1^+)$$
$$- W_{mjin}(t_1,t_2)G_{ij}(t_1,t_2^+)G_{nm}(t_2,t_1^+)] \quad (6.7)$$

where $W_{ijkl}(t,t') = \int d\mathbf{x}d\mathbf{x}'\phi_i^*(\mathbf{x}t)\phi_j^*(\mathbf{x}'t')W(\mathbf{x}t,\mathbf{x}'t')\phi_k(\mathbf{x}t)\phi_l(\mathbf{x}'t')$ and for the GFs we used the spectral representation $G(\mathbf{x}t,\mathbf{x}'t') = \sum_{ij} G_{ij}(t,t')\phi_i(\mathbf{x}t)\phi_j^*(\mathbf{x}'t')$. If we consider an instantaneous $W_{ijji}(t_1,t_1') = W_{ijji}\delta(t_1 - t_1')$, than the 1-GF reduces to the 1-RDM which is diagonal in the basis of natural orbitals, one can thus show that the right-hand side becomes zero and the occupation numbers do not change in time. This is the same structure that one gets with the commonly used (ground-state-based) approximations to $\Gamma^{(2)}$. We should hence keep a dynamically screened Coulomb potential. This prevents one to use the 1-RDM on the right-hand side, one has instead to work with the full 1-GF. This means that the EoM is not closed, and that in order to calculate the occupation numbers one needs to calculate the time evolution of the 1-GF as well. Therefore, as such, Eq. (6.7) is not very useful, since one can directly use the formalism of non-equilibrium Green's functions instead of solving Eq. (6.7). However, it (and similar equations obtained with other many-body approximations) could be used as starting point for approximations based on the 1-RDM only. Here we first explore how common many-body approximations, namely, GW, second Born, and T matrix, perform for the site densities and the occupation numbers of the two-site Anderson model.

6.2.2 Approximations from the two-level Anderson model

In Ref. [109] Töws and Pastor derive an explicit analytical form for the Coulomb interaction-energy functional $W[\gamma]$ of the Lattice Density Functional Theory (LDFT) of the Anderson impurity model. The derivation is based on the exact functional of the two-level Anderson model. Application to finite Anderson rings yields very accurate results for various ground-state properties, such as total energy and occupation of the local impurity orbital, for weak as well strong correlations. Here we derive an (adiabatic) approximation for the $\Gamma^{(2)}[\gamma]$ functional along the same line of Ref. [109]. The purpose is to derive an approximate analytical expression for the functional $\Gamma^{(2)}[\gamma]$ in Eq. (6.1) by looking at a two-level system at half filling (singlet state) consisting of a localized impurity orbital f and a delocalized orbital s in the presence of a time-dependent external potential $v_{\text{ext}}(t)$ on the impurity site. The two-level Anderson model is described by the following Hamiltonian

$$\hat{H}^{2L}(t) = \sum_\sigma \left[\epsilon_f \hat{n}_{f\sigma} + v_{sf}(\hat{c}_{s\sigma}^\dagger \hat{f}_\sigma + \hat{f}_\sigma^\dagger \hat{c}_{s\sigma}) + v_{\text{ext}}(t)\hat{n}_{f\sigma}\right] + U\hat{n}_{f\uparrow}\hat{n}_{f\downarrow},$$

where we explicitly indicated the spin index σ. Here we introduced the impurity site energy ϵ_f, the hybridization parameter v_{sf} and the on-site Coulomb interaction U. The equation of motion (6.6) then becomes

$$\mathrm{i}\,\dot{\gamma}_{ff}^\sigma(t) = v_{sf}\gamma_{sf}^\sigma(t) - v_{sf}(t^+)\gamma_{fs}^\sigma(t), \tag{6.8}$$

$$\mathrm{i}\,\dot{\gamma}_{ss}^\sigma(t) = v_{sf}\gamma_{fs}^\sigma(t) - v_{sf}(t^+)\gamma_{sf}^\sigma(t), \tag{6.9}$$

$$\mathrm{i}\,\dot{\gamma}_{sf}^\sigma(t) = v_{sf}\gamma_{ff}^\sigma(t) - [\epsilon_f + v_{\text{ext}}(t)]\gamma_{sf}^\sigma(t) - v_{sf}(t^+)\gamma_{ss}^\sigma(t) + U\Gamma_{sfff}^{(2),\sigma\bar{\sigma}\sigma\bar{\sigma}}(t), \tag{6.10}$$

where $\bar{\sigma}$ indicates a spin opposite to σ. The functional $\Gamma^{(2),\sigma\bar{\sigma}\sigma\bar{\sigma}}_{sfff}(t)$ is approximated by its exact ground-state expression evaluated at the time-dependent 1-RDM components $\gamma_{ff}(t)$ and $\gamma_{sf}(t)$ (see App. G for details). This reads

$$\Gamma^{(2),\sigma\bar{\sigma}\sigma\bar{\sigma}}_{sfff}(t) = \begin{cases} \frac{\gamma_{sf}(t)}{4}\left[-1+\frac{1-\gamma_{ff}(t)}{1-\sqrt{|\gamma^0_{sf}|^2-|\gamma_{sf}(t)|^2}}\right] & \text{if } |\gamma_{sf}(t)| > \gamma^{\infty}_{sf}(t) \\ \Gamma^{(2),\sigma\bar{\sigma}\sigma\bar{\sigma},\infty}_{sfff}(t) & \text{if } |\gamma_{sf}(t)| \leq \gamma^{\infty}_{sf}(t), \end{cases}$$

with

$$\Gamma^{(2),\sigma\bar{\sigma}\sigma\bar{\sigma},\infty}_{sfff}(t) = \begin{cases} 0 & \text{if } \gamma_{ff}(t) \leq 1 \\ -\gamma^{\infty}_{sf}(t)/2 & \text{if } \gamma_{ff}(t) > 1, \end{cases}$$

$$\gamma^{\infty}_{sf}(t) = \begin{cases} \sqrt{2\gamma_{ff}(t)[1-\gamma_{ff}(t)]} & \text{if } \gamma_{ff}(t) \leq 1 \\ \sqrt{2[2-\gamma_{ff}(t)][\gamma_{ff}(t)-1]} & \text{if } \gamma_{ff}(t) > 1, \end{cases}$$

and $\gamma^0_{sf}(t) = \sqrt{\gamma_{ff}(t)[2-\gamma_{ff}(t)]}$. Note that here $\gamma_{ij} = \sum_\sigma \gamma^\sigma_{ij}$. These equations are valid only for an integer particle number $N = \gamma_{ss} + \gamma_{ff} = 2$. To extend the formulation to the case with more conduction bands, one should extend the two-level functional (6.11) to fractional particle numbers $N \in [0, 4]$, to take into account the charge fluctuations due to the presence of the other conduction-band orbitals. Moreover, one can adopt an effective two-level model approximation having the density matrix

$$\gamma^{\sigma,2L} = \begin{pmatrix} \tilde{\gamma}^\sigma_{ss} & \Gamma^{(2),\sigma}_{sf} \\ (\Gamma^{(2),\sigma}_{sf\sigma})^* & \gamma^\sigma_{ff} \end{pmatrix},$$

where $\Gamma^{(2),\sigma}_{sf}$ and $\tilde{\gamma}^\sigma_{ss}$ are given in Eqs (22) and (24), respectively, of Ref. [109], and coincide with γ^σ_{sf} and γ^σ_{ss} in the case of two levels. Here we will focus only on a pure two-level Anderson model.

6.3 Illustration on the two-level Anderson impurity model

We will now explore how the approximations derived above perform on the simple two-level Anderson model, which can be solved exactly.

6.3.1 MBPT

We first start to look at the performance of GW, second Born, T-matrix approximations for the impurity site density γ^σ_{ff} and the occupation numbers. For comparison we also report the HF results. The time evolution of the non-equilibrium GFs has been

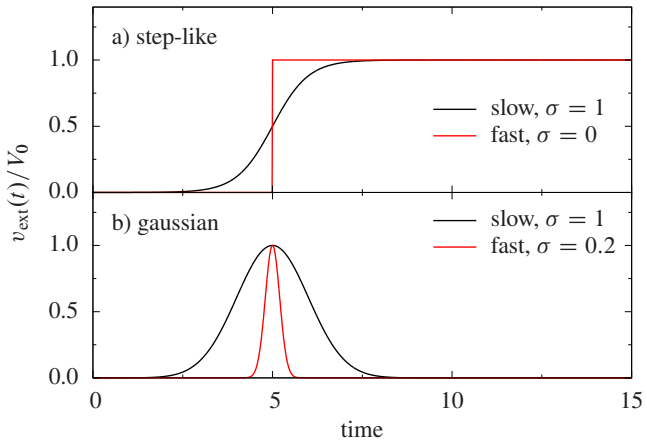

Figure 6.1: Time-dependent perturbations $v_{\text{ext}}(t)$: (a) step-like and (b) Gaussian perturbations. We consider perturbations with a slower or faster onset/offset.

obtained by propagating the equation of motion according to the scheme proposed in Ref. [92, 115].

For $t \leq 0$ the system is in its ground state. At $t > 0$, a time-dependent external perturbation $v_{\text{ext}}(t)$ is applied. In the following we consider both a step-like perturbation $v_{\text{ext}}(t) = V_0/2\{1 + \tanh[(t - t_0)/\sigma]\}$ and a Gaussian perturbation $v_{\text{ext}}(t) = V_0 \exp[-(t - t_0)^2/(2\sigma^2)]$, which for $\sigma \to 0$ tend to the Heaviside step function and the Dirac-delta function, respectively. Varying σ allows us to consider perturbations with a slow or fast onset/offset, whereas V_0 controls the strength of the perturbation. An example is reported in Fig. 6.1.

Site density

Figure 6.2 shows the time-dependent density per spin channel $\gamma^{\sigma}_{ff}(t)$ at the impurity site after a slow (Figs 6.2(a)–6.2(d)) or a fast (Figs 6.2(e)–6.2(h)) step-like perturbation is applied at the impurity site. In case of weak electron correlation (left panels of Fig. 6.2) all MB approximations perform rather well, except in presence of a fast strong perturbation (panel (g)) for which damping is observed over time. Damping in finite systems, when using approximations with memory, has already been observed in literature in the context of Many-Body Perturbation Theory [92, 115] or also in density functionals (see, *e.g.*, [29, 110, 118]). This is due to the fact that these approximations produce an infinite number of excitations, which is correct in infinite systems, but not in finite systems, where the number of electrons and holes which the system can accommodate is finite. This results in an artificial bath with which the system is in contact during the time evolution. Also HF performs well, and, moreover, being an instantaneous approximation, it does not show any damping. In case of strong correlations (right panels of Fig. 6.2) 2B, GWA, and TMA perform much better than HF, but the agreement with the exact results worsens over time: they show an increasing dephasing with the exact density and, in case of a fast strong perturbation (panel (h)), damping occurs. Similar trends are observed when considering other perturbations, as shown, for example, in Fig. 6.3, where the time-dependent density for both a slow and a fast Gaussian perturbation is reported.

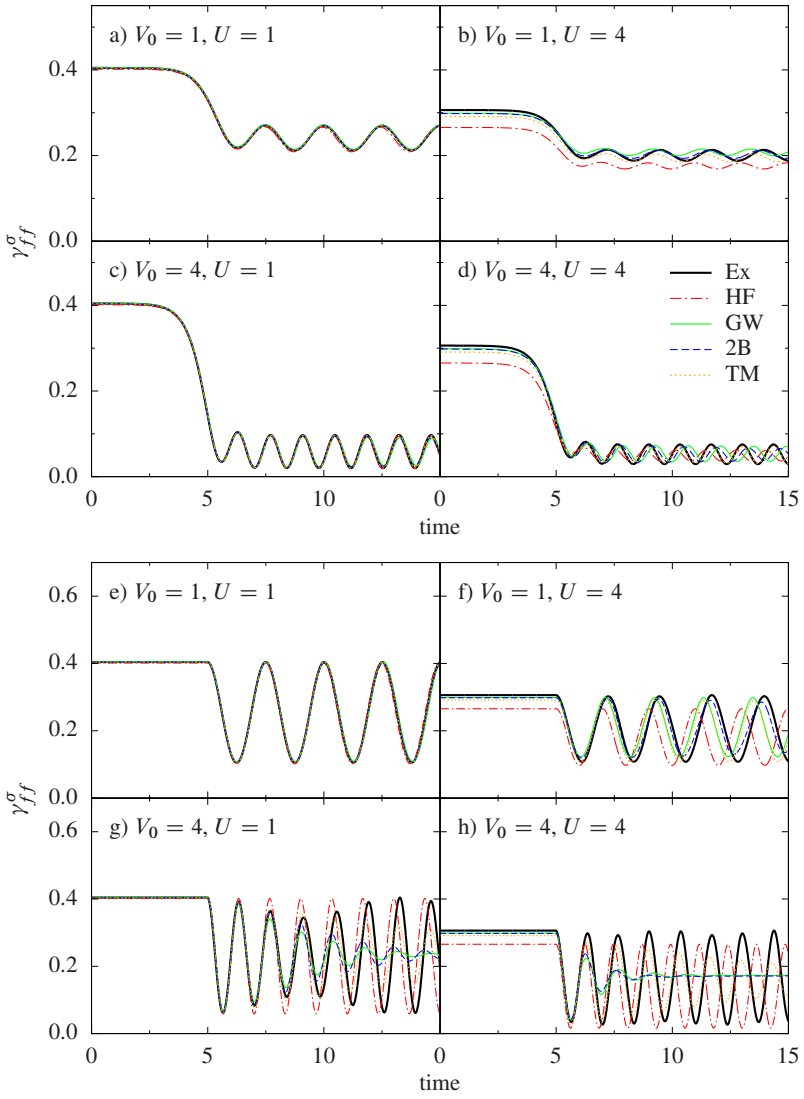

Figure 6.2: Time evolution of the density at the impurity site for the Anderson model after a slow (top) and fast (bottom) step-like external perturbation is applied on the impurity side: exact (thick solid black lines) *vs.* Hartree-Fock (HF, dashed-dotted red lines), *GW* (solid green lines), second Born (2B, dashed blue lines), and T-matrix (TM, dotted orange lines) approximations.

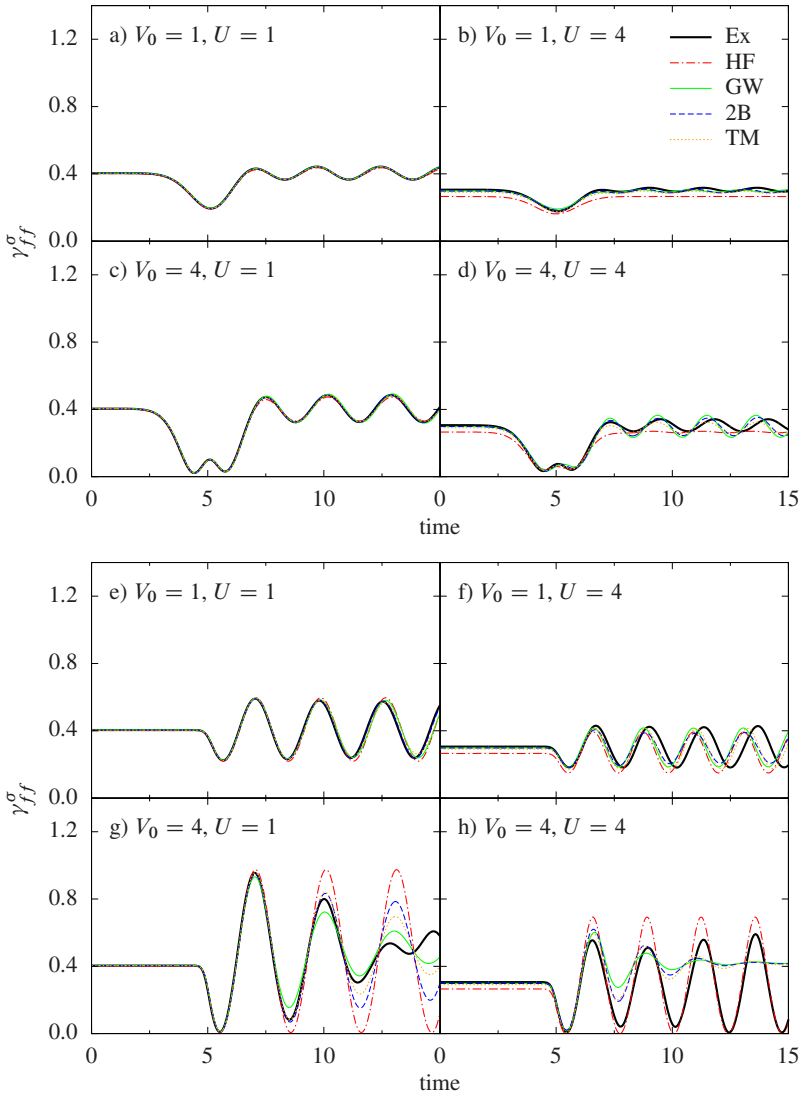

Figure 6.3: Time evolution of the density at the impurity site for the Anderson model after a slow (top) and fast (bottom) Gaussian external perturbation is applied on the impurity site: exact (thick solid black lines) *vs.* Hartree-Fock (HF, dashed-dotted red lines), *GW* (solid green lines), second Born (2B, dashed blue lines), and T-matrix (TM, dotted orange lines) approximations.

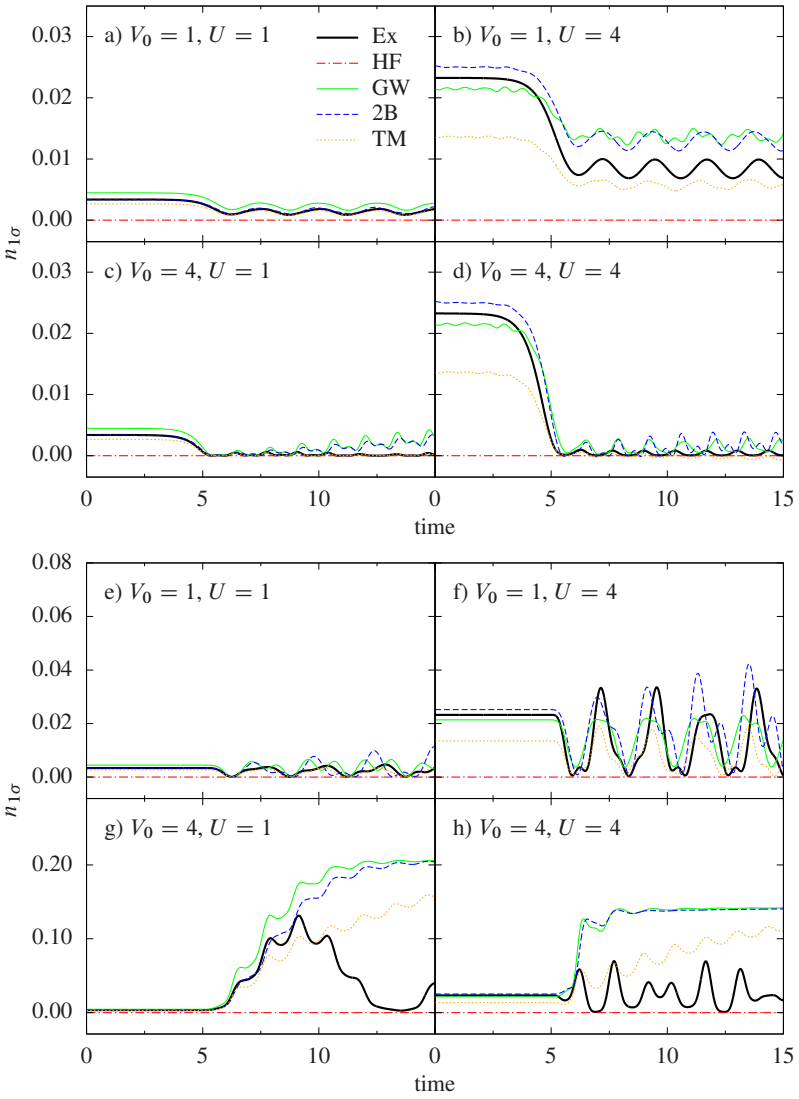

Figure 6.4: Time evolution of the lowest occupation number for the Anderson model after a slow (top) and fast (bottom) step-like external perturbation is applied on this side: exact (thick solid black lines) *vs.* Hartree-Fock (HF, dashed-dotted red lines), *GW* (solid green lines), second Born (2B, dashed blue lines), and T-matrix (TM, dotted orange lines) approximations.

Occupation numbers

In Fig. 6.4 and Fig. 6.5 we reported the lowest occupation number $n_{1\sigma}$ (the other one being $n_{2\sigma} = 1 - n_{1\sigma}$). We observe that in general the trends are not as good as for the site density γ_{ff}. As expected, within HF the occupation numbers do not change in time and are equal to 0 or 1, ($n_{1\sigma} = 0$). At weak correlation and for a step-like perturbation (left panels of Figs 6.4) TMA performs overall much better

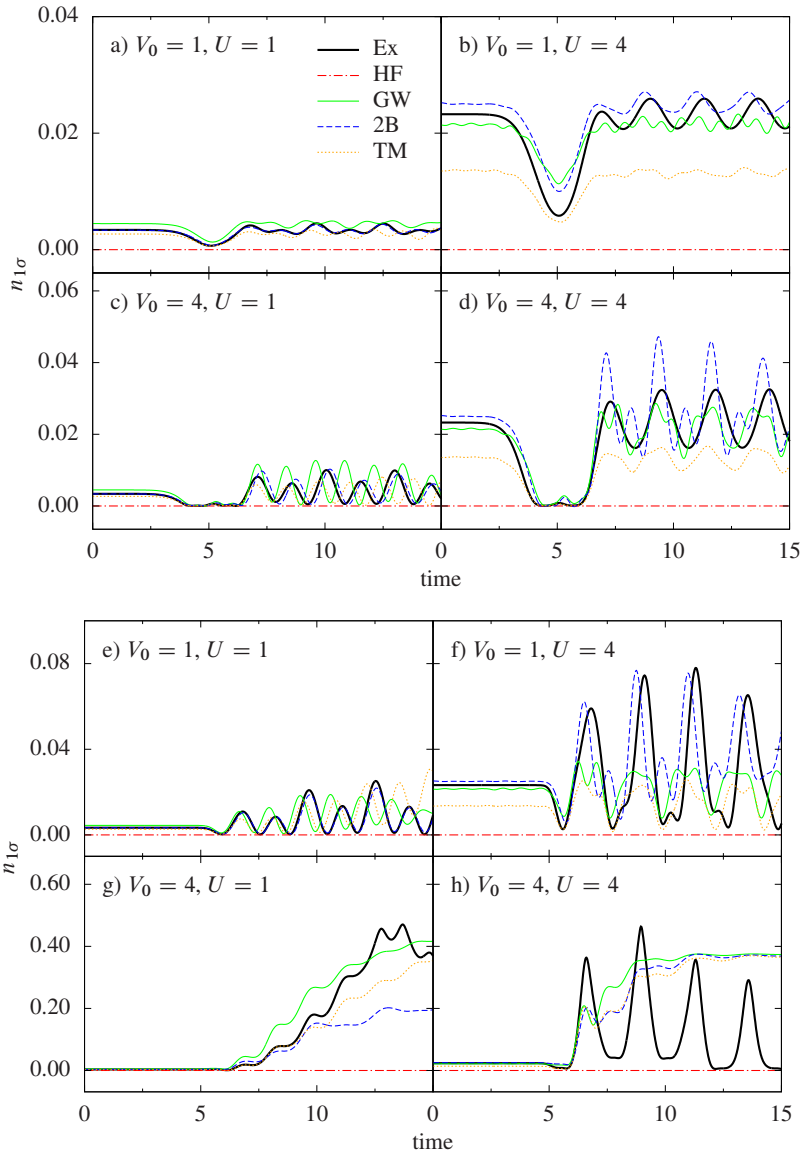

Figure 6.5: Time evolution of the lowest occupation number for the Anderson model after a slow (top) and fast (bottom) Gaussian external perturbation is applied on this side: exact (thick solid black lines) *vs.* Hartree-Fock (HF, dashed-dotted red lines), *GW* (solid green lines), second Born (2B, dashed blue lines), and T-matrix (TM, dotted orange lines) approximations.

than the other MBAs, in particular over small time, before completely departing from the exact results in case of fast and strong perturbations (panel (g) of Figs 6.4). For a Gaussian-like perturbation, instead, the 2B gives better results (left panels of Fig. 6.5). In case of strong correlations (right panels of Figs 6.4 and Fig. 6.5) the situation is rather dramatic: all many-body approximations deviate at $t = 0$. This is because already the ground state is not correctly described.

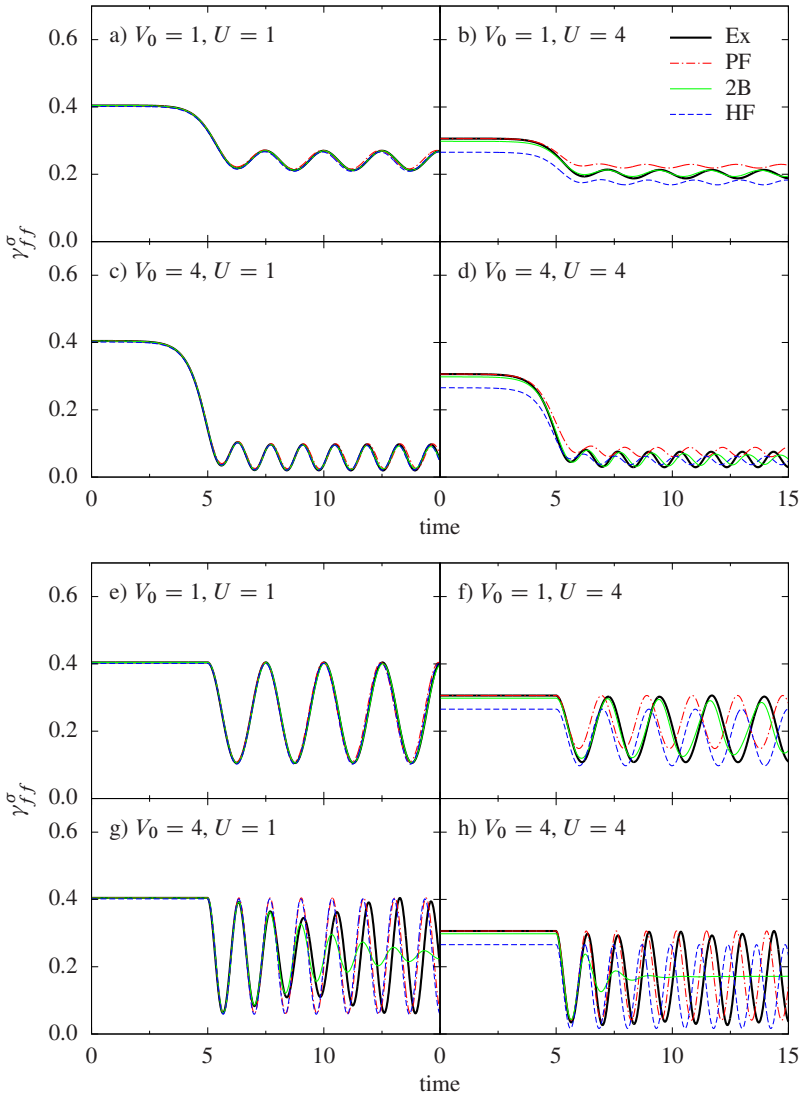

Figure 6.6: Time evolution of the density at the impurity site for the Anderson model after a slow (top) and fast (bottom) step-like external perturbation is applied on this side: exact (thick solid black lines) *vs.* (adiabatic) Pastor functional (PF, dashed-dotted red lines), second Born (2B, solid green lines) and Hartree-Fock (HF, dashed blue lines).

6.3.2 Adiabatic Pastor approximation

In the following we illustrate the performance of the approximation derived in Sec. 6.2.2. We solved numerically the EoM given by Eqs (6.8)–(6.10) with the adiabatic approximation (6.11) (the adiabatic Pastor functional) using a one-step Euler method. We also checked the convergence with more accurate methods.

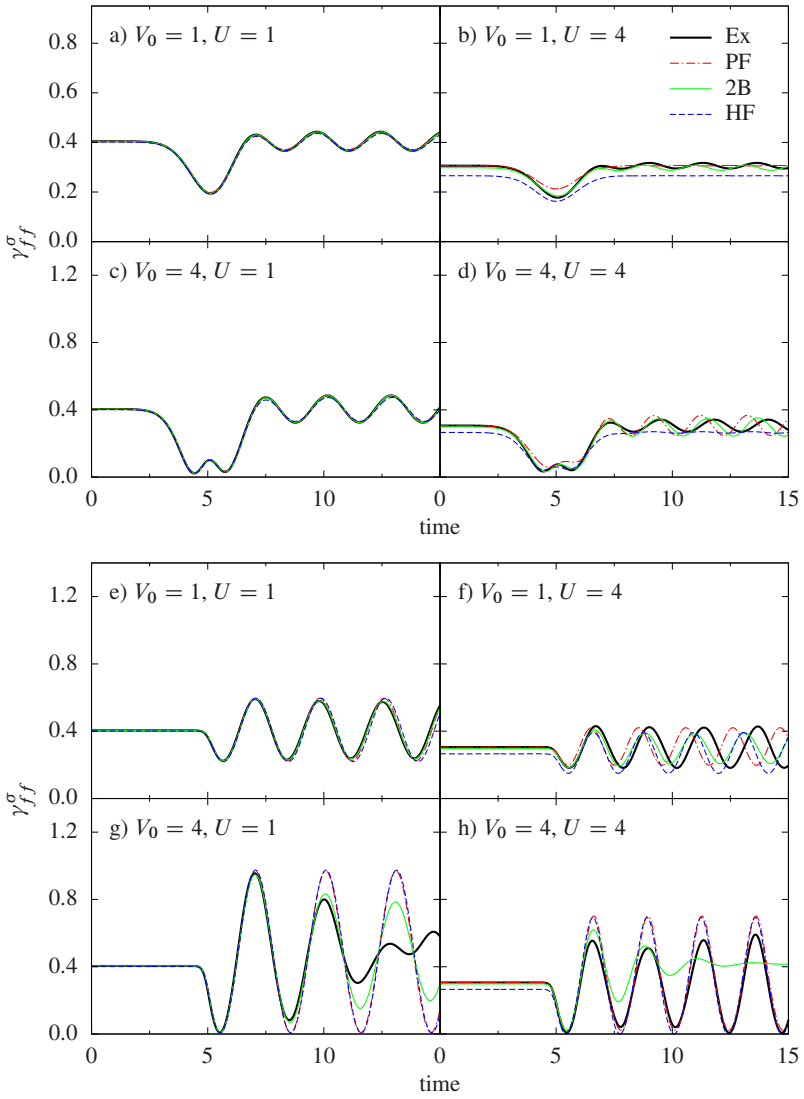

Figure 6.7: Time evolution of the density at the impurity site for the Anderson model after a slow (top) and fast (bottom) Gaussian external perturbation is applied on this side: exact (thick solid black lines) *vs.* (adiabatic) Pastor functional (PF, dashed-dotted red lines), second Born (2B, solid green lines) and Hartree-Fock (HF, dashed blue lines).

In Figs 6.6 and 6.7 we compare the time-dependent density γ^{σ}_{ff} obtained with the adiabatic Pastor approximation with the exact, 2B and HF solutions. In the weakly correlated case ($U = 1$) and for a slow perturbation (Figs 6.6(a), (c) and 6.7(a), (c)) the Pastor functional performs well and it is comparable to the MBAs. When a fast perturbation is considered, the agreement remains good only for weak perturbations (6.6(e) and 6.7 (e)). For strong perturbations (Figs 6.6(g) and 6.7(g)), instead, the Pastor solution follows the exact one only for small times, moreover we note that it is very close to the HF solution and, being adiabatic, does not present the damping

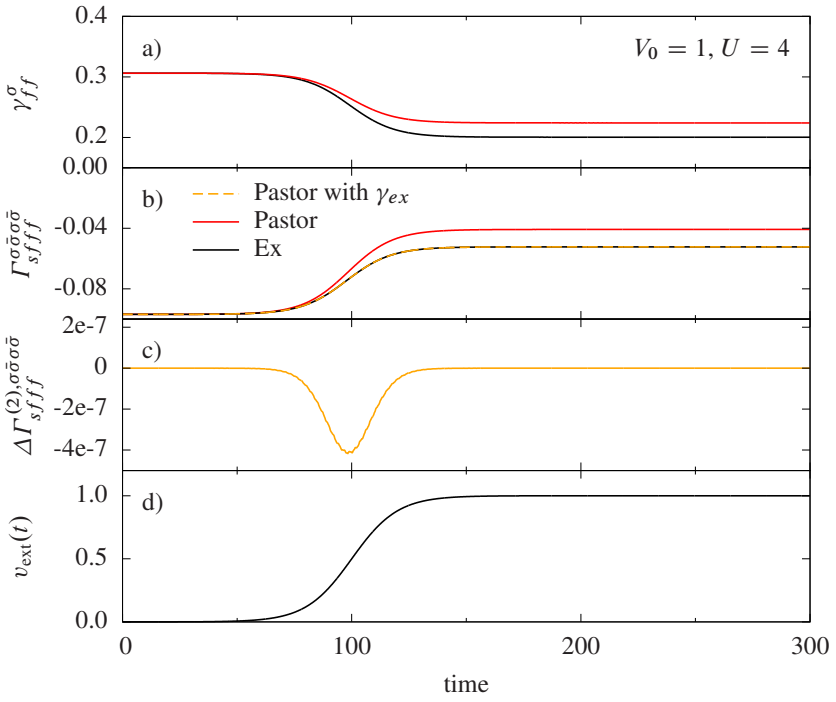

Figure 6.8: Time evolution of the density at the impurity site (a) for the Anderson model after the adiabatic step-like external perturbation represented in (d) is applied on this side: exact (black solid lines) *vs.* (adiabatic) Pastor functional (dashed red lines). In panel (b) are reported the exact 2-RDM, the adiabatic Pastor functional evaluated at the exact time-dependent density matrix elements $\gamma^{\rm ex}_{ff}$ and $\gamma^{\rm ex}_{sf}$ (orange dashed line, on top of the exact result) and at the approximate density matrix elements obtained solving the EoM (6.8)-(6.10) with the Pastor functional. In panel (c) is reported the difference $\Delta\Gamma^{(2),\sigma\bar{\sigma}\sigma\bar{\sigma}}_{sfff}$ between the exact 2-RDM and the adiabatic Pastor functional evaluated at the exact density matrix elements.

problem of 2B.

For strong interaction the Pastor functional is not superior to 2B, except for the case reported in Figs 6.6(h) and 6.7(h), where the performance of 2B is highly worsened by the damping.

The performance of the adiabatic Pastor functional, in particular in the strong correlation regime, is not what one would expect, considering the very good results obtained for the ground state [109]. In order to better understand our results we look at the case in which the perturbation is very slowly switched on at the impurity site f. The form of the perturbation is reported in Fig. 6.8(d). For sufficiently slow perturbation, the system under study can be seen as if it remains always in its instantaneous ground-state (consistently with the adiabatic theorem). In this case the adiabatic Pastor approximation should give, hence, the exact result, since it is an adiabatic extension of the exact ground-state functional. In Fig. 6.8(a) we present the

time evolution of the site density at the impurity site; the exact result is compared with the solution of the EoM using the adiabatic Pastor approximation. We observe that, even if the perturbation is switched on adiabatically, the approximate site density deviates from the exact one at relatively short times. We checked that the dynamics fulfills time-reversal symmetry. To analyze this discrepancy let us inspect $\Gamma^{(2),\sigma\bar{\sigma}\sigma\bar{\sigma}}_{sfff}$. In Fig. 6.8(b) we compare the exact 2-RDM $\Gamma^{(2),\sigma\bar{\sigma}\sigma\bar{\sigma}}_{sfff}$ (black solid line) with the adiabatic Pastor functional evaluated at the exact time-dependent 1-RDM elements $\gamma^{\mathrm{ex}}_{ff}$ and $\gamma^{\mathrm{ex}}_{sf}$ (blue dotted line, on top of the exact result) and at the approximate 1-RDM elements obtained solving the EoM (6.8)-(6.10) with the Pastor functional (red dashed line). The same trend observed for the site density occurs: the approximate solution deviates appreciably from the exact one at relatively short times. If evaluated at the exact density matrix elements, at each time, the Pastor functional gives a value close to, but not the same as, the exact one. The difference between the exact 2-RDM and the Pastor functional evaluated at the exact density matrix elements is plotted in panel (c) of Fig. 6.8; the maximum deviation is of the order of 10^{-7}, which occurs at the point of largest change (maximum slope) in the perturbation. When we consider the EoM this small deviation is amplified and the approximate site density deviates from the exact one.

Although the situation seems quite dramatic for the adiabatic Pastor approximation, we should also consider that here we look at a very small system, which might be quite pathological, and that going to larger systems might mitigate some of these pathologies. Our findings also raise the question whether a nonlocal and adiabatic approximation, such as the one we use, may violate some fundamental constraints when applied on a lattice. This clearly requires some further analysis.

6.4 Conclusions and outlooks

In this chapter we explored new approximations to the electron correlation in Time-Dependent Reduced Density-Matrix Functional Theory. We did this using as test case the two-site Anderson model, which is suitable for studying the effects of electron correlations. We derived approximations to the two-body reduced density matrix (2-RDM) which enters into the equation of motion of the one-body reduced density matrix (1-RDM) from two different perspectives. First, we derived approximations from well-known approximations (GW, second Born, and T matrix) to the self-energy of Many-Body Perturbation Theory (MBPT). The advantage of these approximations is that memory effects are automatically built-in. The disadvantage is that approximations to the 2-RDM derived from MBPT depends on the one-body Green's function (and not on the 1-RDM), which requires to evolve the one-body Green's function as well; moreover, given their perturbative nature, these MB approximations might break down at strong electron correlation. Tests on the Anderson model showed that in general second Born and T matrix perform quite well for the site impurity density, except in

presence of a fast strong perturbation, where they show damping (GW as well), and at strong correlation, where they perform initially well, but then suffer an increasing dephasing with respect to the exact density. The situation is less positive in case of occupation numbers, in particular at strong correlation.
Along a completely different line, we derived the analytic expression for the exact ground-state 2-RDM of the two-site Anderson and we extended it to the time domain in an adiabatic fashion. Clearly in this case memory effects are not taken into account, but the approximation depends on the 1-RDM only and it is supposed to deal well with strong correlations. However our results do not show the expected trends: at strong correlation the agreement with the exact results is poor. We analyzed the origin of this problem and we found that, even with an adiabatic switch on of the perturbation, the site density deviates from the exact one. The comparison of the 2-RDM approximate functional calculated with the exact time-dependent 1-RDM and the approximate 1-RDM shows small deviations which are amplified in the time evolution. These findings suggest to explore this approximation on larger systems, which are probably more forgiving than the small two-site Anderson model.

Conclusions and outlooks

The description, comprehension, and prediction of material properties is the ultimate goal for the theoreticians of condensed matter. The difficulty lies in the fact that one deals with so-called many-body phenomena, intrinsically due to the interaction among all the ($\sim 10^{23}$) electrons in a system. The existing approaches allowed us to advance the comprehension, and even to describe a wide range of materials in a realistic way. Nevertheless, the present level of approximations does not provide yet with a predictive theory that can design materials without relying too much on hypotheses. A way to treat the many-body problem is to use a reduced quantity, such as the electron density $\rho(\mathbf{r})$ for example, which is simpler than the full many-body wavefunction, but it still provides us with the necessary information about the N-electron system. However the price to pay for such a simplified framework is the need for approximations to effective potentials that describe electron correlations. An example of such an approach is Density Functional Theory (DFT) which allows one to calculate all the properties of interest in terms of the density alone. However in this case an accurate description of correlation will require very complicated approximations. Moreover, the expression of the physical observables as functional of the density is not always known. A remedy can be sought using a reduced quantity with more information than only the density, to have a better tool to build approximations. A well suited quantity is the one-body reduced density matrix γ (1-RDM), which is the fundamental variable of Reduced Density-Matrix Functional Theory (RDMFT). Thanks to the one-to-one mapping between the ground-state wavefunction of a given system and the corresponding 1-RDM, all the ground-state physical properties of the system can be calculated as functionals of the 1-RDM. In particular the total energy. Total energy minimization under the constraint of an ensemble N-representable γ, delivers the exact γ. In practice one has to make approximations to the energy functional. The advantage over DFT is that now the kinetic energy part is known in terms of the 1-RDM, and one has to make approximations only to the exchange-correlation part. Various approximations to electron correlation have been proposed in literature. Most of them are functionals of the natural orbitals and occupation numbers (*i.e.*, the eigenvectors and eigenvalues, respectively, of γ), and many can be traced back to the work of Müller, who has proposed an approximation to the correlation which is similar to the Hartree-Fock

approximation but which can produce fractional occupation numbers. This is not always sufficient. Moreover, the expression of the observables of the system in terms of the 1-RDM is not always known. This is the case, for example, for the spectral function, which is closely related to photoemission spectra. In this case there are error cancellations between the approximation to correlation and the approximation to the observable, which can weaken the theory.

In this thesis we addressed the description of electron correlation as well as physical observables within the context of RDMFT. To this aim we exploited the link between reduced density matrices (RDMs) and Green's functions (GFs), which are the basic variables of Many-Body Perturbation Theory (MBPT). The advantage of using MBPT is that one has to approximate only the electron correlation, whereas most of the observables of interest in this thesis have an exact expression in terms of the one-body GF (1-GF). In particular the spectral function is obtained from the imaginary part of 1-GF. Nevertheless, MBPT is in general computationally more expensive than RDMFT and, moreover, state-of-the art approximations to electron correlation, such as GW, do not describe strong correlation (without using spin polarization). Take as an example NiO, which is an antiferromagnetic insulator below the Néel temperature, and a paramagnetic insulator above. The GW approximation (as well as static mean-field theories as DFT within the local density approximation (LDA) and Hartree Fock) gives a metal in the paramagnetic phase. To illustrate the physical contents of the various approximations studied in the thesis as well as for benchmarking we used the Hubbard model, which in many cases can be solved exactly, and which is suitable to describe strong correlation.

First we analyzed the currently used approximations to correlation and observables within RDMFT. We used Müller-like functionals to describe electron correlation. As regards the observables, removal/addition energies and spectral functions are approximated. Our results using the extended Koopmans theorem confirm its reliability for the calculation of removal energies and the lowest addition energy (for finite systems), if a good approximation to the two-body density matrix is used. However, the calculation of the addition energy relies on the $(N+1)$-electron system; in this case, one has an anion, which might not be stable. Moreover, the EKT does not give higher addition energies nor the spectral function. These can be obtained using the approximate DIF/DER method. However, our results suggest a cancellation of errors between this method and Müller-like approximations to electron correlations. Moreover, we found that the spectral peaks are fewer than the exact ones and can have a mixed removal and addition nature as well as a mixed quasiparticle and satellite nature. These findings indicate that although an *ab initio* simulation of the spectral function of a real material using the DIF/DER method could be in agreement with experiment, the underlying physics is not correct. For comparison we also reported the G_0W_0 results. At moderately strong interaction, the G_0W_0 method is superior. In the strongly correlated electron regime we found that both the DIF/DER method and G_0W_0 fail for a fully symmetric ground-state, whereas they give the exact results for

the spin-symmetry-broken case.

Our analysis shows that the failure of the DIF/DER method is mainly due to the approximation of removal/addition energies, rather than to the approximation of the spectral function itself. Therefore one should focus on better approximations to these energies, to improve the description of photoemission spectra. We therefore looked for more accurate approximations by exploiting the link between RDMs and Green's functions. We started from the spectral representation of the 1-GF and we introduced two effective energies, δ^R and δ^A, which account for all removal and addition energy poles of the 1-GF, respectively. These effective energies are represented as series of the one-body, two-body, and higher-order density matrices. In practice one has to truncate these series and several ways to do this are possible. Our choice guarantees the following features for the approximate $\delta^{R/A}$: i) the first moment up to the n-th one of the spectral function generated by the approximation $\delta^{R/A,(n)}$, which involves the 1- up to the $(n+1)$-RDMs, correspond to the exact moments; ii) the total energy obtained from the approximate GF is exact for each $\delta^{R/A,(n)}$, with $n \geq 1$, provided that the exact RDMs are used; iii) the energies generated by the approximation $\delta^{R/A,(1)}$, which involves the 1- and 2-RDMs, are clearly linked to the poles obtained with the Hartree-Fock self-energy, when the Hartree-Fock approximation is used for the 2-RDM. We showed that simple approximations ($\delta^{R/A,(1)}$ and $\delta^{R/A,(2)}$) can give accurate spectra for the Hubbard model in the weak as well as in the strong correlation regimes. In particular the method correctly reproduces the atomic limit without breaking the symmetry of the system. This is an exceptional result, since state-of-the-art methods such as *GW* fail in this regime. We used the simple approximation depending only on the 1- and 2-RDMs to calculate the photoemission spectrum of bulk NiO within RDMFT. Our method produces qualitatively good photoemission spectra for the antiferromagnetic and paramagnetic phases, although the band gap is largely overestimated. Our results on Hubbard chains indicate that this is due to the use of $\delta^{R/A,(1)}$. Indeed the approximation based only on the 1- and 2-RDMs tends to overestimate the band gap with increasing system size, although the spectral shape remains good. Going beyond the 2-RDM and including also the 3-RDM tends to close the gap. One could think of including the effects of higher order RDMs in an effective way. Preliminary tests on NiO with a modified approximation show a global improvement of the spectrum. Another possibility is to explore other ways to cut the $\delta^{R/A}$ series. We think that this method has a great potential and opens the way to a more accurate and computationally efficient description of strongly correlated materials.

In the last part of the thesis we explored new approximations to the electron correlation in Time-Dependent Reduced-Density-Matrix Functional Theory (TDRDMFT). We did this using as test case the two-site Anderson model, which is suitable for studying the effects of electron correlations. We derived approximations to the 2-RDM which enters into the equation of motion of the 1-RDM from two different perspectives. First, we derived approximations from well-known approximations (*GW*, second Born, and T matrix) to the self-energy of Many-Body Perturbation Theory (MBPT). The main

advantage of these approximations is that memory effects are automatically taken into account. The disadvantage is that approximations to the 2-RDM derived from MBPT depends on the 1-GF (and not on the 1-RDM), which requires to evolve the 1-GF as well; moreover, given their perturbative nature, these MB approximations might break down at strong electron correlation. Tests on the Anderson model showed that in general second Born and T matrix perform quite well for the site impurity density, except in presence of a fast strong perturbation, where they show damping (GW as well), and at strong correlation, where they perform initially well but then suffers an increasing dephasing with respect to the exact density. The situation is less positive in case of occupation numbers, in particular at strong correlation.
Along a completely different line, we derived the exact expression for the ground-state 2-RDM of the two-site Anderson model and we extended it to time domain in an adiabatic fashion. Clearly in this case memory effects are not taken into account, but the approximation depends on the 1-RDM only and it is supposed to deal well with strong correlations. However our results do not show the expected trends: at strong correlation the agreement with the exact results is poor. We analyzed the origin of this problem and we found that, even with an adiabatic switch-on of the perturbation, the site density deviates from the exact one. The comparison of the 2-RDM approximate functional calculated with the exact time-dependent 1-RDM and the approximate 1-RDM shows small deviations which are amplified in the time evolution. These findings suggest to explore this approximation on larger systems, which are probably more forgiving than the small two-site Anderson model. They also raise the question whether a nonlocal and adiabatic approximation, such as the one we use, may violate some fundamental constraints when applied on a lattice. This clearly requires some further analysis.

Appendix A

Bonding/antibonding basis and eigenstates for the Hubbard dimer

The bonding/antibonding basis is defined as follows

$$|b\sigma\rangle = \frac{1}{\sqrt{2}}|1\sigma\rangle + \frac{1}{\sqrt{2}}|2\sigma\rangle\,,$$
$$|a\sigma\rangle = \frac{1}{\sqrt{2}}|1\sigma\rangle - \frac{1}{\sqrt{2}}|2\sigma\rangle\,,$$

where $|1\sigma\rangle$ and $|2\sigma\rangle$ are the elements of the site basis. Here 1 and 2 indicate the site and $\sigma = \uparrow, \downarrow$ the spin.

1/4 filling

The coefficients of the transformation from the site basis to the bonding/antibonding basis are given in Tab. A.1. The eigenstates of the Hamiltonian at 1/4 filling are $|b\uparrow\rangle$, $|b\downarrow\rangle$, $|a\uparrow\rangle$, $|a\downarrow\rangle$ with energies $\epsilon_0 - t$, $\epsilon_0 - t$, $\epsilon_0 + t$, $\epsilon_0 + t$, respectively. We chose as ground state $|b\uparrow\rangle$ (one can imagine to remove the spin degeneracy with a small magnetic field). The coefficients of the transformation from the site basis to the bonding/antibonding basis are given in Tab. A.1.

1/2 filling

The coefficients of the transformation from the site basis to the bonding/antibonding basis are given in Tab. A.2. The eigenstates of the Hamiltonian at 1/2 filling in the bonding/antibonding representation are given in Tab. A.3. We defined $c = \sqrt{16t^2 + U^2}$, $a = \sqrt{2\left[16t^2/(c-U)^2 + 1\right]}$ and $b = \sqrt{2\left[16t^2/(c+U)^2 + 1\right]}$. In particular the ground-state ket, in site basis, reads as

$$|\Psi_0\rangle = C_1\left[|1\uparrow, 2\downarrow\rangle - |1\downarrow, 2\uparrow\rangle\right] + C_2\left[|1\uparrow, 1\downarrow\rangle + |2\uparrow, 2\downarrow\rangle\right],$$

	$\|b\uparrow\rangle$	$\|b\downarrow\rangle$	$\|a\uparrow\rangle$	$\|a\downarrow\rangle$
$\|1\uparrow\rangle$	$1/\sqrt{2}$	0	$1/\sqrt{2}$	0
$\|1\downarrow\rangle$	0	$1/\sqrt{2}$	0	$1/\sqrt{2}$
$\|2\uparrow\rangle$	$1/\sqrt{2}$	0	$-1/\sqrt{2}$	0
$\|2\downarrow\rangle$	0	$1/\sqrt{2}$	0	$-1/\sqrt{2}$

Table A.1: Coefficients of the transformation from site to bonding/antibonding basis for 1 electron (1/4 filling).

	$\|b\uparrow, b\downarrow\rangle$	$\|b\uparrow, a\uparrow\rangle$	$\|b\uparrow, a\downarrow\rangle$	$\|b\downarrow, a\uparrow\rangle$	$\|b\downarrow, a\downarrow\rangle$	$\|a\uparrow, a\downarrow\rangle$
$\|1\uparrow, 2\downarrow\rangle$	1/2	0	-1/2	-1/2	0	-1/2
$\|1\downarrow, 2\uparrow\rangle$	-1/2	0	-1/2	-1/2	0	1/2
$\|1\uparrow, 2\uparrow\rangle$	0	-1	0	0	0	0
$\|1\downarrow, 2\downarrow\rangle$	0	0	0	0	-1	0
$\|1\uparrow, 1\downarrow\rangle$	1/2	0	1/2	-1/2	0	1/2
$\|2\uparrow, 2\downarrow\rangle$	1/2	0	-1/2	1/2	0	1/2

Table A.2: Coefficients of the transformation from site to bonding/antibonding basis for 2 electrons (1/2 filling).

with $C_1 = 4t/[a(c-U)]$ and $C_2 = 1/a$. In the bonding/antibonding basis the ground-state ket reads as $|\Psi_0\rangle = B\,|b\uparrow, b\downarrow\rangle + A\,|a\uparrow, a\downarrow\rangle$ where $B = [1 + 4t/(c-U)]/a$ and $A = [1 - 4t/(c-U)]/a$.

E_i	$\|b\uparrow, b\downarrow\rangle$	$\|b\uparrow, a\uparrow\rangle$	$\|b\uparrow, a\downarrow\rangle$	$\|b\downarrow, a\uparrow\rangle$	$\|b\downarrow, a\downarrow\rangle$	$\|a\uparrow, a\downarrow\rangle$
$2\epsilon_0 + (U-c)/2$	$[1+4t/(c-U)]/a$	0	0	0	0	$[1-4t/(c-U)]/a$
$2\epsilon_0 + (U+c)/2$	$[1-4t/(c+U)]/b$	0	0	0	0	$[1+4t/(c+U)]/b$
$2\epsilon_0 + U$	0	0	$-1/\sqrt{2}$	$1/\sqrt{2}$	0	0
$2\epsilon_0$	0	0	0	0	-1	0
$2\epsilon_0$	0	-1	0	0	0	0
$2\epsilon_0$	0	0	$-1/\sqrt{2}$	$-1/\sqrt{2}$	0	0

Table A.3: Eigenenergies and coefficients of the expansion of the eigenstates in the bonding/antibonding basis for the two electron system (1/2 filling).

Appendix B

Hubbard dimer: exact and non-interacting 1-GF

For the Hubbard dimer, the exact and the non-interacting 1-GF can be constructed directly from the definition (3.10). The eigenstates $|\Psi_0\rangle$, $\left|\Psi_k^{N+1}\right\rangle$, and $\left|\Psi_k^{N-1}\right\rangle$, which enter in the definition of the Feynman-Dyson amplitudes, and the corresponding energies E_0, E_k^{N+1}, and E_k^{N-1} can be obtained diagonalizing the Hamiltonian for the system with N, $N+1$ and $N-1$ electrons, respectively.

B.1 Hubbard dimer at 1/4 filling

Exact 1-GF

At 1/4 filling the exact 1-GF in the site basis reads as

$$G_{ij}^{\uparrow}(\omega) = \frac{1}{2}\left[\frac{(-1)^{i-j}}{\omega - (\epsilon_0 + t) + \mathrm{i}\eta} + \frac{1}{\omega - (\epsilon_0 - t) - \mathrm{i}\eta}\right],$$

$$\begin{aligned} G_{ij}^{\downarrow}(\omega) = \frac{1}{2}&\left[\frac{\frac{1}{a^2}\left(1 + \frac{4t}{c-U}\right)^2}{\omega - (\epsilon_0 + (U-c)/2 + t) + \mathrm{i}\eta} + \frac{\frac{1}{b^2}\left(1 - \frac{4t}{c+U}\right)^2}{\omega - (\epsilon_0 + (U+c)/2 + t) + \mathrm{i}\eta}\right] \\ &+ \frac{(-1)^{i-j}}{4}\left[\frac{1}{\omega - (\epsilon_0 + U + t) + \mathrm{i}\eta} + \frac{1}{\omega - (\epsilon_0 + t) + \mathrm{i}\eta}\right], \end{aligned}$$

where $c = \sqrt{16t^2 + U^2}$, $a = \sqrt{2[16t^2/(c-U)^2 + 1]}$, $b = \sqrt{2[16t^2/(c+U)^2 + 1]}$. The 1-GF is spin diagonal; the spin-down block has only the addition part, whereas the spin-up block has both removal and addition parts.
The exact 1-GF in the bonding/antibonding basis can be obtained using the transformations of App. A. It reads as

$$G_{bb}^{\uparrow}(\omega) = \frac{1}{\omega - (\epsilon_0 - t) - \mathrm{i}\eta},$$

$$G^{\downarrow}_{bb}(\omega) = \frac{\frac{1}{a^2}\left(1+\frac{4t}{c-U}\right)^2}{\omega-(\epsilon_0+(U-c)/2+t)+\mathrm{i}\eta} + \frac{\frac{1}{b^2}\left(1-\frac{4t}{c+U}\right)^2}{\omega-(\epsilon_0+(U+c)/2+t)+\mathrm{i}\eta},$$

$$G^{\uparrow}_{aa}(\omega) = \frac{1}{\omega-(\epsilon_0+t)+\mathrm{i}\eta},$$

$$G^{\downarrow}_{aa}(\omega) = \frac{1}{2}\left[\frac{1}{\omega-(\epsilon_0+U+t)+\mathrm{i}\eta} + \frac{1}{\omega-(\epsilon_0+t)+\mathrm{i}\eta}\right],$$

$$G^{\sigma}_{ab} = G^{\sigma}_{ba} = 0.$$

As it can be noted the 1-GF is diagonal in the bonding/antibonding basis.

Non-interacting 1-GF

The non-interacting 1-GF in the site basis can be obtained from the interacting 1-GF taking the limit $U \to 0$. It reads as

$$G^{\uparrow}_{0,ij}(\omega) = \frac{1}{2}\left[\frac{1}{\omega-(\epsilon_0-t)-\mathrm{i}\eta} + \frac{(-1)^{i-j}}{\omega-(\epsilon_0+t)+\mathrm{i}\eta}\right],$$

$$G^{\downarrow}_{0,ij}(\omega) = \frac{1}{2}\left[\frac{1}{\omega-(\epsilon_0-t)+\mathrm{i}\eta} + \frac{(-1)^{i-j}}{\omega-(\epsilon_0+t)+\mathrm{i}\eta}\right].$$

The non-interacting 1-GF in the bonding/antibonding basis reads as

$$G^{\uparrow}_{0,bb}(\omega) = \frac{1}{\omega-(\epsilon_0-t)-\mathrm{i}\eta},$$

$$G^{\downarrow}_{0,bb}(\omega) = \frac{1}{\omega-(\epsilon_0-t)+\mathrm{i}\eta},$$

$$G^{\uparrow}_{0,aa}(\omega) = G^{\downarrow}_{0,aa}(\omega) = \frac{1}{\omega-(\epsilon_0+t)+\mathrm{i}\eta}.$$

B.2 Hubbard dimer at 1/2 filling

Exact 1-GF

At 1/2 filling the exact 1-GF in the site basis reads as

$$\begin{aligned} G^{\uparrow}_{ij}(\omega) &= G^{\downarrow}_{ij}(\omega) \\ &= \frac{1}{2a^2}\left[\frac{\left(1-\frac{4t}{c-U}\right)^2}{\omega-(\epsilon_0+t+(c+U)/2)+\mathrm{i}\eta} + \frac{\left(1+\frac{4t}{c-U}\right)^2}{\omega-(\epsilon_0+t-(c-U)/2)-\mathrm{i}\eta}\right] \\ &+ \frac{(-1)^{i-j}}{2a^2}\left[\frac{\left(1+\frac{4t}{c-U}\right)^2}{\omega-(\epsilon_0-t+(c+U)/2)+\mathrm{i}\eta} + \frac{\left(1-\frac{4t}{c-U}\right)^2}{\omega-(\epsilon_0-t-(c-U)/2)-\mathrm{i}\eta}\right]. \end{aligned}$$

The exact 1-GF in the bonding/antibonding basis reads as

$$\begin{aligned} G^{\uparrow}_{bb}(\omega) &= G^{\downarrow}_{bb}(\omega) \\ &= \frac{1}{a^2}\left[\frac{\left(1-\frac{4t}{c-U}\right)^2}{\omega-(\epsilon_0+t+(c+U)/2)+\mathrm{i}\eta}+\frac{\left(1+\frac{4t}{c-U}\right)^2}{\omega-(\epsilon_0+t-(c-U)/2)-\mathrm{i}\eta}\right], \end{aligned}$$

$$\begin{aligned} G^{\uparrow}_{aa}(\omega) &= G^{\downarrow}_{aa}(\omega) \\ &= \frac{1}{a^2}\left[\frac{\left(1+\frac{4t}{c-U}\right)^2}{\omega-(\epsilon_0-t+(c+U)/2)+\mathrm{i}\eta}+\frac{\left(1-\frac{4t}{c-U}\right)^2}{\omega-(\epsilon_0-t-(c-U)/2)-\mathrm{i}\eta}\right]. \end{aligned}$$

Non-interacting 1-GF

The non-interacting 1-GF in the site basis reads as

$$G^{\uparrow}_{0,ij}(\omega) = G^{\downarrow}_{0,ij}(\omega) = \frac{1}{2}\left[\frac{1}{\omega-(\epsilon_0-t)-\mathrm{i}\eta}\right]+\frac{(-1)^{i-j}}{2}\left[\frac{1}{\omega-(\epsilon_0+t)+\mathrm{i}\eta}\right].$$

The non-interacting 1-GF in the bonding/antibonding basis reads as

$$G^{\uparrow}_{0,bb}(\omega) = G^{\downarrow}_{0,bb}(\omega) = \frac{1}{\omega-(\epsilon_0-t)-\mathrm{i}\eta},$$

$$G^{\uparrow}_{0,aa}(\omega) = G^{\downarrow}_{0,aa}(\omega) = \frac{1}{\omega-(\epsilon_0+t)+\mathrm{i}\eta}.$$

Appendix C

Hubbard dimer: exact RDMs

The matrix elements of the exact 1-RDM can be directly obtained from the definition $\gamma_{ij}^{\sigma} \equiv \langle \Psi_0 | \, \hat{c}_{j\sigma}^{\dagger} \hat{c}_{i\sigma} \, | \Psi_0 \rangle$ or alternatively from the 1-GF derived in App. B, using the fact that $\gamma_{ij}^{\sigma} = -\mathrm{i} \int d\omega/(2\pi) G_{ij}^{\sigma}(\omega) e^{\mathrm{i}\omega 0^+}$.

C.1 1-RDM

At 1/4 filling the matrix elements of the 1-RDM in the site basis read as $\gamma_{11}^{\uparrow} = \gamma_{22}^{\uparrow} = 1/2$ and $\gamma_{12}^{\uparrow} = \gamma_{21}^{\uparrow} = 1/2$, while for the spin down channel the 1-RDM vanishes. Diagonalizing the 1-RDM we obtain the occupation numbers

$$n_{b\uparrow} = 1,$$

$$n_{b\downarrow} = n_{a\uparrow} = n_{a\downarrow} = 0,$$

and the natural orbitals are the bonding/antibonding states given in App. A.

At 1/2 filling the matrix elements of the 1-RDM in the site basis read as

$$\gamma_{11}^{\sigma} = \gamma_{22}^{\sigma} = \frac{1}{2a^2} \left(1 + \frac{4t}{c-U} \right)^2 + \frac{1}{2a^2} \left(1 - \frac{4t}{c-U} \right)^2,$$

$$\gamma_{12}^{\sigma} = \gamma_{21}^{\sigma} = \frac{1}{2a^2} \left(1 + \frac{4t}{c-U} \right)^2 - \frac{1}{2a^2} \left(1 - \frac{4t}{c-U} \right)^2.$$

Diagonalizing the 1-RDM we obtain the occupation numbers

$$n_{b\uparrow} = n_{b\downarrow} = \frac{1}{a^2} \left(1 + \frac{4t}{c-U} \right)^2,$$

$$n_{a\uparrow} = n_{a\downarrow} = \frac{1}{a^2} \left(1 - \frac{4t}{c-U} \right)^2.$$

The natural orbitals are the bonding/antibonding states given in App. A.

Here we note that the coefficients A and B introduced in App. A can be easily related to the occupation numbers; we have $B = \sqrt{n_b}$ and $A = -\sqrt{n_a}$. Thus the ground-state ket in the bonding/antibonding basis is $|\Psi_0\rangle = \sqrt{n_b} \, |b\uparrow, b\downarrow\rangle - \sqrt{n_a} \, |a\uparrow, a\downarrow\rangle$.

C.2 2-RDM

The matrix elements of the 2-RDM can be evaluated using the definition

$$\Gamma^{(2),\sigma_i\sigma_j\sigma_k\sigma_l}_{ijkl} \equiv \langle \Psi_0 | \, \hat{c}^\dagger_{l\sigma_l} \hat{c}^\dagger_{k\sigma_k} \hat{c}_{j\sigma_j} \hat{c}_{i\sigma_i} \, | \Psi_0 \rangle \, .$$

At 1/4 filling we have $\Gamma^{(2)} = 0$. At 1/2 filling the only non-zero matrix elements of the 2-RDM in the bonding/antibonding basis are

$$\Gamma^{(2),\sigma\bar{\sigma}\bar{\sigma}\sigma}_{bbbb} = B^2 = n_b, \tag{C.1}$$

$$\Gamma^{(2),\sigma\bar{\sigma}\bar{\sigma}\sigma}_{aaaa} = A^2 = n_a, \tag{C.2}$$

$$\Gamma^{(2),\sigma\bar{\sigma}\bar{\sigma}\sigma}_{bbaa} = \Gamma^{(2),\sigma\bar{\sigma}\bar{\sigma}\sigma}_{aabb} = AB = -\sqrt{n_b n_a}, \tag{C.3}$$

where $\bar{\sigma}$ is the spin opposite to σ.

C.3 Total energy functional

Using Eqs (C.1)–(C.3) we can calculate the exact total energy functional, which reads as

$$\begin{aligned} E[\{n_{i\sigma_i}\}, \{\phi_i\}] &= \int d\mathbf{x} d\mathbf{x}' \delta(\mathbf{x} - \mathbf{x}') h(\mathbf{x}) \gamma(\mathbf{x}, \mathbf{x}') + \int d\mathbf{x} d\mathbf{x}' v_c(\mathbf{x}, \mathbf{x}') \Gamma^{(2)}(\mathbf{x}, \mathbf{x}'; \mathbf{x}, \mathbf{x}') \\ &= \sum_{j=a,b} \sum_{\sigma_j} h_{jj} n_{j\sigma_j} + \frac{U}{4} \sum_{j=a,b} \sum_{\sigma_j} n_{j\sigma_j} - \frac{U}{4} \sum_{\substack{j,k=a,b \\ j \neq k}} \sum_{\sigma_j} \sqrt{n_{j\sigma_j} n_{k\sigma_j}}. \end{aligned} \tag{C.4}$$

Here we note that the Müller functional, which, for the Hubbard dimer, reads as

$$E[\{n_{i\sigma}\}, \{\phi_i\}] = \sum_{j=a,b} \sum_{\sigma_j} h_{jj} n_{j\sigma_j} + \frac{U}{4} \sum_{j,k=a,b} \sum_{\sigma_j \sigma_k} n_{j\sigma_j} n_{k\sigma_k} - \frac{U}{4} \sum_{j,k=a,b} \sum_{\sigma_j} n^\alpha_{j\sigma_j} n^\alpha_{k\sigma_j},$$

reduces to the exact functional (C.4) when we restrict ourselves to ensemble N-representable 1-RDMs. This means, for the Hubbard dimer, to consider the constraint $n_{a\sigma} = 1 - n_{b\sigma}$.

Appendix D

$\tilde{n}_i^{R/A}$ and $\tilde{\tilde{n}}_i^{R/A}$ in terms of reduced density matrices

Here we show how $\tilde{n}_i^{R/A}$ and $\tilde{\tilde{n}}_i^{R/A}$ can be expressed in terms of reduced density matrices. First, we derive some useful relations by using the anti-commutation relations of the creation and annihilation operators

$$\begin{aligned} \{\hat{c}_i, \hat{c}_j\} = \left\{\hat{c}_i^\dagger, \hat{c}_j^\dagger\right\} = 0, \\ \left\{\hat{c}_i^\dagger, \hat{c}_j\right\} = \delta_{ij}. \end{aligned} \tag{D.1}$$

Let us evaluate the following commutator

$$\begin{aligned} [\hat{c}_i, \hat{c}_j^\dagger \hat{c}_k] &= \hat{c}_i \hat{c}_j^\dagger \hat{c}_k - \hat{c}_j^\dagger \hat{c}_k \hat{c}_i \\ &= \left[\delta_{ij} - \hat{c}_j^\dagger \hat{c}_i\right] \hat{c}_k - \hat{c}_j^\dagger \hat{c}_k \hat{c}_i \\ &= \delta_{ij} \hat{c}_k - \hat{c}_j^\dagger \{\hat{c}_i, \hat{c}_k\} \\ &= \delta_{ij} \hat{c}_k. \end{aligned} \tag{D.2}$$

Taking the Hermitian conjugate of Eq. (D.2) one arrives at

$$[\hat{c}_i^\dagger, \hat{c}_j^\dagger \hat{c}_k] = -\delta_{ik} \hat{c}_j^\dagger. \tag{D.3}$$

In evaluating the commutators of the annihilation operator $\hat{c}_i$ with the interaction potential operator $\hat{V}$ one has to deal with commutators of the kind $[\hat{c}_i, \hat{c}_j^\dagger \hat{c}_k^\dagger \hat{c}_m \hat{c}_l]$, which can be worked out as follows

$$\begin{aligned} [\hat{c}_i, \hat{c}_j^\dagger \hat{c}_k^\dagger \hat{c}_m \hat{c}_l] &= [\hat{c}_i, \hat{c}_j^\dagger \hat{c}_l] \delta_{km} - [\hat{c}_i, \hat{c}_j^\dagger \hat{c}_m \hat{c}_k^\dagger \hat{c}_l] \\ &= \delta_{km} \delta_{ij} \hat{c}_l - \hat{c}_j^\dagger \hat{c}_m [\hat{c}_i, \hat{c}_k^\dagger \hat{c}_l] - [\hat{c}_i, \hat{c}_j^\dagger \hat{c}_m] \hat{c}_k^\dagger \hat{c}_l \\ &= \delta_{km} \delta_{ij} \hat{c}_l - \delta_{ik} \hat{c}_j^\dagger \hat{c}_m \hat{c}_l - \delta_{ij} \hat{c}_m \hat{c}_k^\dagger \hat{c}_l \\ &= \delta_{km} \delta_{ij} \hat{c}_l - \delta_{ik} \hat{c}_j^\dagger \hat{c}_m \hat{c}_l - \delta_{ij} (\delta_{mk} - \hat{c}_k^\dagger \hat{c}_m) \hat{c}_l \\ &= -\delta_{ik} \hat{c}_j^\dagger \hat{c}_m \hat{c}_l + \delta_{ij} \hat{c}_k^\dagger \hat{c}_m \hat{c}_l, \end{aligned} \tag{D.4}$$

where we used Eqs (D.1) and (D.2). Taking the Hermitian conjugate of Eq. (D.4) one arrives at the following relation

$$\left[\hat{c}_i^\dagger, \hat{c}_j^\dagger \hat{c}_k^\dagger \hat{c}_m \hat{c}_l\right] = -\delta_{il}\hat{c}_j^\dagger \hat{c}_k^\dagger \hat{c}_m + \delta_{im}\hat{c}_j^\dagger \hat{c}_k^\dagger \hat{c}_l.$$

The commutators involving the operator $\hat{H}$ can now be evaluated. We first separate the Hamiltonian into the non-interacting part $\hat{H}_0$ and the interacting part $\hat{V}$, obtaining

$$[\hat{c}_i, \hat{H}] = [\hat{c}_i, \hat{H}_0] + [\hat{c}_i, \hat{V}] = h_{ii}\hat{c}_i + [\hat{c}_i, \hat{V}], \tag{D.5}$$

$$[\hat{H}, \hat{c}_i^\dagger] = [\hat{H}_0, \hat{c}_i^\dagger] + [\hat{V}, \hat{c}_i^\dagger] = h_{ii}\hat{c}_i^\dagger + [\hat{c}_i^\dagger, \hat{V}], \tag{D.6}$$

where we made use of Eqs (D.2) and (D.3). From Eqs (D.5) and (D.6) it follows that

$$\begin{aligned}
\hat{c}_i^\dagger[\hat{c}_i, \hat{H}] &= h_{ii}\hat{c}_i^\dagger \hat{c}_i + \hat{c}_i^\dagger[\hat{c}_i, \hat{V}], \\
[\hat{c}_i, \hat{H}]\hat{c}_i^\dagger &= h_{ii}(1 - \hat{c}_i^\dagger \hat{c}_i) + [\hat{c}_i, \hat{V}]\hat{c}_i^\dagger, \\
[\hat{H}, \hat{c}_i^\dagger][\hat{c}_i, \hat{H}] &= h_{ii}^2 \hat{c}_i^\dagger \hat{c}_i + h_{ii}\left(\hat{c}_i^\dagger[\hat{c}_i, \hat{V}] + [\hat{V}, \hat{c}_i^\dagger]\hat{c}_i\right) + [\hat{V}, \hat{c}_i^\dagger][\hat{c}_i, \hat{V}], \\
[\hat{c}_i, \hat{H}][\hat{H}, \hat{c}_i^\dagger] &= h_{ii}^2(1 - \hat{c}_i^\dagger \hat{c}_i) + h_{ii}\left([\hat{c}_i, \hat{V}]\hat{c}_i^\dagger + \hat{c}_i[\hat{V}, \hat{c}_i^\dagger]\right) + [\hat{c}_i, \hat{V}][\hat{V}, \hat{c}_i^\dagger].
\end{aligned}$$

We then evaluate the following commutator

$$\begin{aligned}
[\hat{c}_i, \hat{V}] &= \frac{1}{2}\sum_{jklm} V_{jklm}[\hat{c}_i, \hat{c}_j^\dagger \hat{c}_k^\dagger \hat{c}_m \hat{c}_l] \\
&= \frac{1}{2}\sum_{jklm} V_{jklm}(-\delta_{ik}\hat{c}_j^\dagger \hat{c}_m \hat{c}_l + \delta_{ij}\hat{c}_k^\dagger \hat{c}_m \hat{c}_l) \\
&= \frac{1}{2}\sum_{jkl}(-V_{jikl}\hat{c}_j^\dagger \hat{c}_l \hat{c}_k + V_{ijkl}\hat{c}_j^\dagger \hat{c}_l \hat{c}_k) \\
&= \frac{1}{2}\sum_{jkl}(V_{jilk} + V_{ijkl})\hat{c}_j^\dagger \hat{c}_l \hat{c}_k \\
&= \sum_{jkl} V_{ijkl}\hat{c}_j^\dagger \hat{c}_l \hat{c}_k,
\end{aligned} \tag{D.7}$$

where we used the fact that $V_{ijkl} = V_{jilk}$, which follows directly from the definition of the matrix elements $V_{ijkl} = \int d\mathbf{x}d\mathbf{x}'\phi_i^*(\mathbf{x})\phi_j^*(\mathbf{x}')v_c(\mathbf{r},\mathbf{r}')\phi_k(\mathbf{x})\phi_l(\mathbf{x}')$ interchanging the indices. From the Hermitian conjugate of Eq. (D.7) we arrive at the following relation

$$[\hat{V}, \hat{c}_i^\dagger] = \sum_{jkl} V_{ijkl}^* \hat{c}_k^\dagger \hat{c}_l^\dagger \hat{c}_j = \sum_{jkl} V_{klij}\hat{c}_k^\dagger \hat{c}_l^\dagger \hat{c}_j. \tag{D.8}$$

Here we used the fact that $V_{ijkl}^* = V_{klij}$, which follows from the definition of the Coulomb matrix elements.

The terms appearing in Eqs (5.14), (5.17), and (5.18) can be worked out using Eqs (D.7) and (D.8) giving the following expressions

$$\begin{aligned}
[\hat{V},\hat{c}_i^\dagger][\hat{c}_i,\hat{V}] &= \sum_{jklpqs} V_{klij}V_{ipqs}\hat{c}_k^\dagger\hat{c}_l^\dagger\hat{c}_j\hat{c}_p^\dagger\hat{c}_s\hat{c}_q \\
&= \sum_{jklpqs} V_{klij}V_{ipqs}\hat{c}_k^\dagger\hat{c}_l^\dagger(\delta_{jp}-\hat{c}_p^\dagger\hat{c}_j)\hat{c}_s\hat{c}_q \\
&= \sum_{jklqs} V_{klij}V_{ijqs}\hat{c}_k^\dagger\hat{c}_l^\dagger\hat{c}_s\hat{c}_q \\
&\quad + \sum_{jklpqs} V_{klij}V_{ipqs}\hat{c}_k^\dagger\hat{c}_l^\dagger\hat{c}_p^\dagger\hat{c}_s\hat{c}_j\hat{c}_q,
\end{aligned}$$

$$\begin{aligned}
[\hat{c}_i,\hat{V}]\hat{c}_i^\dagger &= \sum_{jkl} V_{ijkl}\hat{c}_j^\dagger\hat{c}_l\hat{c}_k\hat{c}_i^\dagger \\
&= \sum_{jkl} V_{ijkl}\hat{c}_j^\dagger\hat{c}_l(\delta_{ki}-\hat{c}_i^\dagger\hat{c}_k) \\
&= \sum_{jl} V_{ijil}\hat{c}_j^\dagger\hat{c}_l - \sum_{jkl} V_{ijkl}\hat{c}_j^\dagger(\delta_{li}-\hat{c}_i^\dagger\hat{c}_l)\hat{c}_k \\
&= \sum_{jl} V_{ijil}\hat{c}_j^\dagger\hat{c}_l - \sum_{jk} V_{ijki}\hat{c}_j^\dagger\hat{c}_k + \sum_{jkl} V_{ijkl}\hat{c}_j^\dagger\hat{c}_i^\dagger\hat{c}_l\hat{c}_k \\
&= \sum_{jl} V_{ijil}\hat{c}_j^\dagger\hat{c}_l - \sum_{jk} V_{ijki}\hat{c}_j^\dagger\hat{c}_k - \sum_{jkl} V_{ijkl}\hat{c}_i^\dagger\hat{c}_j^\dagger\hat{c}_l\hat{c}_k,
\end{aligned}$$

$$\begin{aligned}
[\hat{c}_i,\hat{V}][\hat{V},\hat{c}_i^\dagger] &= \sum_{jklspq} V_{ijkl}V_{pqis}\hat{c}_j^\dagger\hat{c}_l\hat{c}_k\hat{c}_p^\dagger\hat{c}_q^\dagger\hat{c}_s \\
&= \sum_{jklspq} V_{ijkl}V_{pqis}\hat{c}_j^\dagger\hat{c}_l(\delta_{kp}-\hat{c}_p^\dagger\hat{c}_k)\hat{c}_q^\dagger\hat{c}_s \\
&= \sum_{jklspq} \delta_{kp}V_{ijkl}V_{pqis}\hat{c}_j^\dagger(\delta_{lq}-\hat{c}_q^\dagger\hat{c}_l)\hat{c}_s - \sum_{jklspq} V_{ijkl}V_{pqis}\hat{c}_j^\dagger(\delta_{lp}-\hat{c}_p^\dagger\hat{c}_l)\hat{c}_k\hat{c}_q^\dagger\hat{c}_s \\
&= \sum_{jklspq} \delta_{kp}\delta_{lq}V_{ijkl}V_{pqis}\hat{c}_j^\dagger\hat{c}_s - \sum_{jklspq} \delta_{kp}V_{ijkl}V_{pqis}\hat{c}_j^\dagger\hat{c}_q^\dagger\hat{c}_l\hat{c}_s \\
&\quad - \sum_{jklspq} \delta_{lp}V_{ijkl}V_{pqis}\hat{c}_j^\dagger(\delta_{kq}-\hat{c}_q^\dagger\hat{c}_k)\hat{c}_s + \sum_{jklspq} V_{ijkl}V_{pqis}\hat{c}_j^\dagger\hat{c}_p^\dagger\hat{c}_l(\delta_{kq}-\hat{c}_q^\dagger\hat{c}_k)\hat{c}_s \\
&= \sum_{jklspq} \delta_{kp}\delta_{lq}V_{ijkl}V_{pqis}\hat{c}_j^\dagger\hat{c}_s - \sum_{jklspq} \delta_{kp}V_{ijkl}V_{pqis}\hat{c}_j^\dagger\hat{c}_q^\dagger\hat{c}_l\hat{c}_s \\
&\quad - \sum_{jklspq} \delta_{lp}\delta_{kq}V_{ijkl}V_{pqis}\hat{c}_j^\dagger\hat{c}_s + \sum_{jklspq} \delta_{lp}V_{ijkl}V_{pqis}\hat{c}_j^\dagger\hat{c}_q^\dagger\hat{c}_k\hat{c}_s \\
&\quad + \sum_{jklspq} \delta_{kq}V_{ijkl}V_{pqis}\hat{c}_j^\dagger\hat{c}_p^\dagger\hat{c}_l\hat{c}_s - \sum_{jklspq} V_{ijkl}V_{pqis}\hat{c}_j^\dagger\hat{c}_p^\dagger(\delta_{lq}-\hat{c}_q^\dagger\hat{c}_l)\hat{c}_k\hat{c}_s
\end{aligned}$$

$$
\begin{aligned}
&= \sum_{jklspq} \delta_{kp}\delta_{lq} V_{ijkl} V_{pqis} \hat{c}_j^\dagger \hat{c}_s - \sum_{jklspq} \delta_{lp}\delta_{kq} V_{ijkl} V_{pqis} \hat{c}_j^\dagger \hat{c}_s \\
&\quad - \sum_{jklspq} \delta_{kp} V_{ijkl} V_{pqis} \hat{c}_j^\dagger \hat{c}_q^\dagger \hat{c}_l \hat{c}_s + \sum_{jklspq} \delta_{lp} V_{ijkl} V_{pqis} \hat{c}_j^\dagger \hat{c}_q^\dagger \hat{c}_k \hat{c}_s \\
&\quad + \sum_{jklspq} \delta_{kq} V_{ijkl} V_{pqis} \hat{c}_j^\dagger \hat{c}_p^\dagger \hat{c}_l \hat{c}_s - \sum_{jklspq} \delta_{lq} V_{ijkl} V_{pqis} \hat{c}_j^\dagger \hat{c}_p^\dagger \hat{c}_k \hat{c}_s \\
&\quad + \sum_{jklspq} V_{ijkl} V_{pqis} \hat{c}_j^\dagger \hat{c}_p^\dagger \hat{c}_q^\dagger \hat{c}_l \hat{c}_k \hat{c}_s .
\end{aligned}
$$

Equations (5.22)-(5.25) can be obtained from Eqs (5.10), (5.14), (5.17), and (5.18) respectively making use of the expressions so far derived. We have

$$
\begin{aligned}
\tilde{n}_i^R &= \langle \Psi_0 | \, \hat{c}_i^\dagger [\hat{c}_i, \hat{H}] \, | \Psi_0 \rangle \\
&= h_{ii} \langle \Psi_0 | \, \hat{c}_i^\dagger \hat{c}_i \, | \Psi_0 \rangle + \sum_{jkl} V_{ijkl} \langle \Psi_0 | \, \hat{c}_i^\dagger \hat{c}_j^\dagger \hat{c}_l \hat{c}_k \, | \Psi_0 \rangle \\
&= h_{ii} n_i + \sum_{jkl} V_{ijkl} \Gamma^{(2)}_{klji},
\end{aligned}
$$

$$
\begin{aligned}
\tilde{\tilde{n}}_i^R &= \langle \Psi_0 | \, [\hat{H}, \hat{c}_i^\dagger][\hat{c}_i, \hat{H}] \, | \Psi_0 \rangle \\
&= h_{ii}^2 n_i + h_{ii} \sum_{jkl} \left(V_{ijkl} \Gamma^{(2)}_{klji} + V_{klij} \Gamma^{(2)}_{ijlk} \right) + \sum_{jklqs} V_{klij} V_{ijqs} \Gamma^{(2)}_{qslk} + \sum_{jklpqs} V_{klij} V_{ipqs} \Gamma^{(3)}_{qjsplk},
\end{aligned}
$$

$$
\begin{aligned}
\tilde{n}_i^A &= \langle \Psi_0 | \, [\hat{c}_i, \hat{H}] \hat{c}_i^\dagger \, | \Psi_0 \rangle \\
&= h_{ii}(1 - n_i) + \sum_j V_{ijij} n_j - \sum_j V_{ijji} n_j - \sum_{jkl} V_{ijkl} \Gamma^{(2)}_{klji},
\end{aligned}
$$

$$
\begin{aligned}
\tilde{\tilde{n}}_i^A &= \langle \Psi_0 | \, [\hat{c}_i, \hat{H}][\hat{H}, \hat{c}_i^\dagger] \, | \Psi_0 \rangle \\
&= h_{ii}^2 (1 - n_i) + 2 h_{ii} \sum_j (V_{ijij} n_j - V_{jiij} n_j) - \sum_{jlk} V_{klij} \Gamma^{(2)}_{ijlk} - \sum_{jlk} V_{ijkl} \Gamma^{(2)}_{klji} \\
&\quad + \sum_{jkl} V_{ijkl} V_{klij} n_j - \sum_{jkl} V_{ijkl} V_{lkij} n_j + \sum_{jklspq} \delta_{kp} V_{ijkl} V_{pqis} \Gamma^{(2)}_{lsqj} \\
&\quad - \sum_{jklspq} V_{ijkl} V_{pqis} \left(\delta_{lp} \Gamma^{(2)}_{ksqj} + \delta_{kq} \Gamma^{(2)}_{sljp} + \delta_{lq} \Gamma^{(2)}_{ksjp} \right) \\
&\quad - \sum_{jklspq} V_{ijkl} V_{pqis} \Gamma^{(3)}_{klsqjp},
\end{aligned}
$$

where we used the definitions $\Gamma^{(2)}_{ijkl} = \langle \Psi_0 | \, \hat{c}_l^\dagger \hat{c}_k^\dagger \hat{c}_j \hat{c}_i \, | \Psi_0 \rangle$, and

$$
\Gamma^{(3)}_{ijklmn} = \langle \Psi_0 | \hat{c}_n^\dagger \hat{c}_m^\dagger \hat{c}_l^\dagger \hat{c}_k \hat{c}_j \hat{c}_i | \Psi_0 \rangle .
$$

Appendix E

EET on the Hubbard dimer

E.1 Exact density matrices

Here we derive the expressions for $\delta^{R/A,(1)}$ for the Hubbard dimer at half filling, using the exact 2-RDM given in App. C. Using Eqs (C.1)–(C.3), Eq. (5.22) gives

$$\begin{aligned}\tilde{n}^R_{b\sigma} &= h_{bb}n_{b\sigma} + \frac{U}{2}\left(\Gamma^{(2),\sigma\bar{\sigma}\bar{\sigma}\sigma}_{bbbb} + \Gamma^{(2),\sigma\bar{\sigma}\bar{\sigma}\sigma}_{bbaa}\right)\\ &= h_{bb}n_{b\sigma} + \frac{U}{2}(B^2 + AB),\end{aligned}$$

$$\begin{aligned}\tilde{n}^R_{a\sigma} &= h_{aa}n_{a\sigma} + \frac{U}{2}\left(\Gamma^{(2),\sigma\bar{\sigma}\bar{\sigma}\sigma}_{aaaa} + \frac{U}{2}\Gamma^{(2),\sigma\bar{\sigma}\bar{\sigma}\sigma}_{aabb}\right)\\ &= h_{aa}n_{a\sigma} + \frac{U}{2}(A^2 + AB),\end{aligned}$$

while Eq. (5.24) gives

$$\begin{aligned}\tilde{n}^A_{b\sigma} &= h_{bb}(1 - n_{b\sigma}) + \frac{U}{2}\sum_{i\sigma_i} n_{i\sigma_i} - \frac{U}{2}\sum_i n_{i\sigma} - \tilde{n}^R_{b\sigma}\\ &= h_{bb}(1 - n_{b\sigma}) + \frac{U}{2} - \frac{U}{2}(B^2 + AB),\end{aligned}$$

$$\begin{aligned}\tilde{n}^A_{a\sigma} &= h_{aa}(1 - n_{a\sigma}) + \frac{U}{2}\sum_{i\sigma_i} n_{i\sigma_i} - \frac{U}{2}\sum_i n_{i\sigma} - \tilde{n}^R_{a\sigma}\\ &= h_{aa}(1 - n_{a\sigma}) + \frac{U}{2} - \frac{U}{2}(A^2 + AB).\end{aligned}$$

We finally obtain

$$\begin{aligned}
\delta^{R,(1)}_{b\sigma} &= \frac{\tilde{n}^R_{b\sigma}}{n_{b\sigma}} = \epsilon_0 - t + \frac{U}{2}\frac{B+A}{B}, \\
\delta^{R,(1)}_{a\sigma} &= \frac{\tilde{n}^R_{a\sigma}}{n_{a\sigma}} = \epsilon_0 + t + \frac{U}{2}\frac{A+B}{A}, \\
\delta^{A,(1)}_{b\sigma} &= \frac{\tilde{n}^A_{b\sigma}}{1-n_{b\sigma}} = \epsilon_0 - t + \frac{U}{2}\frac{A-B}{A}, \\
\delta^{A,(1)}_{a\sigma} &= \frac{\tilde{n}^A_{a\sigma}}{1-n_{a\sigma}} = \epsilon_0 + t + \frac{U}{2}\frac{B-A}{B}.
\end{aligned}$$

Using the definition of the coefficients A and B, given in App. A, we retrieve the exact poles of the 1-GF (see App. B). We found that also using $\delta^{R/A,(n)}$ with $n > 2$ we retrieve the exact solution.

E.2 Approximate density matrices

Here we derive the expression for $\delta^{R/A,(1)}$ for the Hubbard dimer at half filling, using an approximate 2-RDM. Inserting in Eqs (5.22) and (5.24) the power functional

$$\Gamma^{(2),\sigma_i\sigma\sigma\sigma_i}_{klji} = n_{i\sigma_i} n_{j\sigma_j}\delta_{ik}\delta_{jl} - n^\alpha_{i\sigma_i} n^\alpha_{j\sigma_j}\delta_{il}\delta_{jk}\delta_{\sigma_j\sigma_i},$$

we obtain

$$\begin{aligned}
\tilde{n}^R_{i\sigma_i} &= h_{ii} n_{i\sigma_i} + \sum_{jkl}\sum_{\sigma} V_{ijkl}\left(n_{i\sigma_i} n_{j\sigma}\delta_{ik}\delta_{jl} - n^\alpha_{i\sigma_i} n^\alpha_{j\sigma}\delta_{il}\delta_{jk}\delta_{\sigma\sigma_i}\right) \\
&= h_{ii} n_{i\sigma_i} + \sum_{j}\sum_{\sigma} V_{ijij} n_{i\sigma_i} n_{j\sigma} - \sum_j V_{ijji} n^\alpha_{i\sigma_i} n^\alpha_{j\sigma_i} \\
&= h_{ii} n_{i\sigma_i} + \frac{U}{2}\left(n_{i\sigma_i}\sum_j\sum_\sigma n_{j\sigma} - n^\alpha_{i\sigma_i}\sum_j n^\alpha_{j\sigma_i}\right) \\
&= h_{ii} n_{i\sigma_i} + \frac{U}{2}\left(n_{i\sigma_i} N - n^\alpha_{i\sigma_i}\sum_j n^\alpha_{j\sigma_i}\right),
\end{aligned} \tag{E.1}$$

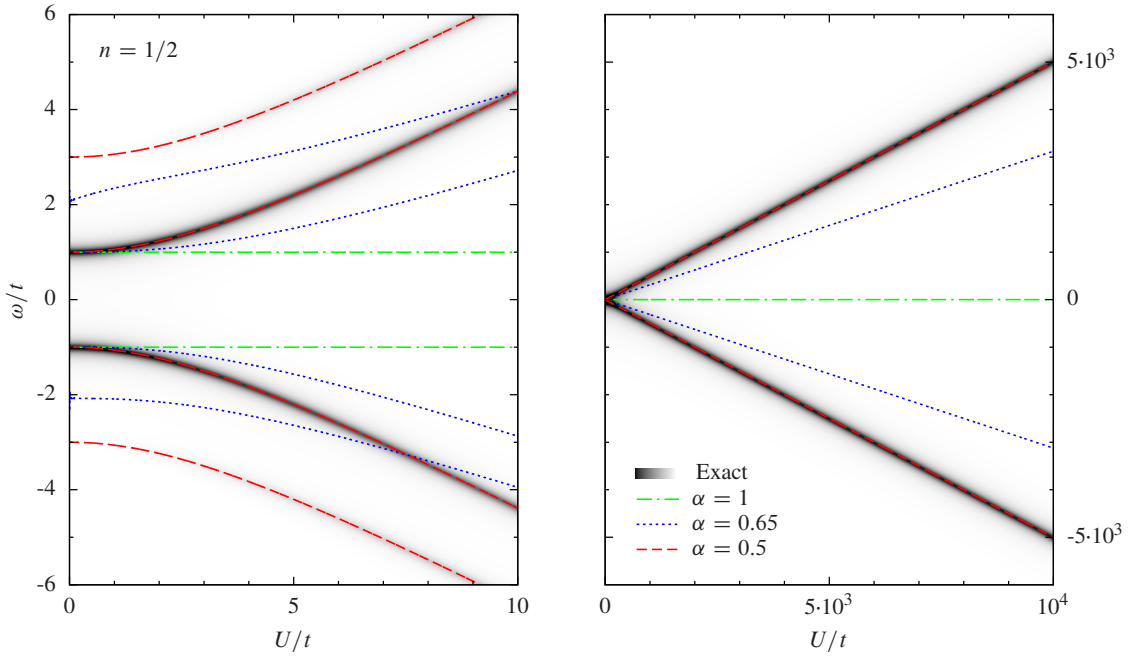

Figure E.1: Addition and removal energies for the Hubbard dimer at 1/2 filling: exact *vs.* EET ($\delta^{(1)}$) with approximate density matrices for different values of α.

where N is the total number of electrons. Here we used the fact that $V_{ijij} = V_{ijji} = U/2$ for the Hubbard dimer in the bonding/antibonding basis. For the addition we have

$$\begin{aligned}
\tilde{n}^{A}_{i\sigma_i} &= h_{ii}(1 - n_{i\sigma_i}) + \sum_j \sum_\sigma V_{ijij} n_{j\sigma} - \sum_j V_{ijji} n_{j\sigma_i} - \tilde{n}^{R}_{i\sigma_i} \\
&= h_{ii}(1 - n_{i\sigma_i}) + \frac{U}{2}\left(\sum_j \sum_\sigma n_{j\sigma} - \sum_j n_{j\sigma_i}\right) - \tilde{n}^{R}_{i\sigma_i} \\
&= h_{ii}(1 - n_{i\sigma_I}) + \frac{U}{2}\left(N - N_{\sigma_i}\right) - \tilde{n}^{R}_{i\sigma_i} \\
&= h_{ii}(1 - n_{i\sigma_I}) + \frac{U}{2}\left(N - N_{\sigma_i} - n_{i\sigma_i} N + n^{\alpha}_{i\sigma_i} \sum_j n^{\alpha}_{j\sigma_i}\right),
\end{aligned} \tag{E.2}$$

where N_{σ_i} is the number of electrons with spin σ_i. Using Eqs (E.1) and (E.2) in Eqs (5.15) and (5.19), respectively, we get ($N = 2$, $N_{\sigma_i} = 1$ at half filling)

$$\delta^{R,(1)}_{i\sigma_i} = h_{ii} + U - \frac{U}{2} n^{\alpha-1}_{i\sigma_i} \sum_j n^{\alpha}_{j\sigma_i}, \tag{E.3}$$

and

$$\delta^{A,(1)}_{i\sigma_i} = h_{ii} + U - \frac{U}{2}\frac{1}{1 - n_{i\sigma_i}}\left(N_{\sigma_i} - n^{\alpha}_{i\sigma_i} \sum_j n^{\alpha}_{j\sigma_i}\right). \tag{E.4}$$

If we use in Eqs (E.3) and (E.4) the occupation numbers obtained from the minimization of the total energy functional within the Müller approximation ($\alpha = 0.5$), we obtain the exact removal and addition energies. In Fig. E.1 we compare the removal and addition energies obtained using $\delta^{(1)}$, for various values of the parameter α, with the exact energies. For $\alpha = 1$ we have $n_{b\sigma} = 1$ and $n_{a\sigma} = 0$, which give the removal and addition energies $\delta^{R,(1)}_{b\sigma} = \epsilon_0 - t + U/2$ and $\delta^{A,(1)}_{a\sigma} = \epsilon_0 + t + U/2$. For $0.5 < \alpha < 1$ we have an intermediate situation were the gap is smaller than the exact one.

Appendix F

RDMFT and EET for the infinite Hubbard model

Let us consider the infinite Hubbard model. Here we will restrict ourselves to the case of a 1D, 2D square and 3D simple cubic lattices. The 1-RDM is diagonal in momentum space, *i.e.*, the natural orbitals are the momentum operator eigenstates $|\mathbf{k},\sigma\rangle$; the 1-RDM is thus given by

$$\gamma_{\sigma\sigma'}(\mathbf{k},\mathbf{k}') = \delta(\mathbf{k}-\mathbf{k}')\delta_{\sigma\sigma'}n_\sigma(\mathbf{k}).$$

The total energy functional within the power-functional approximation reads as

$$\begin{aligned} E[\{n_\sigma(\mathbf{k})\}] = &-2t\sum_{\sigma'}\int\frac{d\mathbf{k}'}{(2\pi)^D}\sum_i\cos(k_i')n_{\sigma'}(\mathbf{k}') \\ &+\frac{U}{2}\sum_{\sigma'\sigma''}\int\frac{d\mathbf{k}'}{(2\pi)^D}\frac{d\mathbf{k}''}{(2\pi)^D}[n_{\sigma'}(\mathbf{k}')n_{\sigma''}(\mathbf{k}'')-n^\alpha_{\sigma'}(\mathbf{k}')n^\alpha_{\sigma''}(\mathbf{k}'')\delta_{\sigma'\sigma''}], \end{aligned} \tag{F.1}$$

where $D=1,2,3$ is the dimension of the k-space considered and k_i is the i-th component of the D-dimensional vector $\mathbf{k}$. Here we will consider only the case of a spin-symmetric system, *i.e.*, $n_\uparrow(\mathbf{k}) = n_\downarrow(\mathbf{k}) \equiv n(\mathbf{k})$. In this case the functional (F.1) reduces to

$$\begin{aligned} E[n(\mathbf{k})] = &-4t\int\frac{d\mathbf{k}'}{(2\pi)^D}\sum_i\cos(k_i')n(\mathbf{k}') \\ &+\frac{U}{2}\int\frac{d\mathbf{k}'}{(2\pi)^D}\frac{d\mathbf{k}''}{(2\pi)^D}[4n(\mathbf{k}')n(\mathbf{k}'')-2n^\alpha(\mathbf{k}')n^\alpha(\mathbf{k}'')]. \end{aligned}$$

Moreover, the momentum distribution function $n(\mathbf{k})$ is normalized in such a way that

$$\int\frac{d\mathbf{k}}{(2\pi)^D}n(\mathbf{k}) = \frac{n}{2}, \tag{F.2}$$

with $n = N/N_s$ the ratio between the number of electrons N and the number of the sites of the lattice N_s. Using (F.2), the integrals in the Hartree term can be performed giving

$$E[\{n(\mathbf{k})\}] = -4t \int \frac{d\mathbf{k}'}{(2\pi)^D} \sum_i \cos(k_i') n(\mathbf{k}') + \frac{U}{2} n^2 - U \int \frac{d\mathbf{k}'}{(2\pi)^D} \frac{d\mathbf{k}''}{(2\pi)^D} n^\alpha(\mathbf{k}') n^\alpha(\mathbf{k}'').$$

The stationarity condition (2.22) with respect to the variation in $n(\mathbf{k})$ reads as

$$\frac{\delta E[\{n(\mathbf{k})\}]}{\delta n(\mathbf{k})} = -\frac{4t}{(2\pi)^D} \sum_i \cos(k_i) - \frac{2U}{(2\pi)^D} \alpha n^{\alpha-1}(\mathbf{k}) \int \frac{d\mathbf{k}'}{(2\pi)^D} n^\alpha(\mathbf{k}') = \mu, \qquad \text{(F.3)}$$

where μ is the Lagrange multiplier introduced in Eq. (2.19). The common coefficient $1/(2\pi)^D$ is unessential, as the constant μ can be redefined in such a way to make it disappear ($\tilde{\mu} \equiv (2\pi)^D \mu$). Equation (F.3) can be formally solved with respect to $n(\mathbf{k})$ giving

$$n(\mathbf{k}) = \left[\frac{-4t \sum_i \cos(k_i) - \tilde{\mu}}{2\alpha U \int d\mathbf{k}'/(2\pi)^D n^\alpha(\mathbf{k}')} \right]^{\frac{1}{\alpha-1}}.$$

The optimal $n(\mathbf{k})$ can be now found iteratively: we start with some guess for $n(\mathbf{k})$ (*e.g.*, the Hartree-Fock solution), $\tilde{\mu}$ is then calculated with an iterative bisection method until $\int d\mathbf{k}/(2\pi)^D n(\mathbf{k})$ converges to $n/2$. Once $\tilde{\mu}$ is obtained, we can calculate the new $n(\mathbf{k})$. The procedure can be repeated until the global convergence is reached. At each step the condition $0 \leq n(\mathbf{k}) \leq 1$ is imposed by setting $n(\mathbf{k}) = 1$ ($n(\mathbf{k}) = 0$) if $n(\mathbf{k}) > 1$ ($n(\mathbf{k}) < 0$).

In Fig. F.1 we report the momentum distribution function $n(\mathbf{k})$ for the 1D, 2D square and 3D simple cubic lattices for various values of the interaction strength U/t and α. The ground-state energy and the fundamental gap are shown as a function of the interaction strength in Fig. 5.7 in Chap. 5. Using the momentum distribution function $n(\mathbf{k})$ we can calculate the EET (at the level of $\delta^{(1)}$) removal and addition energies, and the spectral function. The EET (at the level of $\delta^{(1)}$) spectral functions for the infinite Hubbard model on 1D, 2D square and 3D simple cubic lattices are reported in Fig. F.2 for different values of the Coulomb repulsion U. The results refer to the power functional ($\alpha = 0.5, 0.6, 1$). As can be noticed the EET method with the power functional and $0.5 \leq \alpha < 1$ produces always a gap at 1/2 filling for any $U/t \neq 0$.

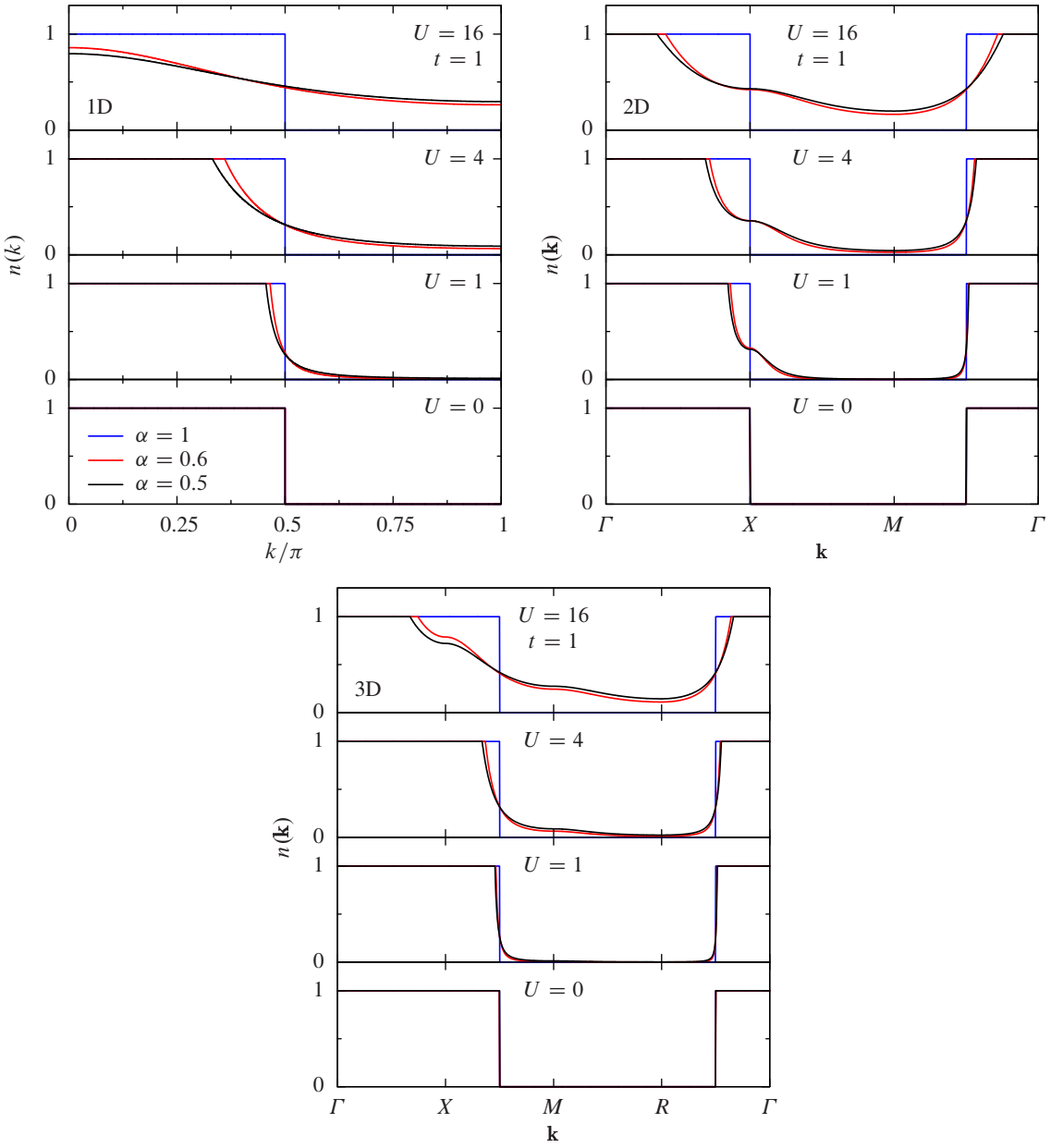

Figure F.1: Momentum distribution function $n(\mathbf{k})$ for the 1D (top left), 2D square (top right) and 3D simple cubic (bottom) lattices for various values of the interaction strength U/t, obtained from the minimization of the power functional with different values of α. For the 2D square and 3D simple cubic lattices the momentum $\mathbf{k}$ follows a path along high symmetry directions of the respective first Brillouin zone.

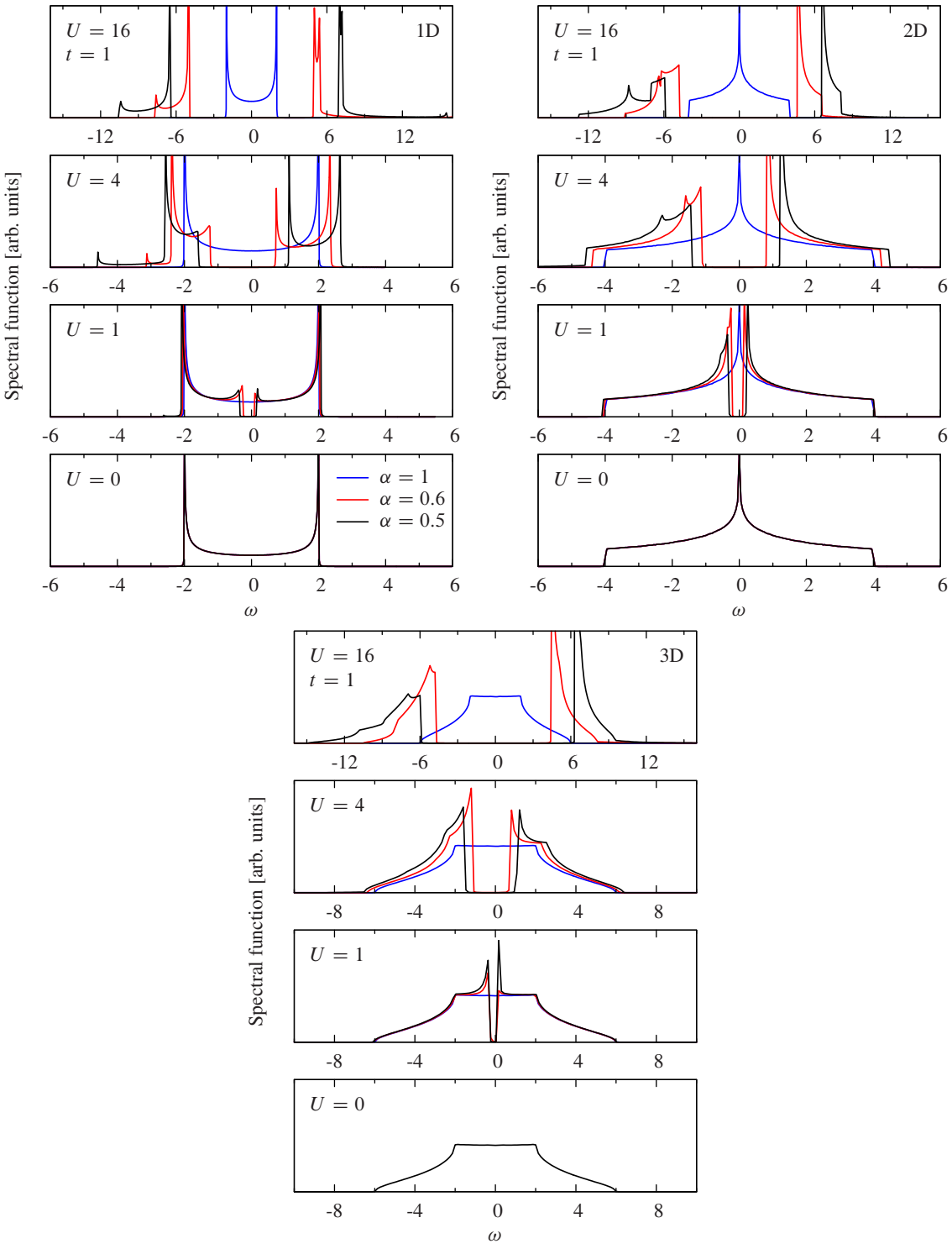

Figure F.2: Spectral function of the infinite 1D (top left), 2D square (top right) and 3D simple cubic (bottom) lattices Hubbard model at half filling, for different values of the interaction strength U/t, calculated using the EET method with the power functional.

Appendix G

Derivation of 2-RDM in the two-level Anderson model

In this Appendix we derive the two-body reduced density matrix element $\Gamma^{(2)}_{sfff}$ for the ground (singlet) state of a two-level Anderson model. First we focus on pure-state N representable density matrices γ at half filling and then we extend the functional to ensemble N representable γ. More details can be found in Ref. [109]. The singlet ground-state of the system reads

$$|\Psi\rangle = \alpha_1 \hat{c}^\dagger_{s\uparrow}\hat{c}^\dagger_{s\downarrow}|0\rangle + \alpha_2 \hat{f}^\dagger_\uparrow \hat{f}^\dagger_\downarrow |0\rangle + \frac{\alpha_3}{\sqrt{2}}\left(\hat{f}^\dagger_\uparrow \hat{c}^\dagger_{s\downarrow} - \hat{f}^\dagger_\downarrow \hat{c}^\dagger_{s\uparrow}\right)|0\rangle\,,$$

with

$$\begin{aligned} 2\alpha_2^2 + \alpha_3^2 &= \gamma_{ff}, \\ 2\alpha_1^2 + \alpha_3^2 &= 2 - \gamma_{ff}, \\ \sqrt{2}(\alpha_1 + \alpha_2)\alpha_3 &= \gamma_{sf}, \end{aligned}$$

from which

$$\Gamma^{(2),\sigma\bar{\sigma}\sigma\bar{\sigma}}_{sfff} = -\frac{\alpha_2\alpha_3}{\sqrt{2}} = \frac{\gamma_{sf}}{4}\left[-1 + \frac{1-\gamma_{ff}}{1-\sqrt{|\gamma^0_{sf}|^2 - |\gamma_{sf}|^2}}\right]. \tag{G.1}$$

Note that here $\gamma_{ij} = \sum_\sigma \gamma^\sigma_{ij}$. We note that in the uncorrelated limit, for which $\gamma_{sf} = \gamma^0_{sf} = \sqrt{\gamma_{ff}(2-\gamma_{ff})}$ [109], Eq. (G.1) reduces to the HF solution $\Gamma^{(2),\sigma\bar{\sigma}\sigma\bar{\sigma}}_{sfff} \approx -\gamma^{\bar{\sigma}}_{ff}\gamma^\sigma_{sf}$.

To extend the functional (G.1) to ensemble N representable γ we follow the same arguments of Ref. [109]. We arrive at Eqs (6.11)-(6.13).

List of publications

- S. Di Sabatino, J. A. Berger, L. Reining, and P. Romaniello, *Reduced Density-Matrix Functional Theory: correlation and spectroscopy*, J. Chem. Phys. **143**, 024108 (2015).
- S. Di Sabatino, J. A. Berger, L. Reining, and P. Romaniello, *Photoemission spectra from reduced density matrices: Band gap in strongly correlated systems*, submitted to Phys. Rev. Lett.
- S. Di Sabatino, C. Verdozzi, and P. Romaniello, *Time-dependent Reduced Density-Matrix Functional Theory: an exploration of memory effects and strong correlation*, in preparation.

Acknowledgments

Firstly, I would like to express my sincere gratitude to my advisor Pina Romaniello for the continuous support of my Ph.D study and related research, for her patience, motivation and valuable advice. Her guidance helped me in all the time of research and writing of this thesis.
Special thanks go to Arjan Berger, Lucia Reining and Claudio Verdozzi for the help and useful discussions.
Some of the work in this thesis was done at the Mathematical Physics group at Lund University, Sweden. I thank Claudio Verdozzi for his hospitality.
I would like to thank the members of the jury, and in particular the referees Silke Biermann and Eberhard K. U. Gross, who accepted to read my thesis and gave me precious comments. I equally thank Arjan Berger, Christoph Meier, Pina Romaniello, and Francesco Sottile for the interesting and pertinent questions during my thesis defense.
I would like also to thank Sangeeta Sharma, Matteo Gatti, Matteo Guzzo, Florian Eich, Nektarios N. Lathiotakis for useful discussions.
I thank the current and former members of the Cluster Physics group of the Laboratoire de Physique Théorique, IRSAMC in Toulouse, and in particular my colleagues Congzhang Gao, Phillipp Wopperer, and Nader Slama.

Stefano Di Sabatino,
Toulouse, November 2015

Bibliography

[1] A. Abrikosov, L. P. Gorkov, and I. E. Dzyaloshinski. *Methods of Quantum Field Theory in Statistical Physics*. Dover publications, 1975.

[2] A. Akbari, M. J. Hashemi, A. Rubio, R. M. Nieminen, and R. van Leeuwen. *Phys. Rev. B*, 85:235121, 2012.

[3] G. Alvarez. DMRG++, http://www.ornl.gov/ gz1/dmrgPlusPlus.

[4] P. W. Anderson. *Phys. Rev.*, 124:41–53, 1961.

[5] H. Appel and E. K. U. Gross. *Europhys. Lett.*, 92(2):23001, 2010.

[6] F. Aryasetiawan and O. Gunnarsson. *Rep. Prog. Phys.*, 61(3):237–312, 1998. and references therein.

[7] W. G. Aulbur, L. Jönsson, and J. W. Wilkins. *Solid State Phys.*, 54:1, 1999. and references therein.

[8] E. J. Baerends. *Phys. Rev. Lett.*, 87:133004, 2001.

[9] J. A. Berger, L. Reining, and F. Sottile. *Phys. Rev. B*, 82:041103, 2010.

[10] J. A. Berger, L. Reining, and F. Sottile. *Phys. Rev. B*, 85:085126, 2012.

[11] J. A. Berger, P. Romaniello, F. Tandetzky, B. S. Mendoza, C. Brouder, and L. Reining. *New J. Phys.*, 16(11):113025, 2014.

[12] S. Biermann, F. Aryasetiawan, and A. Georges. *Phys. Rev. Lett.*, 90:086402, 2003.

[13] G. H. Booth, A. Gruneis, G. Kresse, and A. Alavi. *Nature*, 493(24):365, 2013.

[14] M. A. Buijse and E. J. Baerends. *Mol. Phys.*, 100(4):401–421, 2002.

[15] F. Caruso, P. Rinke, X. Ren, M. Scheffler, and A. Rubio. *Phys. Rev. B*, 86:081102, 2012.

[16] F. Caruso, D. R. Rohr, M. Hellgren, X. Ren, P. Rinke, A. Rubio, and M. Scheffler. *Phys. Rev. Lett.*, 110:146403, 2013.

[17] A. N. Chantis, M. van Schilfgaarde, and T. Kotani. *Phys. Rev. B*, 76:165126, 2007.

[18] J. Cioslowski and K. Pernal. *J. Chem. Phys.*, 111(8):33963400, 1999.

[19] J. Cioslowski, K. Pernal, and P. Ziesche. *J. Chem. Phys.*, 117(21):95609566, 2002.

[20] Cohen A.J. and Baerends E.J. *Chemi. Phys. Lett.*, 364(34):409419, 2002.

[21] A. J. Coleman. *Rev. Mod. Phys.*, 35:668–686, 1963.

[22] G. Csanak, H. Taylor, and R. Yaris. Green's Function Technique in Atomic and Molecular Physics. volume 7 of *Advances in Atomic and Molecular Physics*, page 287361. Academic Press, 1971.

[23] G. Csányi and T. A. Arias. *Phys. Rev. B*, 61:7348–7352, 2000.

[24] E. Dagotto. *Rev. Mod. Phys.*, 66:763–840, 1994.

[25] N. E. Dahlen, R. van Leeuwen, and U. von Barth. *Phys. Rev. A*, 73:012511, 2006.

[26] O. W. Day, D. W. Smith, and C. Garrod. *Int. J. Quantum Chem.*, 8(S8):501509, 1974.

[27] A. Einstein. *Annalen der Physik*, 322(6):132148, 1905.

[28] Elk, http://elk.sourceforge.net, 2004.

[29] J. M. Escartín, M. Vincendon, P. Romaniello, P. M. Dinh, P.-G. Reinhard, and E. Suraud. *J. Chem. Phys.*, 142(8), 2015.

[30] S. V. Faleev, M. van Schilfgaarde, and T. Kotani. *Phys. Rev. Lett.*, 93(12):126406, 2004.

[31] S. V. Faleev, M. van Schilfgaarde, and T. Kotani. *Phys. Rev. Lett.*, 93:126406, 2004.

[32] A. Fetter and J. D. Walecka. *Quantum Theory of Many-Particle Systems*. Dover publications, 2003.

[33] R. L. Frank, E. H. Lieb, R. Seiringer, and H. Siedentop. *Phys. Rev. A*, 76:052517, 2007.

[34] M. Fuchs, Y.-M. Niquet, X. Gonze, and K. Burke. *J. Chem Phys.*, 122(9):, 2005.

[35] S. Fuchs, E. Gull, M. Troyer, M. Jarrell, and T. Pruschke. *Phys. Rev. B*, 83:235113, 2011.

[36] V. M. Galitskii and A. B. Migdal. *Sov. Phys.-JETP*, 7:96, 1958.

[37] M. Gatti, F. Bruneval, V. Olevano, and L. Reining. *Phys. Rev. Lett.*, 99:266402, 2007.

[38] A. Georges and G. Kotliar. *Phys. Rev. B*, 45:6479–6483, 1992.

[39] A. Georges, G. Kotliar, W. Krauth, and M. J. Rozenberg. *Rev. Mod. Phys.*, 68:13–125, 1996.

[40] K. J. H. Giesbertz. *Time-Dependent One-Body Reduced Density Matrix Functional Theory*. PhD thesis Vrije Universiteit Amsterdam, 2010.

[41] K. J. H. Giesbertz, E. J. Baerends, and O. V. Gritsenko. *Phys. Rev. Lett.*, 101:033004, 2008.

[42] K. J. H. Giesbertz and R. van Leeuwen. *J. Chem Phys.*, 139(10):104110, 2013.

[43] K. J. H. Giesbertz and R. van Leeuwen. *J. Chem Phys.*, 139(10):104109, 2013.

[44] T. L. Gilbert. *Phys. Rev. B*, 12:2111–2120, 1975.

[45] S. Goedecker and C. J. Umrigar. *Phys. Rev. Lett.*, 81:866–869, 1998.

[46] E. K. U. Gross, R. E., and H. O. *Many-particle Theory*. A. Hilger, 1991.

[47] A. Grüneis, G. Kresse, Y. Hinuma, and F. Oba. *Phys. Rev. Lett.*, 112:096401, 2014.

[48] M. Guzzo, J. J. Kas, L. Sponza, C. Giorgetti, F. Sottile, D. Pierucci, M. G. Silly, F. Sirotti, J. J. Rehr, and L. Reining. *Phys. Rev. B*, 89:085425, 2014.

[49] M. Guzzo, G. Lani, F. Sottile, P. Romaniello, M. Gatti, J. J. Kas, J. J. Rehr, M. G. Silly, F. Sirotti, and L. Reining. *Phys. Rev. Lett.*, 107:166401, 2011.

[50] L. Hedin. *Phys. Rev.*, 139:A796–A823, 1965.

[51] L. Hedin and S. Lundqvist. *Solid State Phys.*, volume 23. Ehrenreich, H. and Seitz, F. and Turnbull, D., Academic Press, New York, 1969.

[52] N. Helbig, N. N. Lathiotakis, M. Albrecht, and E. K. U. Gross. *Europhys. Lett.*, 77(6):67003, 2007.

[53] H. Hertz. *Annalen der Physik*, 267(8):9831000, 1887.

[54] P. Hohenberg and W. Kohn. *Phys. Rev.*, 136:B864–B871, 1964.

[55] J. Hubbard. *Proc. R. Soc. A*, 276(1365):238–257, 1963.

[56] S. Huotari, J. A. Soininen, T. Pylkkänen, K. Hämäläinen, A. Issolah, A. Titov, J. McMinis, J. Kim, K. Esler, D. M. Ceperley, M. Holzmann, and V. Olevano. *Phys. Rev. Lett.*, 105:086403, 2010.

[57] L. P. Kadanoff and G. Baym. *Quantum Statistical Mechanics*. W.A. Benjamin Inc., New York, 1964.

[58] W. Kohn and L. J. Sham. *Phys. Rev.*, 140:A1133–A1138, 1965.

[59] J. Kuneš, V. I. Anisimov, A. V. Lukoyanov, and D. Vollhardt. *Phys. Rev. B*, 75:165115, 2007.

[60] J. Kuneš, V. I. Anisimov, S. L. Skornyakov, A. V. Lukoyanov, and D. Vollhardt. *Phys. Rev. Lett.*, 99:156404, 2007.

[61] G. Lani, P. Romaniello, and L. Reining. *New J. Phys.*, 14(1):013056, 2012.

[62] N. N. Lathiotakis, N. Helbig, and E. K. U. Gross. *Phys. Rev. B*, 75:195120, 2007.

[63] N. N. Lathiotakis, S. Sharma, J. K. Dewhurst, F. G. Eich, M. A. L. Marques, and E. K. U. Gross. *Phys. Rev. A*, 79:040501, 2009.

[64] D. A. Liberman. *Phys. Rev. B*, 62:6851–6853, 2000.

[65] E. H. Lieb. *Int. J. Quantum Chem.*, 24(3):243277, 1983.

[66] E. H. Lieb and F. Y. Wu. *Phys. Rev. Lett.*, 20:1445–1448, 1968.

[67] L. Y. Lim, S. Lany, Y. J. Chang, E. Rotenberg, A. Zunger, and M. F. Toney. *Phys. Rev. B*, 86:235113, 2012.

[68] J. Lischner, D. Vigil-Fowler, and S. G. Louie. *Phys. Rev. Lett.*, 110:146801, 2013.

[69] P.-O. Löwdin. *Phys. Rev.*, 97:1474–1489, 1955.

[70] P.-O. Löwdin and H. Shull. *Phys. Rev.*, 101:1730–1739, 1956.

[71] P. C. Martin and J. Schwinger. *Phys. Rev.*, 115:1342–1373, 1959.

[72] L. F. Mattheiss. *Phys. Rev. B*, 5:290–306, 1972.

[73] D. A. Mazziotti. *Phys. Rev. A*, 57:4219–4234, 1998.

[74] D. A. Mazziotti and R. M. Erdahl. *Phys. Rev. A*, 63:042113, 2001.

[75] M. M. Morrell, R. G. Parr, and M. Levy. *J. Chem Phys.*, 62(2):549554, 1975.

[76] R. C. Morrison. *J. Chem Phys.*, 96(5):37183722, 1992.

[77] N. F. Mott. *Proceedings of the Physical Society. Section A*, 62(7):416, 1949.

[78] A. Müller. *Phys. Lett. A*, 105(9):446 – 452, 1984.

[79] I. A. Nechaev, R. C. Hatch, M. Bianchi, D. Guan, C. Friedrich, I. Aguilera, J. L. Mi, B. B. Iversen, S. Blügel, P. Hofmann, and E. V. Chulkov. *Phys. Rev. B*, 87:121111, 2013.

[80] W. Nelson, P. Bokes, P. Rinke, and R. W. Godby. *Phys. Rev. A*, 75:032505, 2007.

[81] V. Olevano, A. Titov, M. Ladisa, K. Hämäläinen, S. Huotari, and M. Holzmann. *Phys. Rev. B*, 86:195123, 2012.

[82] T. Olsen and K. S. Thygesen. *J. Chem. Phys.*, 140(16), 2014.

[83] C. Overy, G. H. Booth, N. S. Blunt, J. J. Shepherd, D. Cleland, and A. Alavi. *J. Chem. Phys.*, 141(24), 2014.

[84] E. Papalazarou, M. Gatti, M. Marsi, V. Brouet, F. Iori, L. Reining, E. Annese, I. Vobornik, F. Offi, A. Fondacaro, S. Huotari, P. Lacovig, O. Tjernberg, N. B. Brookes, M. Sacchi, P. Metcalf, and G. Panaccione. *Phys. Rev. B*, 80:155115, 2009.

[85] R. G. Parr and W. Yang. *Density-functional theory of atoms and molecules*, volume 16. Oxford university press, 1989.

[86] Peng Hai Yang, Li Yong Feng, Lin Wei Nan, Wang Yu Zhan, Gao Xing Yu, and Wu Tom. *Scientific Reports*, 2:442, 2012.

[87] J. P. Perdew and Y. Wang. *Phys. Rev. B*, 45:13244–13249, 1992.

[88] K. Pernal and J. Cioslowski. *Chem. Phys. Lett.*, 412(13):71 – 75, 2005.

[89] M. Piris and J. M. Ugalde. *J. Comput. Chem.*, 30(13):20782086, 2009.

[90] T. J. Pollehn, A. Schindlmayr, and R. W. Godby. *J. Phys.: Condens. Matter*, 10(6):1273, 1998.

[91] M. Puig von Friesen, C. Verdozzi, and C.-O. Almbladh. *Phys. Rev. Lett.*, 103:176404, 2009.

[92] M. Puig von Friesen, C. Verdozzi, and C.-O. Almbladh. *Phys. Rev. B*, 82:155108, 2010.

[93] X. Ren, P. Rinke, C. Joas, and M. Scheffler. *J. Mater. Sci.*, 47(21):74477471, 2012.

[94] P. Romaniello, F. Bechstedt, and L. Reining. *Phys. Rev. B*, 85:155131, 2012.

[95] P. Romaniello, S. Guyot, and L. Reining. *J. Chem. Phys*, 131(15):154111, 2009.

[96] G. A. Sawatzky and J. W. Allen. *Phys. Rev. Lett.*, 53:2339–2342, 1984.

[97] J. Schwinger. *Proc. Natl. Acad. Sci. U.S.A.*, 37(7):452–455, 1951.

[98] S. Sharma, J. K. Dewhurst, N. N. Lathiotakis, and E. K. U. Gross. *Phys. Rev. B*, 78:201103, 2008.

[99] S. Sharma, J. K. Dewhurst, S. Shallcross, and E. K. U. Gross. *Phys. Rev. Lett.*, 110:116403, 2013.

[100] M. Springer, F. Aryasetiawan, and K. Karlsson. *Phys. Rev. Lett.*, 80:2389–2392, 1998.

[101] A. Stan, N. E. Dahlen, and R. van Leeuwen. *Europhys. Lett.*, 76(2):298, 2006.

[102] A. Stan, N. E. Dahlen, and R. van Leeuwen. *J. Chem Phys.*, 130(11), 2009.

[103] V. N. Staroverov and G. E. Scuseria. *J. Chem. Phys.*, 117(6):24892495, 2002.

[104] G. Strinati. *Riv. Nuovo Cimento*, 11:1–86, 1988.

[105] D. Sundholm and J. Olsen. *J. Chem Phys.*, 98(5):39994002, 1993.

[106] K. Terakura, T. Oguchi, A. R. Williams, and J. Kübler. *Phys. Rev. B*, 30:4734–4747, 1984.

[107] O. Tjernberg, S. Söderholm, G. Chiaia, R. Girard, U. O. Karlsson, H. Nylén, and I. Lindau. *Phys. Rev. B*, 54:10245–10248, 1996.

[108] O. Tjernberg, S. Söderholm, G. Chiaia, R. Girard, U. O. Karlsson, H. Nylén, and I. Lindau. *Phys. Rev. B*, 54:10245–10248, 1996.

[109] W. Töws and G. M. Pastor. *Phys. Rev. B*, 83:235101, 2011.

[110] C. A. Ullrich. *J. Chem. Phys.*, 125(23), 2006.

[111] R. van Meer, O. V. Gritsenko, and E. J. Baerends. *J. Chem. Phys.*, 140(2), 2014.

[112] M. van Schilfgaarde, T. Kotani, and S. Faleev. *Phys. Rev. Lett.*, 96:226402, 2006.

[113] J. Vidal, S. Botti, P. Olsson, J.-F. m. c. Guillemoles, and L. Reining. *Phys. Rev. Lett.*, 104:056401, 2010.

[114] J. Vidal, X. Zhang, L. Yu, J.-W. Luo, and A. Zunger. *Phys. Rev. B*, 84:041109, 2011.

[115] M. P. von Friesen, C. Verdozzi, and C.-O. Almbladh. *Phys. Rev. Lett.*, 103:176404, 2009.

[116] R. Žitko, J. Bonča, and T. Pruschke. *Phys. Rev. B*, 80:245112, 2009.

[117] D. Waroquiers, A. Lherbier, A. Miglio, M. Stankovski, S. Poncé, M. J. T. Oliveira, M. Giantomassi, G.-M. Rignanese, and X. Gonze. *Phys. Rev. B*, 87:075121, 2013.

[118] H. O. Wijewardane and C. A. Ullrich. *Phys. Rev. Lett.*, 95:086401, 2005.

[119] Q. Wu, C.-L. Cheng, and T. Van Voorhis. *J. Chem Phys.*, 127(16), 2007.

[120] J. Zaanen and G. Sawatzky. *J. Solid State Chem.*, 88(1):827, 1990.

[121] A. Zangwill and P. Soven. *Phys. Rev. Lett.*, 45:204–207, 1980.

[122] A. Zangwill and P. Soven. *Phys. Rev. B*, 24:4121–4127, 1981.

[123] E. N. Zarkadoula, S. Sharma, J. K. Dewhurst, E. K. U. Gross, and N. N. Lathiotakis. *Phys. Rev. A*, 85:032504, 2012.

[124] V. P. Zhukov, E. V. Chulkov, and P. M. Echenique. *Phys. Rev. Lett.*, 93:096401, 2004.